

NORTHWESTERN UNIVERSITY

Metabolic Reprogramming of Macrophage During Inflammation Resolution and Cardiac Wound  
Healing

A DISSERTATION

SUBMITTED TO THE GRADUATE SCHOOL IN PARTIAL FULFILLMENT OF THE REQUIREMENTS

for the degree

DOCTOR OF PHILOSOPHY

Field of Driskill Graduate Training Program in Life Sciences

By

Shuang Zhang

EVANSTON, ILLINOIS

December 2018

© Copyright by Shuang Zhang 2018

All Rights Reserved

**Abstract**

Macrophages are one of the most versatile immune cells in the immune system. They are found in nearly every tissue and organ throughout the body. Macrophages play important roles of orchestrating initiation and resolution of inflammation, such as sentineling against pathogens or engulfing apoptotic cells. Macrophages are able to respond to a variety of different stimuli and secrete an array of different cytokines in response to different stimuli, which can further license a large amount of other types of cells such as B cells, T cells, neutrophils, or fibroblasts. Thus, this thesis work has been dedicated to elucidating the mechanisms that orchestrate macrophage activation.

Each day billions of cells per person turns over during normal homeostatic process or tissue injuries. One of the most important roles of macrophage is clearing dying cells (a process termed efferocytosis). Different from phagocytosis of bacteria, upon efferocytosis, macrophages reprogram to a resolving status where they secrete anti-inflammatory and pro-resolving factors such IL10 and TGF $\beta$  while reduce anti-inflammatory cytokine secretion, such as TNF $\alpha$  and IL1 $\beta$ . However, when efferocytosis is ineffective, it can lead to prolonged inflammation, delayed wound healing, and auto-immune disorders. More importantly, we found that efferocytosis also plays an important role in wound healing in the heart. Heart failure after myocardial infarction is a significant cause of morbidity and mortality. During MI, a burst of cardiomyocyte (CM) triggers recruitment and mobilization of phagocytic monocytes and macrophages that clear myocardial tissue. While prompt phagocytic clearance of dying cardiomyocytes triggers homeostatic tissue remodeling via anti-inflammatory and pro-reparative signaling pathways within phagocyte,

delayed phagocytosis lead to maladaptive tissue repair which can lead to heart failure. Thus, it is of great importance to identify the orchestrating machineries that regulate the anti-inflammatory reprogramming in macrophages after efferocytosis.

It is now well appreciated that intracellular metabolism is integrated with the balance of cell activation and function. In macrophages, glycolysis is required for pro-inflammatory (M1) cell activation and the mobilizing of biosynthetic precursors to combat bacterial infection, while fatty acid oxidation is more required for alternative macrophage (M2) polarization. In the case of efferocytosis, macrophages not only receive anti-inflammatory signaling initiated by apoptotic cell/scavenger receptor contact, but also bring extracellular macromolecules such as lipids into efferocytes. How do macrophages metabolically respond to such stimuli awaits to be discovered. We found that apoptotic cells with different fatty acid loads initiate anti-inflammatory response in macrophages to different degrees. Using a mouse model in which myeloid lineage specific deletion of complex III protein RISP leads to reduced anti-inflammatory IL10 secretion from macrophages after efferocytosis. Myeloid RISP deficiency mice also showed defected wound healing/recover after myocardial infarction. Thus, we elucidated a key role of mitochondrial electron transport chain in efferocytosis mediated macrophage reprogramming. We also found that ETC facilitate IL10 production via regulating NAD<sup>+</sup>/NADH level in macrophages. This further led to SIRT1 activation. These findings highlight a key role for mitochondria/SIRT1 pathway in regulating macrophage reprogramming after efferocytosis and suggest how metabolism can fine-tune macrophage functions during cardiac wound healing.

## Acknowledgement

My special thanks to:

My thesis advisor, Dr. Edward Thorp, for giving me the opportunity to engage in doing exciting projects and providing the most generous support and guidance during my time in his lab.

My thesis committee members, Dr. Paul Schumacker, Dr. Hossein Ardehali, and Dr. Congcong He for their support, guidance, and critical feedbacks for my thesis project.

Dr. Steve Anderson, who was always there to listen when I went through tough times in grad school and always made me feel better after our conversations.

Thorp lab members, Matt, Kris, Connor, Xinyi, Shirley, Luba for their help along the way and making the lab feel like home.

My friends Staci, Matt, Yuanming, Anu, Sherry, Johanna, Nayo, and Laura who supported me along the way, I will not be able to make it through without their love and support.

Last but not least, I want to thank my parents, two most important people in my life, who have been pouring their unconditional love and support for me over the years. Even though they are on the other side of the Earth, they are always there whenever I need them. I cannot imagine finishing my PhD journey without them.

## List of Abbreviations

|               |  |
|---------------|--|
| CCR2          | C-C Chemokine Receptor Type 2                        |
| CM            | Cardiomyocyte  |
| DMEM          | Dulbecco's Modified Eagle Serum                      |
| DNA           | Deoxyribonucleic Acid                                |
| ECAR          | Extracellular Acidification Rate                     |
| ELISA         | Enzyme-Linked Immunosorbent Assay                    |
| ETC           | Electron Transport Chain                             |
| FACS          | Fluorescence-Activated Cell Sorting                  |
| FAO           | Fatty Acid Oxidation                                 |
| FBS           | Fetal Bovine Serum                                   |
| IFN- $\gamma$ | Interferon Gamma                                     |
| IL            | Interleukin  |
| KO            | Knock Out  |
| LPS           | Lipopolysaccharide                                   |
| MCP-1         | monocyte chemoattractant protein 1                   |
| Mertk         | Tyrosine protein Kinase Mer Precursor                |
| MI            | Myocardial Infarction                                |
| NAD           | nicotinamide Adenine Dinucleotide                    |
| NF $\kappa$ B | Nuclear Factor Kappa Light Chain Enhancer of B cells |
| OCR           | Oxygen Consumption Rate                              |

|             |  |
|-------------|--|
| PBS         | Phosphate Buffered Saline  |
| pbx1        | pre-B-cell leukemia transcription factor 1                           |
| PCR         | Polymerase Chain Reaction  |
| PGC1a       | Peroxisome Proliferator-Activated Receptor Gamma Coactivator-1 alpha |
| PHD2        | prolyl hydroxylase domain protein 2                                  |
| PMN         | Polymorphonuclear neutrophils  |
| qPCR        | Quantitative Real Time PCR   |
| RISP        | Rieske Iron Sulfur Protein   |
| RPMI        | Roswell Park Memorial Institute Medium                               |
| RT          | Room Temperature   |
| SIRT1       | Sirtuin1   |
| TGF $\beta$ | Transforming Growth Factor $\beta$                                   |
| TNF         | Tumor Necrosis Factor  |
| VEGF        | Vascular Endothelial Growth Factor                                   |
| WT          | Wild Type  |

**Table of Contents****Abstract—p3****Acknowledgement—p5****List of abbreviations—p6****1 GENERAL INTRODUCTIONS—p11**

1.1 Cardiac innate immune response post myocardial infarction

1.1.1 Innate immune cells in the heart—p12

1.1.2 Macrophage mediated efferocytosis and inflammation resolution in the heart—p15

1.1.3 phagocyte; myocyte interactions: “Eat me” vs “Don’t eat me” signals--019

1.2 Metabolic reprogram and immune cell polarization—p26

**2 CHAPTER 1- Catabolism of apoptotic cells fuels mitochondrial electron transport and anti-inflammatory metabolic polarization of macrophages—p31**

2.1 Introduction—p32

2.2 Materials and Methods—p33

2.3 Results—p39

2.3.1 The efferocytosis transcriptome highlights mobilization of mitochondrial metabolism and the electron transport chain activities.

2.3.2 Global metabolomics profile of efferocytosis suggests heightened mitochondrial metabolism.

2.3.3 Efferocytosis induces oxygen consumption and glycolysis in macrophages

2.3.4 Electron transport chain integrity is required for IL10 production after efferocytosis.

2.3.5 Elevated NAD<sup>+</sup>/NADH ratio after efferocytosis is required for IL10 production and this is dependent on RISP.

2.3.6 SIRT1/PGC1 $\alpha$  is required for NAD dependent IL10 production during efferocytosis.

2.3.7 macrophage mitochondrial dysfunction impairs IL10 dependent cardiac repair.

2.4 Discussion—p66

### **3 CHAPTER 2- Cardiomyocytes induce macrophage receptor shedding to suppress phagocytosis**

3.1 Introduction—p75

3.2 Materials and Methods—p76

3.3 Results—p81

3.3.1 Mertk<sup>+</sup> monocytes juxtapose damaged cardiomyocytes in human myocardium

3.3.2 Mertk localizes to phagocytic cups in ischemic myocardium

3.3.3 Mertk is required for CM-internalization and digestion in cardiac-derived macrophages

3.3.4 Co-cultivations reveal cooperative and piece-meal phagocytic processing of dying cardiomyocytes

3.3.5 Cardiomyocyte efferocytosis is inefficient

3.3.6 Shedding of macrophage apoptotic cell receptor Mertk to reduce efferocytosis efficiency

3.4 Discussion—p106

#### **4 CHAPTER 3- Acute CD47 blockade during ischemic myocardial reperfusion enhances phagocytosis-associated cardiac repair**

4.1 Introduction—p110

4.2 Materials and Methods-p112

4.3 Results—p121

4.3.1 Evidence for cardiomyocyte specific CD47 expression in humans and mouse after experimental MI induction

4.3.2 Ex vivo uptake of cardiomyocytes by macrophages is regulated by the CD47-SIRP $\alpha$  axis

4.3.3 Acute CD47 blockade during reperfusion after MI enhances myocardial phagocytosis

4.3.4 The effects of acute anti-CD47 on infarct size, systolic function and cardiac scarring

4.4 Discussion-p144

#### **5 CONCLUDING REMARKS—p148**

**References—p152**

#### **5 CONCLUDING REMARKS**

## **1. General Introductions**

## **1.1 Cardiac innate immune response post myocardial infarction**

Heart failure after MI is a leading cause of morbidity and mortality in the industrialized world<sup>1</sup>. Even though significant advances have been made, cardiovascular disease is still the leading cause of mortality worldwide<sup>2</sup>. MI often occurs secondary to atherosclerotic plaque destabilization, the precursor to atherothrombosis<sup>3</sup>. Infarction triggers inflammatory cell recruitment, which is a critical component of healing after tissue injury<sup>4</sup>. A diverse population of bone marrow and spleen-derived immune cells are recruited to the heart after ischemia<sup>5</sup> and function to promote clearance of damaged cardiac myocytes and repair of damaged myocardium<sup>6</sup>. In contrast to inflammation during atherosclerosis<sup>7</sup>, immune cell mobilization after a heart attack is relatively acute and resolving. Although the initial inflammatory response may last just a few weeks, the activation state of recruited myocardial immune cells, molded by MI risk factors, may in turn modify cardiac infarct size and subsequently, the extent of cardiac remodeling and heart function<sup>8</sup>.

### **1.1.1 Innate immune cells in the heart**

The mononuclear phagocyte system (MPS) of monocytes, macrophages, and dendritic, collectively scavenge damaged matrix, microparticles, dead cells, and regulate inflammation. Circulating monocytes can differentiate into macrophages, dendritic cells, osteoclasts, microglia, and Kupffer cells<sup>9</sup>. In the heart, in addition to differentiating into macrophages, monocyte alone has the residence time of approximately 20 hours. Sustained levels of monocytes in the heart post MI are supplied by extramedullary splenic hematopoiesis, as well as from bone marrow sources<sup>10</sup>. There are two monocytes subsets in the heart identified by expression of surface

markers and characterized by inflammatory phenotype: Ly6C<sup>HI</sup> monocytic (analogous to CD14<sup>+</sup> CD16<sup>-</sup> in humans) and Ly6C<sup>LO</sup> monocytic/macrophage cells (CD14<sup>+</sup> CD16<sup>+</sup> in humans)<sup>11-13</sup>. In human MI patients, individuals with prolonged prevalence of proinflammatory CD14<sup>+</sup>/CD16<sup>-</sup> cells have decreased myocardial salvage, a measure of the amount of healthy tissue in the infarct<sup>14</sup>. Ly6C<sup>HI</sup> cells exhibit a pro-inflammatory phenotype and are found early in the infarct after occlusion, peaking in mice ~3 days post permanent occlusion of the murine left anterior descending artery. These cells also promote removal of necrotic debris<sup>15</sup>. Ly6C<sup>HI</sup> monocytes express high levels of CCR2, respond to MCP-1, and produce TNF $\alpha$  and proteolytic enzymes. Ly6C<sup>HI</sup> monocytes typically are not associated with high efficiency of apoptotic cell clearance, however, recent studies suggest that cross-talk with macrophages may be partially responsible. For example, 12/15 lipoxygenase (LO), expressed by alternatively activated macrophages (described below), generate phospholipid oxidation motifs on the macrophage that sequester soluble molecules that bridge apoptotic cell receptors and apoptotic targets. This in turn reduces monocyte efferocytosis efficiency<sup>16</sup>. Ly6C<sup>LO</sup>, CX3CR1<sup>HI</sup>, CCR2<sup>LO</sup> monocyte/macrophages emerge in the myocardium soon after Ly6C<sup>HI</sup> subsets and are critical for myocardial repair, where they secrete pro-fibrotic and angiogenic cytokines. Ly6C<sup>LO</sup> pro-reparative functions are tied to the Ly6C<sup>HI</sup> response, as clodronate-mediated depletion during the predominantly Ly6C<sup>HI</sup> monocyte phase delays healing. Ly6C<sup>LO</sup> cells “patrol” endothelial capillaries during homeostasis, and therefore are positioned to respond immediately after MI<sup>17</sup>. Alternatively, Ly6C<sup>LO</sup> cells need not extravasate into tissue to promote wound healing, as *Carlin et al.* reported that Ly6C<sup>LO</sup> cells can be interestingly retained by endothelial cells in the kidney vasculature to recruit PMNs<sup>18</sup>. In this example, recruited PMNs promoted lysis of compromised endothelium, which was subsequently

cleared up by monocytes. In the heart, and in terms of absolute numbers, the vast majority of Ly6C<sup>LO</sup> cells accumulate in the cardiac wound after Ly6C<sup>HI</sup> monocytes peak, eventually outnumbering Ly6C<sup>HI</sup> cells in the later stages of the cardiac inflammatory response<sup>15</sup>. Interestingly, the apoptotic cell receptor MERTK is expressed predominantly by Ly6C<sup>LO</sup> cells post MI, suggesting distinct clearance mechanisms utilized by monocyte subsets<sup>19</sup>.

Monocytes differentiate into macrophage-like cells and proliferate in the presence of Macrophage-Colony Stimulating Factor (M-CSF), which is elevated in canine infarcts<sup>20</sup>. Monocytosis is associated with higher numbers of mature macrophages in the infarct on day 5<sup>8</sup>. Within the myocardium, the early macrophage phenotype is similar to pro-inflammatory/activated M1-like macrophages (F4/80+, CD86+), which is followed by a phenotypically similar anti-inflammatory M2-like macrophage profile (F4/80+, CD206+). Furthermore, increasing the M2/M1 ratio after mesenchymal stem cell therapy was associated with improved regional function at the mid-anterior infarct zone, an effect that was abrogated upon clodronate depletion of phagocytic cells<sup>21</sup>. Besides monocyte derived macrophages, Slava Epelman et al. reported the existence of three different populations of resident macrophages in the heart which are defined by two cell surface markers: MHC-II and CCR2. Embryonic derived macrophages are CCR2<sup>-</sup>, but they can be either MHC-II<sup>hi</sup> or MHC-II<sup>low</sup>. MHC-II<sup>low</sup> Mφs are the primary subset and MHC-II<sup>hi</sup> Mφs develop from MHC-II<sup>low</sup> Mφs<sup>22,23</sup>. Both MHC-II<sup>hi</sup> and MHC-II<sup>low</sup> macrophages are good at clearing apoptotic cardiac debris, suggesting that they serve important roles in maintaining tissue homeostasis during development. The third macrophage subset is CCR2+ macrophages, which are derived from circulating blood monocytes as described earlier.

Different from CCR2<sup>-</sup> macrophages, CCR2<sup>+</sup> macrophages express high level of NLRP3 inflammasome genes<sup>22</sup>. They are critical for inflammation activation during cardiac injury<sup>24-26</sup>.

Dendritic-like cells peak at day 7 in experimental models of MI. Following dendritic cell ablation, mice exhibited enhanced inflammation and extracellular matrix degradation in the infarcted myocardium, leading to wall thinning, impaired neo-angiogenesis, and increased infiltration of Ly6C<sup>Hi</sup> monocytes. This suggested that at least immature CD11c<sup>+</sup> dendritic-like cells may play a protective role in post-MI repair<sup>27</sup>. Other cell lineages classically associated with the adaptive immune arm have been discovered in injured myocardium, including IL-10 and TGF- $\beta$  producing regulatory T cells, and B-cells<sup>28</sup>, both of which may interact with phagocytes to control inflammation and potentially other aspects of chronic heart healing.

#### 1.1.2 Macrophage mediated efferocytosis and inflammation resolution in the heart

A central function of recruited leukocytes to sites of sterile injury is the degradation and phagocytosis of degraded extracellular matrix and dying and necrotic cells. This in turn promotes fibrogenic, and potentially angiogenic, responses that contribute to filling the void of lost and non-regenerative cardiac myocytes. Recent data collectively and directly link efferocytosis by inflammatory immune cells, i.e., the phagocytosis of apoptotic cells, to wound healing in the myocardium and in turn implicate phagocytosis receptors on monocytes and macrophages as a significant link between acute inflammation resolution and organ function<sup>19,29</sup>. Importantly and in the elderly, sub-optimal dying-cell clearance may lead to maladaptive cardiac remodeling and tissue repair, thereby accelerating the transition to heart failure<sup>30</sup>.

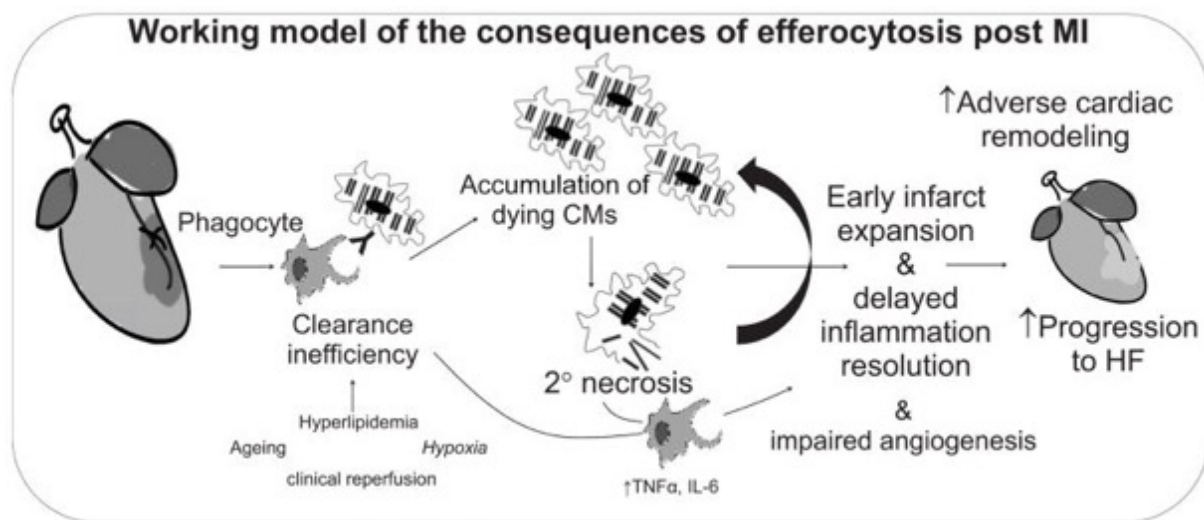


**Figure 1-1 Working Model of How the Cell Biology of Inflammation post Myocardial Infarction regulates Heart Failure.** Advanced atherosclerosis promotes atherothrombotic myocardial infarction (MI), the latter of which is characterized by recruitment of neutrophils and monocyte subsets that can differentiate into macrophages or dendritic-like cells. Phagocytes promote clearance of dying cardiac and immune cells. However, inherent inefficiency or MI associated risk factors promote inefficient dying-cell clearance, leading to secondary necrosis and further loss of non-regenerative cardiomyocytes. These acute events can affect later cardiac remodeling and inflammation that may lead to heart failure.

Here I proposed a testable working model (Figure 1-1) that predict relationships between phagocyte-mediated dying-cell recognition, efferocytosis, infarct size, tissue-reparative signaling, and myocardial remodeling in the hypoxic heart.

Whereas efficient efferocytosis activates pro-resolving/anti-inflammatory pathways in the phagocyte<sup>31,32</sup>, defective efferocytosis leads to secondary post-apoptotic necrosis and expansion of tissue necrosis<sup>29</sup>. Previous studies have linked defective apoptotic cell clearance to diseases of chronic non-resolving inflammation such as atherosclerosis and lupus<sup>33</sup>. In contrast, the extent to which efferocytosis efficiency during acute resolving inflammation may affect long-lasting organ function is much less clear. In particular, inefficient removal of dead cardiac tissue in aged hearts has been linked to progression of heart failure<sup>34</sup>. Clearance of apoptotic PMNs by macrophages initiates the resolution phase of inflammation, inducing the production of IL-10, TGF- $\beta$ , lipoxins, and resolvins. IL-10 appears late in the infarcted myocardium and contributes to the stabilization of the matrix by promoting macrophage production of tissue inhibitor of metallo-proteinases<sup>35</sup>. IL-10 knockout animals display an increased inflammatory response<sup>36</sup>, including heightened TNF- $\alpha$  and MCP-1 mRNA and increased mortality rates during ischemia-reperfusion<sup>37</sup>. Lipoxins and resolvins, derived from poly-unsaturated fatty acids, are protective for cardiomyocyte reperfusion injury and promote efferocytosis of PMNs by macrophages while reducing vascular permeability and PMN infiltration<sup>38-41</sup>. Enhanced clearance of PMNs may feed-back through an IL-23 pathway to affect granulopoiesis and PMN production<sup>42</sup>. In a mouse model of acute kidney ischemia reperfusion injury, PMN-associated production of IL-17/IL-23 was shown to be required for further PMN infiltration and IFN- $\gamma$  production<sup>43</sup>. Finally, If PMNs are cleared by macrophages, the question arises: What cells are responsible for clearing

macrophages that turnover in the heart? Dying macrophages may emigrate to spleen or lymph or alternatively be removed by new resident cardiac macrophages or other resident cardiac cells. Efferocytosis induces TGF- $\beta$ <sup>44-46</sup>, which also plays an important role in tissue remodeling and post-MI inflammation resolution. TGF- $\beta$  activates fibroblasts and induces collagen and fibronectin production<sup>47</sup>. This cytokine also reduces adhesion molecule expression and promotes the differentiation of regulatory T cells<sup>48,49</sup>. After activation by IFN $\gamma$ , LPS, lactate, or hypoxia, macrophages may produce pro-angiogenic factors, including nitric oxide and VEGF (Vascular Endothelial Growth Factor), or. During hypoxia, VEGF is up-regulated through the action of hypoxia transcription factors and through increased mRNA stability<sup>50</sup>. A subset of pro-angiogenic macrophages have been described, termed myeloid angiogenic cells (MACS), which are similar in function to alternatively active/M2 phagocytes, but also express endothelial cell markers including TIE2 (Tunica Internal Endothelial Cell Kinase, or TEK tyrosine kinase) and VEGFR. These cells promote angiogenesis via paracrine signaling, producing MCP-1, MMP9 and IL-8, which act on endothelial cells to activate VEGFR<sup>51</sup>. Interestingly, when these cells were administered intravenously in a rat model of MI, they were found to localize to ischemic areas, causing reduced scarring and improved ventricular function<sup>52</sup>. Whether these cells are capable of differentiating into endothelial cells or maintain their myeloid phenotype once within tissue, however, remains unclear<sup>53</sup>. Of further interest, when CD14<sup>+</sup> monocytes were delivered to ischemic sites of oxygen-induced retinopathy, the result was an enhanced pro-angiogenic M2 macrophage phenotype that improved vascularization and reduced retinopathy-associated inflammation<sup>54</sup>. Furthermore, in a hind-limb ischemia model, deletion of one allele of hypoxia transcription factor-suppressor PHD2 (prolyl hydroxylase domain protein 2), in turn skewed macrophage polarization towards a

pro-arteriogenic phenotype, thereby preventing tissue necrosis and preserving limb perfusion<sup>55</sup>. Finally, *Hochreiter-Hufford* showed that through recognition of externalized phosphatidylserine on neighboring apoptotic cells, BAI1 (brain-specific angiogenesis inhibitor), a member of the adhesion type-G protein coupled receptor family, can signal through the EMLO-DOCK180-Rac1 pathway and enhance myoblast fusion during muscle development, regeneration and repair<sup>56</sup>.

### 1.1.3 phagocyte; myocyte interactions: “Eat me” vs “Don’t eat me” signals

After margination to post capillary venules, immune cells transmigrate past endothelial cells and chemotax towards the site of infarction. Directed migration to the ischemic core of an MI requires trafficking through a gradient of reducing oxygen tension. Apoptotic cells, primarily located in the zone bordering the infarct<sup>57</sup>, likely secrete local so-called *find-me* signals, which is the first essential step for phagocyte recruitment in tissue. *Find-me* molecules are soluble chemo-attractants released by dying cells to establish a chemotactic gradient to attract phagocytes<sup>58</sup>. Many of these signaling pathways act on RhoGTPases, which regulate cytoskeleton rearrangement to promote cellular migration<sup>59</sup>. Known *find-me* signals include lipids, such as lyso-phosphatidyl-choline (LPC) and sphingosine-1-phosphate (S1P). LPC, one of the better-characterized *find-me* signals, is externalized and excreted during apoptosis<sup>60</sup>. Secreted LPC interacts with G-protein-coupled receptor G2A, stimulating macrophage chemotaxis towards apoptotic cells<sup>61</sup>. LPC accumulates during ischemia in myocardium via thrombin activation of Ca<sup>2+</sup>-independent phospholipases<sup>62</sup>, consistent with its role as a *find-me* signal in the damaged heart. S1P, another lipid *find-me* signal is produced by sphingosine kinase 1 (SPHK1) for recognition by S1P receptors on distal cells. Apoptotic stress induces SPHK1 activation, which can

then promote S1P secretion<sup>63</sup>. In addition to lipid *find-me* signals, proteinaceous tissue recruitment factors include cytokines and chemokines, including fractalkine (CX3CL1), which is cleaved by caspase-3 during apoptosis. In turn, the released fractalkine extracellular domain interacts with CX3CR1 on macrophages for cell recruitment<sup>64</sup>. Nucleotides, including ATP and UTP, originate from both apoptotic and necrotic cells, and also likely act as *find-me* signals in the myocardium. In apoptotic cells, the plasma membrane channel pannexin 1 (PANX1) may serve as a conduit for nucleotide release after cleavage by caspases 3 and 7<sup>65</sup>. During ischemia, cellular stress increases glycosylation of PANX1, resulting in enhanced ATP release from myocytes to promote fibroblast transformation<sup>66</sup>. Also, ATP can guide neutrophil chemotaxis via purinergic P2Y2 and A3 adenosine receptors *in vitro* and *in vivo*<sup>67</sup>. Knockdown of P2y2 inhibits migration, all consistent with the possibility that ATP released from PANX1 may act as a *find-me* signal in the heart<sup>68</sup>.

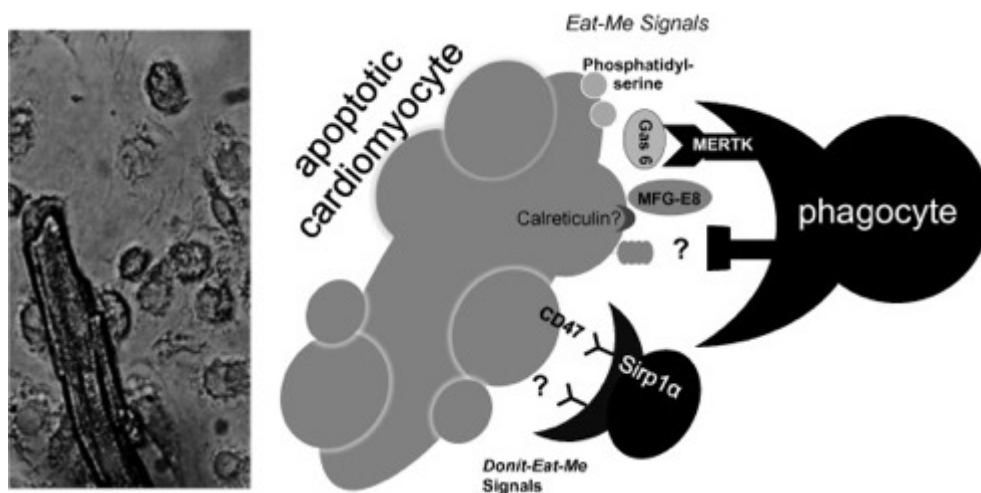


**Figure 1-2 Phagocyte-Myocyte interactions.** To the left is a micrograph of the elongated cardiomyocyte juxtaposed next to multiple circular macrophages. To the right is a schematic exhibiting the unknown spectrum of interacting ligands between macrophages and cardiomyocytes, including putative eat-me signals on the apoptotic cardiomyocyte, such as phosphatidylserine and calreticulin, as well as potential molecules that bridge cardiomyocytes and macrophages, such as Gas6 (growth arrest specific) or MFG-E8 (milk fat globule). Don't eat me signals may include CD47 through interactions with Srp1 $\alpha$ . MERTK is important on the phagocyte side for efferocytosis of cardiomyocyte apoptotic bodies. Other putative cardiac recognition ligands and macrophage receptors are yet to be described.

### Keep-out/Keep-away signals

Local find me signals are balanced by local *keep-out/keep-away* signals. In some instances, apoptotic cells selectively recruit monocytes as opposed to neutrophils. For example, monocytes in contrast to neutrophils are selectively recruited after injecting apoptotic cell supernatants into an air-pouch model of inflammation<sup>69</sup>. Additionally, lactoferrin from apoptotic cell supernatants “kept out” neutrophils but not monocytes<sup>70</sup>. Interestingly, the *apo*-form of lactoferrin can function as a mimetic of hypoxia by stabilizing the hypoxia inducible factor HIF-1 $\alpha$ <sup>71</sup>. Consistent with this, lactoferrin increased in patients during ischemia, just prior to reperfusion<sup>72</sup>. Growth differentiation factor-15 (GDF-15), a TGF- $\beta$ -related cytokine, is also a keep-out signal. For example, GDF-15 is induced in the infarcted heart and *Gdf15* deficient mice exhibit enhanced recruitment of neutrophils to the infarcted myocardium. GDF-15 activates the small Rho GTPase CDC42, inhibits activation of another small GTPase RAP1, and furthermore counteracts chemokine-triggered conformational activation and clustering of adhesive  $\beta$ 2 integrins<sup>73</sup>. Though other inflammatory signals from the surrounding parenchymal pattern recognition receptor response also strongly influence inflammatory cell recruitment, the ratio of *find-me* signals to *keep-away* may be important in regulating local responses of phagocytes in close proximity to dying cells<sup>74</sup>.

The molecular pathways responsible for phagocyte interactions with cardiomyocytes remain largely unknown. A key purpose of the aforementioned recruitment signals and recruited leukocytes is to promote interactions with dying or necrotic cardiac tissue. Phagocytes distinguish viable from non-viable cells through the aid of so-called self *eat-me* and *don't-eat-me* signals, which are presented on the target cell surface and aided by binding of bridging molecules that

interface between the target cell and phagocyte. *Eat-me* signals can be externalized phospholipids, proteins, alterations in cell-surface charge or glycosylation patterns, and nucleotides<sup>56</sup>. Externalization of phosphatidyl-serine (PS) is one of the most conserved apoptotic markers, however, we are still just learning about the mechanism of PS externalization. Just this past year, *Nagata* and colleagues published that Xk-Related Protein 8 (XKR8) is required for PS externalization under apoptotic stimuli. Cells deficient for *Xkr-8* failed to expose PS during apoptosis and were inefficiently engulfed by phagocytes. Interestingly, both cancer cells and terminally differentiated cardiomyocytes were found to express low levels of *Xkr-8* (at the mRNA level), consistent with recent data showing reduced efferocytosis efficiency of cardiac myocytes by macrophages *in vitro* (*data not published*). In the context of the infarcted heart, *eat-me* signals *in vivo* may be affected by low oxygen levels. For example, acute hypoxia alters PS content in erythrocytes, potentially through modulation of phospholipid scramblases, aminophospholipid translocases and ATP-dependent floppases<sup>75</sup>. In addition to PS, annexin 1, a calcium and phospholipid binding protein in the annexin superfamily, is an endogenous *eat-me* signal for macrophages<sup>76</sup>. Annexin 1 is cleaved by ADAM10 (A Disintegrin And Metalloproteinase) during cell necrosis, also contributing as a monocytic chemotactic signal<sup>77</sup>. This pathway may be especially important after MI considering the extensive level of cellular necrosis. Another newly defined *eat-me* signal is the ficolin1-PTX3 heterocomplex, which can interact with late apoptotic or necrotic cells and enhance their clearance<sup>78</sup>.

*Don't-eat-me* signals, such as CD31 and PAI-I (Plasminogen activator inhibitor), can also help prevent viable cells from being engulfed by phagocytes. The most widely studied *don't-eat-me* signal is CD47, which is a membrane protein expressed on the surface of most cells. CD47

interacts with SIRP $\alpha$  on phagocytes, recruits phosphatases, and inhibits downstream activation of the phagocyte actin cytoskeleton, thereby preventing engulfment<sup>79</sup>. It has been shown that CD47 is expressed in abundance on apoptotic neonatal cardiocytes<sup>80</sup>. However, nothing more has been studied in the heart. By showing thrombospondin-2 (a CD47 ligand) knockout mice have higher mortality and dilated cardiomyopathy, it was concluded that TSP-2 protects age-related dilated cardiomyopathy<sup>81</sup>. However, whether this phenomenon requires CD47, or how CD47 may be directly involved in removal of apoptotic cells in the heart, is unknown. Furthermore, the TSP1-CD47 axis is induced in renal tubular epithelial cells (RTEC) under hypoxia<sup>82</sup>. Thus, it will be interesting to see if such an axis is also induced between cardiomyocytes and macrophages within the hypoxic environment of the ischemic heart.

Though pharmacological advances have significantly reduced mortality, the residual risk of post MI-induced heart failure remains high. This necessitates the development of complementary approaches to preserve heart function. It stands to reason that clearance of dying cells after MI by recruited phagocytes may be inherently inefficient as evolutionary pressure has not selected for optimal monocyte interactions with cardiac myocytes during diseases of aging. It is tempting to speculate that enhancing efferocytosis in the heart might help wound healing after heart attack. Efficient clearance of dying cells, both in a timely manner and of a significant quantity, is a pre-requisite for resolution of inflammation and downstream reparative processes after tissue clearance. In addition to clearance efficiency, the downstream signaling responses of phagocytes post engulfment are critical to inflammation resolution. Imbalances between pro- and anti-inflammatory stimuli may contribute to clearance inefficiency. The extent of cell death in the acute inflammatory phase of MI is a critical determinant of the degree of adverse remodeling

leading to heart failure<sup>57</sup>. Therefore, strategies that enhance efficient resolution of inflammation and prevent unnecessary further cell death of terminally differentiated heart myocytes (cardiomyocytes) may be useful in slowing the progression to heart failure and potential autoimmune reactions. Additional MI risk factors, such as hyperlipidemia may further reduce efferocytosis efficiency and repair in the heart.

Though many potential molecular reasons may explain inefficient efferocytosis of cardiomyocytes, one candidate worth noting is at the level of apoptotic cell receptors, which could be rendered naturally dysfunctional in the setting of disease or genetic risk factors. For example, polymorphisms in the apoptotic cell receptor *Mertk* are associated with increased autoimmune inflammation in diseases such as Lupus<sup>83</sup>. In addition, ADAM metallopeptidase 17, which cleaves MERTK into a soluble inhibitory receptor<sup>84,85</sup>, is increased during MI<sup>86</sup>. This may explain the identification of solMER in murine extracts post MI<sup>19</sup> and further provide the impetus for investigation of human MI specimens or blood. MERTK activity may also be limited by availability of its ligand *Gas6*, which is required for binding to apoptotic cells<sup>87</sup>. Future therapeutic approaches must strike a balance as, although the innate immune response has helpful activity in the healing heart, maladaptive inflammation can also be detrimental. Therefore, selective approaches that target specific immune subsets or cellular pathways harbor the most potential, as broad immunosuppressive therapy post MI can be detrimental in mice and humans<sup>88,89</sup>. Targeting of Ly6c<sup>HI</sup> monocytes after reperfusion have shown promise in improving infarct healing in atherosclerosis-prone mice<sup>90</sup>. Also, stimulation of so called pro-resolving pathways downstream of efferocytosis and phosphatidylserine recognition have proven beneficial in animal models<sup>91</sup>.

## 1.2 Metabolic reprogram and immune cell polarization

Tissue injury generates heightened levels of apoptotic and necrotic debris and matrix remnants that once cleared by phagocytes, must be metabolized. Despite the current interest in immunometabolism, the relevance of this process in the heart by immune cells is largely unexplored. For example, emerging roles for metabolism have been linked to stem cell development, cell proliferation, and T-cell activation<sup>92-94</sup>. In particular, mitochondrial metabolism has been linked to many key macrophage functions, including inflammasome activation, bacterial defense, and polarization<sup>95-97</sup>. Given that macrophages can engulf cardiomyocytes and associated debris and cardiomyocytes may have both denser cellular and elevated mitochondria content<sup>98</sup>, it is reasonable to suspect that following engulfment, macrophages need to increase cellular metabolism to process this large metabolic load and that this in turn influences phagocyte intracellular signaling and reprogramming.

Macrophages can polarize to classic M1, alternative M2, or resolving stages in responses to different stimuli. The idea of classical macrophage activation was introduced by Mackaness in 1960. There are a variety of M1 stimuli: IFN $\gamma$ , through IFNGR-1 and IFNGR-2 chains from IFN- $\gamma$  receptor, can recruits Jak1 and Jak2 adaptors that activate STAT1; pathogens and LPS, through pattern recognition receptors, such as TLRs can lead to inflammasome activation through MyD88 and Mal/Tirap-dependent pathways; Granulocyte macrophage colony-stimulating factor (GM-CSF) is recently found to be an M1 stimuli for macrophages, through GM-CSF receptor, the recruited Jak2 leads to STAT5 activation. M1 macrophages are characterized by TNF $\alpha$ , IL1 $\beta$ , IL-6, and NO production. Other the other hand, there are three main M2 stimuli: IL-4/IL-13 through

IL-4R $\alpha$ 1, IL13R $\alpha$ 1, and IL13R $\alpha$ 2; binding of IL4 led to JAK1/JAK3 and STAT6 activation; a less common one is glucocorticoids: glucocorticoids bind to glucocorticoid receptor (GCR) alpha, leads to thrombospondin, IL10, and CD163 expression; IL10 is also an M2 stimuli: IL10 binding to IL10R1 and IL10R2 lead to activation of STAT3, which further leads to macrophage metabolic reprogramming and anti-inflammatory reprogramming.

Recently research has stirred interests in how metabolism regulates macrophage polarization. In contrast to traditional viewpoints that metabolic reprogramming occurs solely in response to nutrient or oxygen availability, newer studies reveal that intracellular metabolism is further linked to receptors of damage-associated molecular patterns (DAMPs), which are present in abundance after myocardial infarction<sup>99</sup>. In response to LPS, macrophages increase glycolysis and the pentose phosphate pathway, and reduce oxidative phosphorylation despite the presence of abundant molecular oxygen<sup>96,100-102</sup>. Approaches utilizing glucose tracers demonstrate conservation of this glycolytic shift in response to other proinflammatory stimuli such as IFN- $\gamma$  and DAMPs<sup>103</sup>. Mechanistically, integrated transcriptional and metabolic network analyzes revealed that proinflammatory macrophages have a so-called “broken TCA cycle,” where the truncation of isocitrate dehydrogenase and succinate dehydrogenase (SDH) leads to an accumulation of succinate<sup>104</sup>. The increase in succinate stabilizes hypoxia inducible factor (HIF)-1 $\alpha$  resulting in an increase in reverse electron transport and ROS production from complex I of the electron transport chain and favoring glycolysis by promoting phosphofructokinase isoform conversion<sup>102,105</sup>. Metabolomic studies also revealed that itaconate modulates proinflammatory macrophage metabolism and effector function by inhibiting the oxidation of succinate to fumarate by SDH<sup>106</sup>. Furthermore, HIF-1 $\alpha$  may also directly be stabilized by ROS generated during

IRI driving a metabolic shift in macrophages toward glycolysis and the subsequent proinflammatory polarization<sup>107</sup>.

While DAMPs and hypoxia may polarize cardiac macrophages toward a glycolysis-dominated, proinflammatory profile early during myocardial injury, increased oxygen tensions due to angiogenesis and increased levels of lipids from engulfed apoptotic debris may promote a metabolic shift toward fatty acid oxidation (FAO) through the mitochondria. In this context, alternatively activated macrophages induced by IL-4 consumed more oxygen<sup>108</sup> and this increase in oxidative metabolism was required for the anti-inflammatory phenotype, as inhibition of FAO with the carnitine palmitoyltransferase (CPT)-1 inhibitor, etomoxir, inhibited IL-4 induced alternative macrophage polarization<sup>96</sup>. However, another group contrasted CPT-2 requirements by showing that CPT-2-deficient macrophages can still fully polarize toward an alternatively activated macrophage phenotype after IL-4 stimulation, despite inhibition of FAO. Thus, the effect of etomoxir on macrophage polarization might be partially due to off target effects<sup>109</sup>. Additionally, few processes are all or none and another recent study reported glucose requirements during alternative macrophage polarization, which was dependent on a mTORC2/Stat6/IRF4 signaling axis<sup>110</sup>. Still the evidence to date largely supports a role for mitochondrial oxidative phosphorylation in anti-inflammatory responses as IL-10 can alter macrophage function by promoting mitophagy of damaged mitochondria to support oxidative phosphorylation and limiting glucose uptake and glycolysis to oppose inflammatory metabolic reprogramming<sup>111</sup>. As IL-10 is actively produced in macrophages after efferocytosis, it is worth exploring whether efferocytosis influences cellular metabolism to promote IL-10 production or whether macrophage secretion of IL-10 after efferocytosis functions in an autocrine manner to

affect macrophage metabolism. Metabolism of small molecules such as amino acids and vitamins are also involved in macrophage activation. For example, L-arginine-derived metabolites are important mediators for inhibiting the production of TNF- $\alpha$  in mouse splenic macrophages after intestinal obstruction<sup>112</sup>. Vitamin A has also been shown to be required for the phenotypic conversion of IL-4 activated macrophages within tissue resident macrophages of the peritoneal cavity<sup>113</sup>. Besides its contribution to alternative macrophage activities, lipid metabolism also likely contributes to macrophage phagocytosis by fulfilling its energetic needs and regulating the membrane fluidity that is required for phagocytosis<sup>114</sup>. Other links to mitochondrial pathways includes mitochondrial UCP2, which is required for continuous uptake of apoptotic cells<sup>115</sup>. Taken together, many of the metabolic links between phagocytosis and macrophage function remain unknown, especially in the heart, and discoveries made in the field of immunometabolism as it pertains to the macrophage will likely influence our understanding of inflammation resolution after cardiac injury and inform new therapeutic strategies.

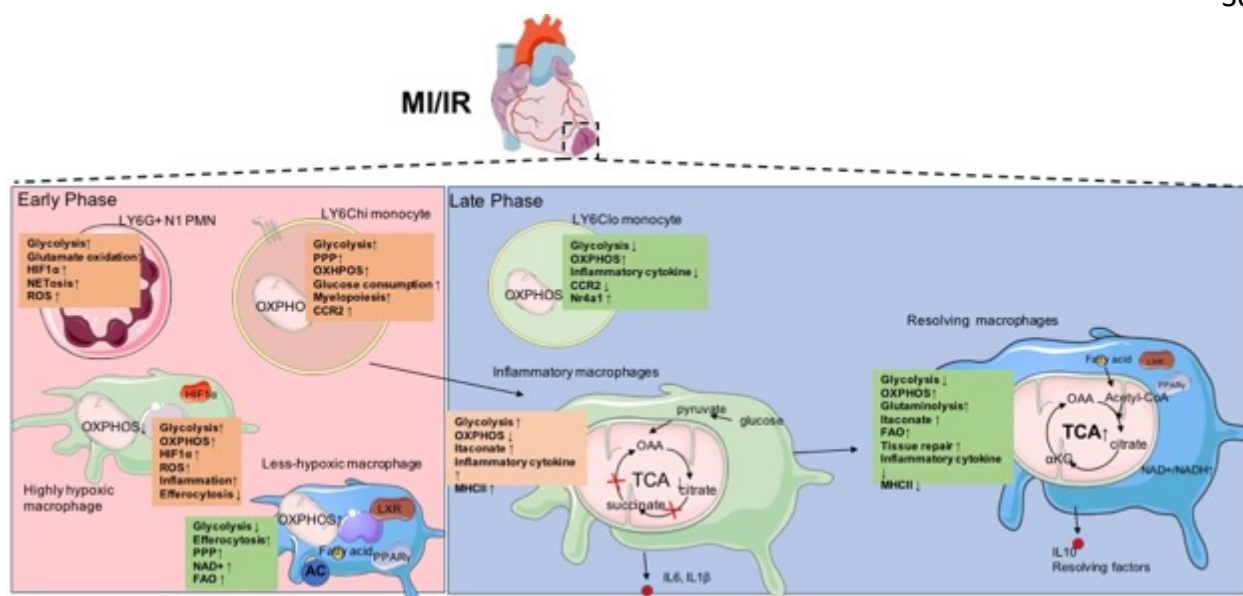


**Figure 1-3 Immunometabolism during wound healing after myocardial infarction.** This figure summarizes early and late inflammatory phase in the heart after ischemia in the area of myocardial infarction. In the early phase (onset of ischemia-D3) there are glycolytic neutrophils, Ly6Chi monocytes, and tissue macrophages. Macrophages in the middle of the infarct core are highly hypoxic, thus are less able to engage in efferocytosis and are more glycolytic; while macrophages at the border zone are less hypoxic, and have higher capacity of clearing tissue debris, thus engaging in more mitochondrial OXPHOS than glycolysis. In late phase (D3-D7), Ly6Clo monocytes from blood infiltrated into myocardium. In the meantime, ly6Chi monocytes differentiate into CCR2+ macrophages. These macrophages first engage in glycolysis and secrete more inflammatory cytokines and MMPs. As time passes and inflammation are dampened, these macrophages are reprogrammed into a resolving state macrophage, probably after efferocytosis of tissue debris. The late resolving state macrophages are less glycolytic and using OXPHOS to produce IL10 and TGF $\beta$  for tissue repair.

**2 CHAPTER 1- Catabolism of apoptotic cells fuels mitochondrial electron transport and anti-inflammatory metabolic polarization of macrophages**

## 2.1 Introduction

Macrophages preserve systemic self-tolerance and promote inflammation resolution and tissue repair through efferocytosis <sup>116</sup>. In addition to the recognition and engulfment of dying cells, efferocytosis triggers the production of anti-inflammatory and tissue reparative cytokines <sup>46</sup> as well as inflammation-resolving bioactive lipids <sup>32</sup>. Whilst these host-protective responses act in part through lipid-activated nuclear receptor transcription factors <sup>117</sup>, the signal transduction role of metabolites during efferocytic reprogramming is largely untested. This is likely important during syndromes of metabolite imbalance, where the anti-inflammatory potential of macrophages is often depressed and contributes to disease progression <sup>33</sup>.

It is now well appreciated that intracellular metabolism is integrated with the balance of cell activation and function. In macrophages, glycolysis is required for both pro-inflammatory cell activation and the mobilizing of biosynthetic precursors to combat bacterial infection <sup>118</sup>. Elevated glucose utilization is also necessary for alternative macrophage polarization, the latter initiated by the cytokine interleukin 4 (IL4) and further accompanied by increased oxidative phosphorylation<sup>110</sup>. In the case of efferocytosis, biosynthetic precursors are in abundant supply within the phagocytic body, raising the interesting prospect that apoptotic cell catabolism may provide substrates that contribute to macrophage reprogramming. Early studies of efferocytosis implicate cellular metabolism for the generation of ATP energetic currency that is necessary for actin-mediated engulfment of external bodies <sup>119</sup>. Separately, mitochondrial uncoupling proteins <sup>115</sup> and components of mitochondrial fission machinery <sup>120</sup> are necessary for multiple rounds of efferocytosis; this is of particular importance during tissue injury, which is characterized by

heightened cell turnover. Taken together, these examples emphasize a conserved interplay between efferocytosis and cellular and mitochondrial metabolism, however what is left unsolved is whether the catabolism of dying cells is integrated to the signature macrophage anti-inflammatory response.

To understand relationships between cellular metabolism, inflammation, and tissue repair, we now report the metabolome of macrophages during efferocytosis. We implemented unbiased global metabolic pathway analyses to reveal a unique association between fatty acid oxidation, mitochondrial respiration and inflammation during the catabolism of apoptotic cells. From our investigation, we discovered that efferocytosis significantly elevated long chain fatty acid content in macrophages, activated the respiratory chain, which was required to program the macrophage anti-inflammatory response through the generation of metabolic signaling intermediates. We reproduced this non-canonical mitochondrial response during tissue injury to validate its significance to the broad pathophysiology of wound healing.

## 2.2 Material and methods

*Mice.* C57BL/6 *Uqcrfs1* (*Risp<sup>fl/fl</sup>*) mice were provided by *Paul Schumacker* (Northwestern University) and crossed to *LysMCre*<sup>121</sup>.  $\alpha$ MHC-mCherry mice (stock no. 021577) were obtained from the Jackson Laboratory. Mice were housed in temperature- and humidity-controlled environments and kept on a 12:12h day/night cycle with access to standard mouse chow and water *ad libitum*. All studies were approved and reviewed by the Institutional Animal Care and Use Committee at Northwestern University (Chicago, Illinois), protocol #IS00000375.

*Reagents.* *Risp* gene silencing was induced with validated GeneSolution siRNAs from *Qiagen*: GS66694 for *Uqcrfs1*: 4 siRNAs for Entrez gene 66694: SI01462895 (FlexiTube siRNA) SI01462902 (FlexiTube siRNA) SI01462909 (FlexiTube siRNA) SI01462916 (FlexiTube siRNA). Fatty acid supplement (F7050) was purchased from Sigma Aldrich.

*Efferocytosis ex-vivo.* Peritoneal macrophages were elicited in mice with thioglycollate broth (*Sigma-Aldrich*) and harvested after lavage. Adherent macrophages were co-cultivated with apoptotic Jurkat T cells. Tcells were induced to apoptosis after ultraviolet irradiation and early apoptotic cells (ACs) were identified as annexin V positive, propidium iodide negative, and overlaid at a ratio of 5 ACs to 1 phagocyte. Non-engulfed Tcells were removed from adherent phagocytes, 1 hours post co-cultivation. Engulfment was confirmed by microscopic and flow cytometric analysis with fluorescently labelled apoptotic cells.

*Unbiased analysis of efferocytic secretome.* Cell culture supernatant was collected 5 hours post co-cultivation. Chemokines and cytokines were analyzed with a *Bio-Plex Pro Mouse cytokine 23-plex* from *Bio Rad* (M60009RDPD) using a *Luminex 200 multiplex* instrument (Luminex, Austin, TX) and MAGPIX analysis. Additional cytokines, including IL-10, were validated by independent ELISA (BD Biosciences).

*RNA-sequencing and bioinformatics.* Adherent peritoneal macrophages were stimulated with apoptotic thymocytes for 6 hours, versus IL-4 and control. RNA was isolated from cells with Trizol

and RNA quality assessed at the Northwestern Genomics core with RNA integrity values of 10 for a minimum of 100 ng per sample. Library construction was performed in lab and sequencing was performed at the Genomics Core facility at the University of Chicago and Northwestern University. Sequencing libraries were constructed using an Illumina TruSeq Stranded mRNA prep kit LT (Illumina, RS-122-2101) for mRNA sequencing and constructs sequenced on NextSeq 500 instrument and HiSeq 2500 System from Illumina. Transcriptome analysis was performed at the bioinformatics core at Northwestern University with assistance from *Matthew Schipma, PhD*.

*Metabolomics of efferocytosis.* Metabolomics analyses were carried out in with *Metabolon, Inc.* (Durham, NC) as previously described (Evans et al., 2009; Masri et al., 2014) and with the University of Michigan Metabolomics Core. Briefly, control and *Risp-deficient* peritoneal macrophages were treated as indicated. Cell lysates were harvested, methanol extracted and analyzed by ultra-high-performance liquid chromatography-tandem mass spectrometry (UPLC-MS/MS; positive mode), UPLC-MS/MS (negative mode) and gas chromatography–mass spectrometry (GC-MS). Metabolites were identified by automated comparison of the ion features in the experimental samples to a reference library of chemical standard entries that included retention time, molecular weight (m/z), preferred adducts, and in-source fragments as well as associated MS spectra, and curated by visual inspection for quality control. Candidate metabolites and other molecules were also independently validated as follows: NAD<sup>+</sup>/NADH levels were measured with Abcam, #ab65348. Succinate measured with BioVision #K649-100. ATP was measured with Abcam, #ab83355.

*Respiratory and glycolytic analyses.* To measure the extracellular acidification rate/ECAR and oxygen consumption rate/OCR, apoptotic cell-treated, Gas6 (R&D systems, 986-GS-025), or MerTK activation antibody (R&D systems, AF591)-treated primary macrophages were plated on an XF24 cell culture microplates coated with CellTak. Experiments were conducted in XF assay medium containing 25 mM glucose, 2 mM L-glutamine, and 1 mM Na pyruvate, and analyzed using a Seahorse XF24 extracellular flux analyzer (*Agilent Technologies*). Where indicated, the following were injected: ATP-synthesis inhibitor oligomycin (1.5  $\mu$ M), carbonyl cyanide 4-(trifluoromethoxy) phenylhydrazone (FCCP; 1.5  $\mu$ M) to uncouple ATP synthesis, rotenone (100 nM) to block complex I, and antimycin A (1  $\mu$ M) (*Sigma*) to block complex III. Basal ECAR, OCR, and spare respiratory capacity were generated by Wave Desktop software (*Agilent Technologies*). Etomoxir, an inhibitor of CPT1, was from *Sigma-Aldrich* as sodium salt hydrate (E1905).

*Transmission electron microscopy.* Macrophages were cultured on sterilized Thermanox plastic coverslips and cultivated with apoptotic cells. Subsequently, coverslip was fixed with 0.1 M sodium cacodylate buffer (pH 7.3) containing 2% paraformaldehyde and 2.5% glutaraldehyde for 30 mins at room temperature and were kept at 4°C and then processed for TEM. Coverslips were flat-embedded in resin and cured in a 60°C oven. Samples were sectioned on a Leica Ultracut UC6 ultramicrotome into 70nm sections and collected on 200 mesh copper grids. Samples were processed and imaged on an FEI Tecnai Spirit G2 TEM at the Advantaged Imaging Center at Feinberg School of Medicine with assistance from Lennell Reynolds Jr.

*Immunoprecipitation.* Whole cell extract was isolated from macrophages treated with or without apoptotic cells. Pbx-1 binding chromatin was pulled down using EMD Millipore chromatin immunoprecipitation assay kit (# 17-295). To be brief, chromatin was sonicated into 200-1000 bp following crosslinking. After overnight incubation with isotype IgG or Pbx-1 antibody (Invitrogen PA5-17223), 100ul of protein A beads were added into the solution and incubated for 1hr at 4C. The protein-bound beads were collected, DNA was eluted and reverse cross-linked. DNA was recovered by phenol/chloroform extraction and ethanol precipitation.

*Immunoblots.* Cells were lysed in RIPA buffer, resolved on 10% polyacrylamide gels and transferred to nitrocellulose membranes. Membranes were blocked using 5% milk and then incubated in the primary antibody overnight. Antibodies were anti-RISP (Abcam, ab14746; used at a 1:500 dilution), anti-SIRT1 (Abcam, ab110304), and anti- $\alpha$ -tubulin. Membranes were rinsed 3 times with tween solution and then incubated with secondary antibody. Secondary antibodies utilized were anti-mouse IgG, HRP-linked and anti-rabbit IgG, HRP-linked.

*In vivo models of inflammation and tissue repair.* For experimental myocardial infarction/MI: Surgeries were performed on mice 12-16 weeks of age and as described <sup>19</sup>. Surgeries were performed by an individual blinded to the genotype. Mice were anesthetized with Avertin and secured in a supine position and endotracheal-intubated and ventilated with an Inspira Advanced Safety Single Animal Pressure/Volume Controlled Ventilator (*Harvard Apparatus, Holliston, MA*) with room air supplemented with oxygen to maintain blood gases within normal physiological limits. The chest wall was shaved and left thoracotomy was performed. With the aid of a

dissecting microscope, the left ventricle was visualized and left coronary artery on the anterior wall was permanently ligated with monofilament nylon 8-0 sutures (Ethicon, Somerville, NJ) 2mm distal to the site of its emergence from under the left atrium. Blanching/pale discoloration and hypokinesis of the anterior wall verified LAD ligation. The chest wall was closed with 7-0 nylon sutures and the skin and subcutaneous tissue was closed. Sham operations were performed on animals by passing the suture beneath the LAD without ligating the vessel.

*Flow cytometric analysis after experimental myocardial infarction/MI.* Infarcted mice were anesthetized with isoflurane and peripheral blood drawn into citrate anticoagulant solution. Hearts were harvested, perfused with saline to remove peripheral cells, minced with fine scissors, and incubated in a cocktail of collagenase and DNase. Cells were filtered through a 70mm strainer and pelleted at 500xg. Total cell numbers were counted by Trypan blue staining and cell suspensions were rinsed with Hank's Balanced Salt Solution supplemented with 0.2% (wt/vol) bovine serum albumin and 1% wt/vol fetal calf serum. Flow cytometry was performed as previously described<sup>19</sup>.

*Statistics.* Statistical analyses were performed with GraphPad Prism (GraphPad Software, La Jolla, CA). Comparisons between two groups were performed using two-tailed, unpaired t-test with 95% confidence interval. For comparisons of more than two variables, ANOVA was utilized with 95% confidence interval. Data are presented as mean +/- SEM.

*Data availability.* The datasets generated during and/or analyzed during the current study are available from the corresponding author on reasonable request.

## 2.3 Results

*2.3.1 Macrophages reprogram to an anti-inflammatory status with significant IL10 production in response to apoptotic cells.* Efferocytosis is a key first step in the resolution of inflammation<sup>32</sup>. We first asked if efferocytes produce anti-inflammatory cytokines in response to apoptotic cells. Apoptosis of Jurkat T cells and autologous splenocytes and thymocytes was induced with either UV treatment or staurosporine. Apoptosis was confirmed with annexin V, PI staining (**Fig 2-1-1A**). We chose to use 5h-treated cells for all subsequent experiment because it gave use high percentage of early stage apoptotic cells (Annexin V<sup>+</sup>, PI<sup>-</sup>) cells (**Fig 2-1-1B, C**). We began with a non-biased screen of secreted chemokines and cytokines. This approach confirmed that apoptotic cells specifically and reproducibly induced macrophages to produce the canonical anti-inflammatory cytokine IL10<sup>46</sup> (**Fig 2-1-2A,B**). This response was also validated with primary apoptotic thymocytes and primary splenocytes (**Fig 2-1-2C**). Pro-reparative TGF- $\beta$  was also induced after efferocytosis, as reported previously by Peter Henson's group (**Fig 2-1-2D**), while pro-inflammatory TNF $\alpha$  was suppressed<sup>122</sup> (**Fig 2-1-2E**). The specificity of the efferocytic cytokine phenotype was underscored by cytokines that were not affected (**Fig 2-1-3**). Unexpectedly, IL-9, the cytokine that was described as a T cell growth factor produced mainly by T cell clones<sup>123</sup> was also induced by apoptotic cells, while *Eotaxin*, the cytokine linked to eosinophil responses<sup>124</sup> was suppressed after efferocytosis.

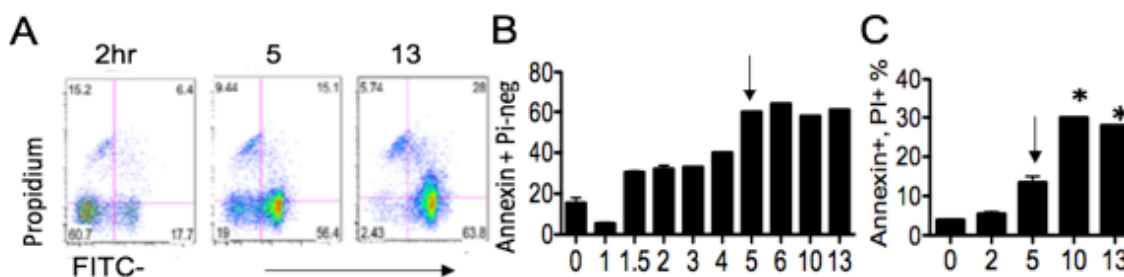


**Figure 2-1-1. Induction of early apoptotic cells for efferocytosis analyses.** (A) T cells were induced to apoptosis as described in *Materials and Methods*. At indicated times post-induction, cells were analyzed by flow cytometry for markers of apoptosis (Annexin V) and necrosis (propidium iodide permeability). Bar graphs are the enumerations of a time course analyses. (B) Quantification of percentage of early apoptotic (Annexin+, PI-) cells. (C) Quantification of late stage apoptotic (Annexin+, PI+) cells.  $p < 0.05$  relative to control. Arrow indicates time point (in hours) selected.

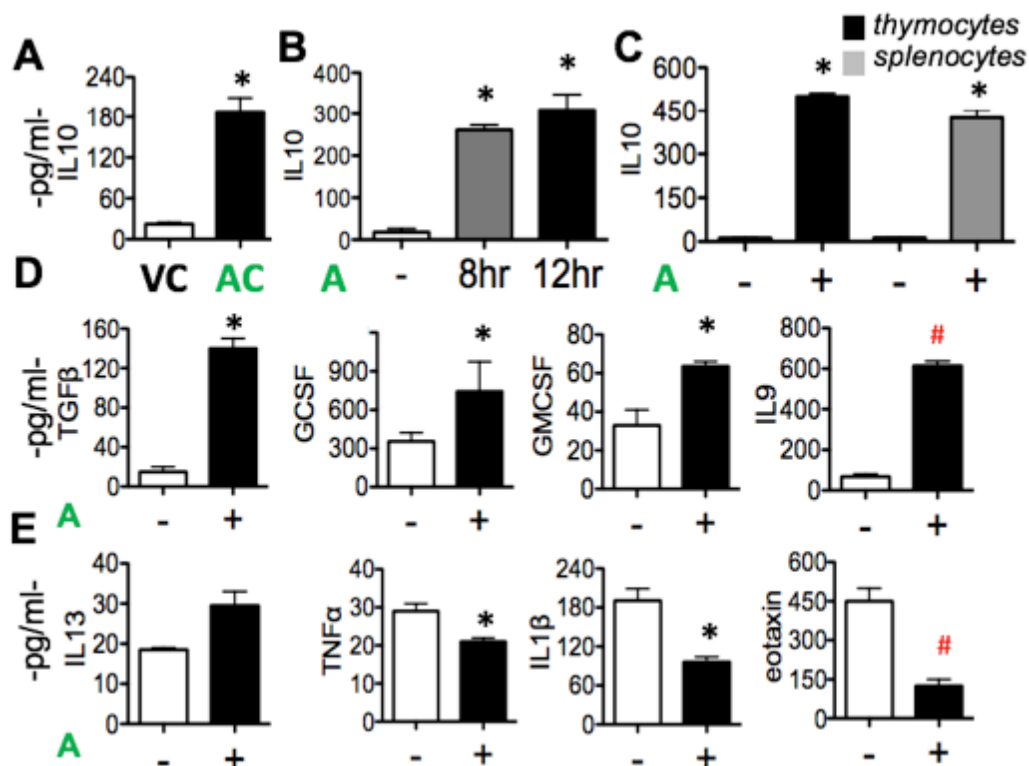


**Figure 2-1-2. Apoptotic cells induce a polarized anti-inflammatory cytokine response in activated macrophages.** Elicited primary macrophages (M $\phi$ ) were co-cultivated (see Materials and Method for further detail) with viable T cells (VCs) versus early apoptotic cells (ACs). Non-engulfed cells were removed from adherent phagocytes and cell culture media analyzed for secreted cytokines. IL10, interleukin 10; TGF $\beta$ , fibroblast growth factor  $\beta$ ; GCSF, granulocyte colony stimulating factor; GMCSF, granulocyte-macrophage colony-stimulating factor; IL9, interleukin 9; IL13, interleukin 13; TNF $\alpha$ , tumor necrosis factor  $\alpha$ , IL1 $\beta$ , interleukin 1 $\beta$ . Asterisks indicate  $p < 0.05$ . # indicates newly identified efferocytic-induced molecules.

*Efferocytic respiration exerts an increased mitochondrial respiratory capacity that is dependent on MerTK.* In addition to drastic anti-inflammatory reprogramming, we found that efferocytosis also altered metabolic status in macrophages. Seahorse analysis revealed that basal oxygen consumption rate (OCR) was significantly elevated in macrophages that were fed apoptotic cells (**Fig 2-2-1A**). This was in contrast to macrophages co-cultivated with either live cells or inert polystyrene beads (**Fig 2-2-1B**). Remarkably, efferocytes exhibited heightened mitochondrial spare respiratory capacity, consistent with an elevated bioenergetics reserve that was provided by the introduction of exogenous metabolic substrates. Even though we observed an increase in aerobic glycolysis as measured by extracellular acidification rate/ECAR, the ratio of OCR to ECAR was still significantly higher during apoptotic cell engulfment relative to non-efferocytes, consistent with a mitochondrial bias during efferocytosis (**2-2-1A**). Intriguingly, elevated OCR was not measured upon the feeding of necrotic cells (**Fig 2-2-1C**) even though similar levels of engulfment were documented by microscopy (*data not shown*). It has been shown that PtdSer-dependent receptor tyrosine kinases MERTK and AXL are receptors responsible for apoptotic cell clearance and are required for IL-4/IL13 mediated type 2 immune response in macrophages<sup>125,126</sup>. We further sought to test whether apoptotic cells signal to mitochondria through Mertk/Axl. We found that Mertk/axl ligand gas6 rapidly induced OCR in WT peritoneal macrophages (**Fig 2-2-2A**). Interestingly, Mertk activating antibody, instead of Axl activating antibody, increased OCR in WT macrophages (**Fig 2-2-2A, B**). This is further proved by using MerTK vs Axl knockout macrophages that gas6 and activating antibodies can only induce OCR in Axl<sup>-/-</sup> macrophages while not in Mertk<sup>-/-</sup> macrophages (**Fig 2-2-1C**).

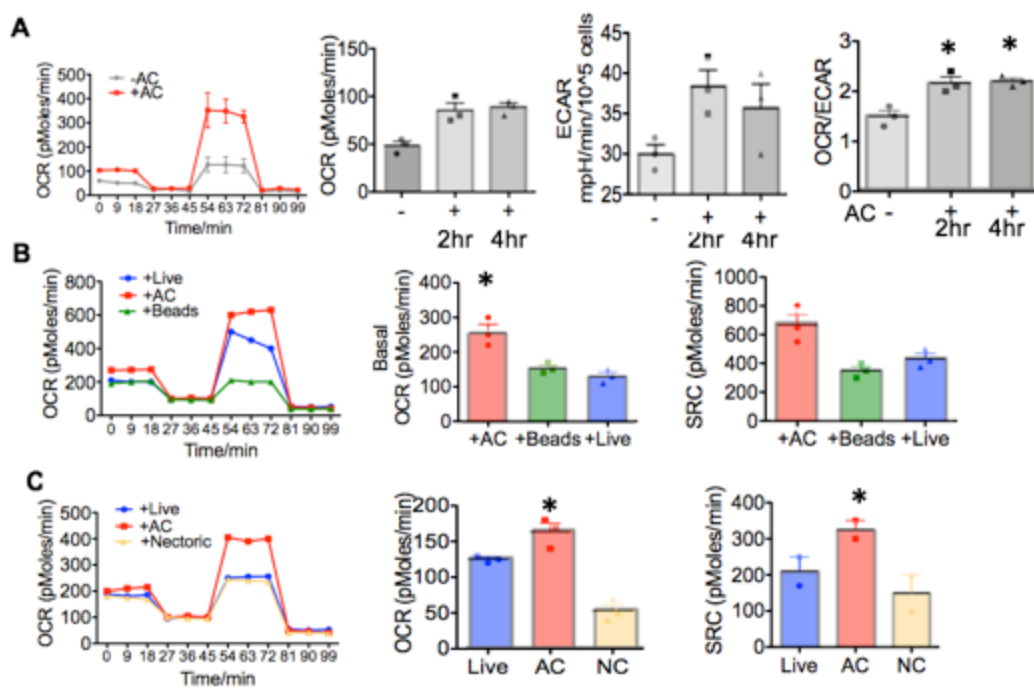


**Figure 2-2-1. Oxygen consumption is specific to the phagocytosis of apoptotic cells (ACs).** (A) Oxygen consumption rate/OCR of primary elicited macrophages +/- indicated treatments. (B) Macrophages were cocultivated with inert beads and or live cells. (C) Macrophages were co-cultivated with necrotic cells (NCs) in comparison to live and ACs.

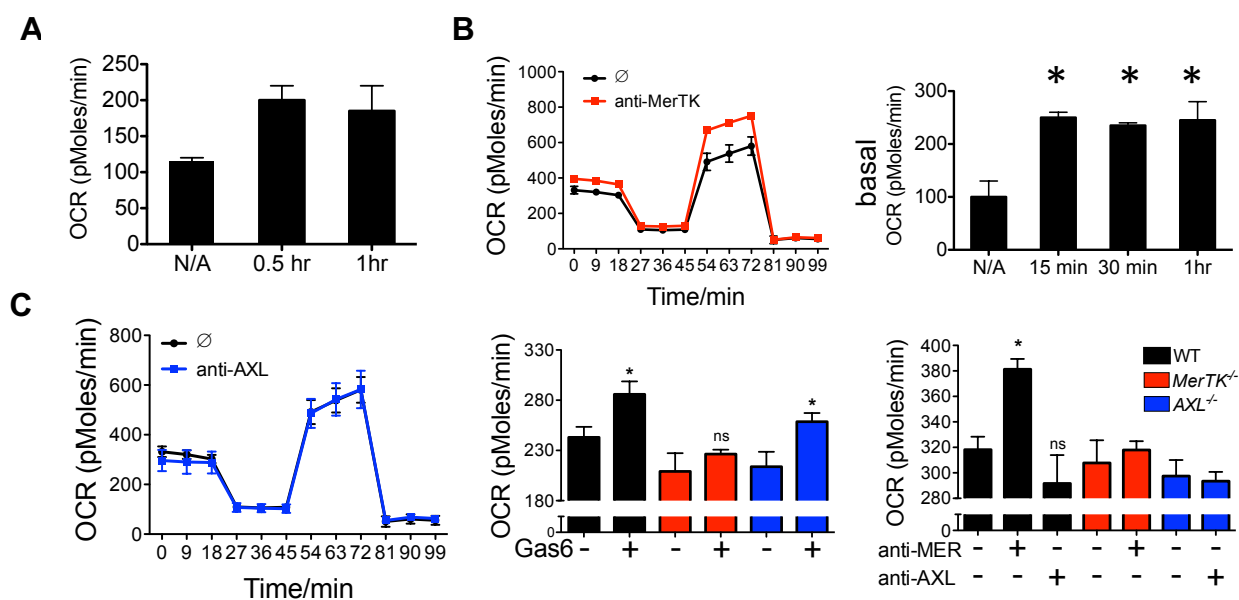


**Figure 2-2-2. Oxygen consumption is MerTK dependent. (A)** OCR was measured after effero at indicated time point. **(B)** OCR was measured after Mertk activation. **(C)** OCR in *Mertk* or *Axl* <sup>-/-</sup> macrophages with either Gas6 or activating antibodies. Both apoptotic cells and gas6 activated mTOR pathway in WT macrophages but not in MerTK macrophages. \*  $p < 0.05$  versus control

Together these results indicate that apoptotic cells reprogram macrophages metabolism towards mitochondrial respiration in a MerTK dependent manner.

*Apoptotic cells introduce extra lipids and induce fatty acid oxidation in macrophages.*

Apoptotic cells contain a rich content of lipids. To determine if apoptotic cell engulfment changes metabolome of macrophages, we performed parallel unbiased liquid chromatography with tandem mass spectrometry. Over 255 total biochemicals were altered with a  $p < 0.05$ , with 181 induced and 74 downregulated (**Table I**). Unbiased analysis of the LC/MS readings identified reproducible global changes in metabolites (**Fig 2-3-1A and Table I**). Metabolite set-enrichment highlighted noteworthy escalations in long chain free fatty acids, as well as fatty acid metabolism (**Fig 2-3-1B**). Random Forest Analysis<sup>127</sup> revealed that lipid metabolites such as 3-hydroxybutyrylcarnitine, behenoylcarnitine, and arachidoylcarnitine etc are top enriched metabolites in macrophages after efferocytosis (**Fig 2-3-3**). We further looked into lipid metabolites that are involved in fatty acid oxidation. Long chain fatty acids hexadecanedioate, myristoylglycerol, and linoleoylcarnitine are increased in efferocytes. More importantly, acetylcarnitine, the fatty acid that is transported from cytosol into mitochondria, is also increased in macrophages that have engulfed apoptotic cells (**Fig 2-3-1C**). Consistent with metabolomics data, we found apoptotic cell stimulation of primary macrophages induced expression of genes involved in fatty acid oxidation, ETC, and OXPHOS pathways (**Fig 2-3-2A**). Importantly, the induction is not due to contamination from apoptotic cell RNAs and requires AC engulfment. Because cocultivation of apoptotic cells with macrophages under 4C doesn't induce FAO or OXPHOS gene signatures (**Fig 2-3-2B**). Gene ontology enrichment analysis of canonical pathways

from our RNAseq data also revealed most significantly mobilized pathways, which interestingly included mitochondrial electron transport (**Fig 2-3-2C**). At first approximation, these parallel analyses of principal cytokine, transcriptional, and metabolic modules revealed an efferocytic signature that coupled anti-inflammatory cytokine production to fatty acid breakdown and mitochondrial metabolism.

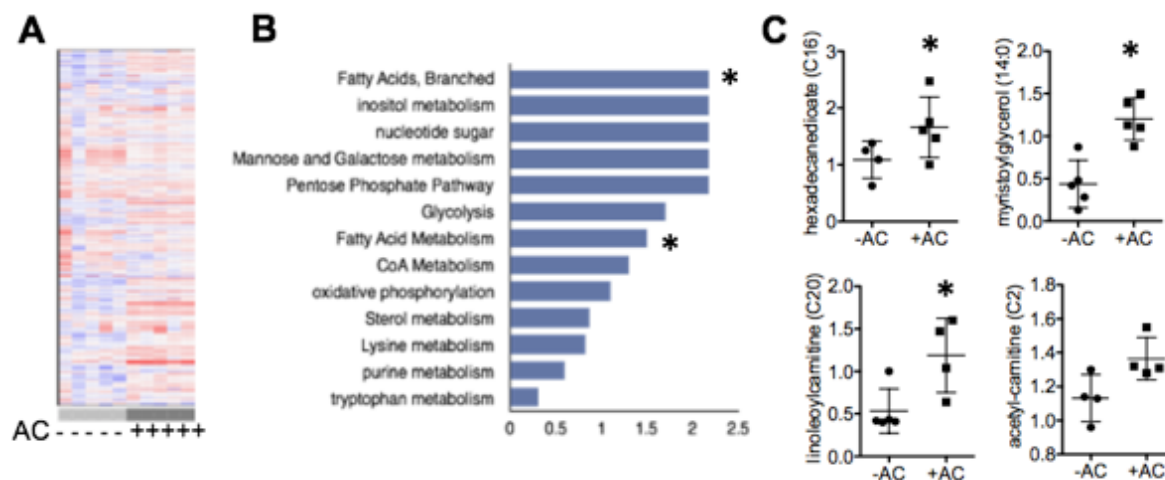


**Figure 2-3-1. The efferocytosis transcriptome and metabolome highlight enhanced fatty acid oxidation.** (A) Gene Ontology enrichment of canonical pathways after efferocytosis. \* highlights top induced pathways. # highlights immune response pathways. (B) qPCR validation of FAO, lipolysis, TCA, and inflammatory genes in macrophage treated with vs without AC. (C) qPCR validation of FAO, lipolysis, TCA, and inflammatory genes in macrophage treated with AC under 4 degree to block AC uptake vs macrophage treated without AC.

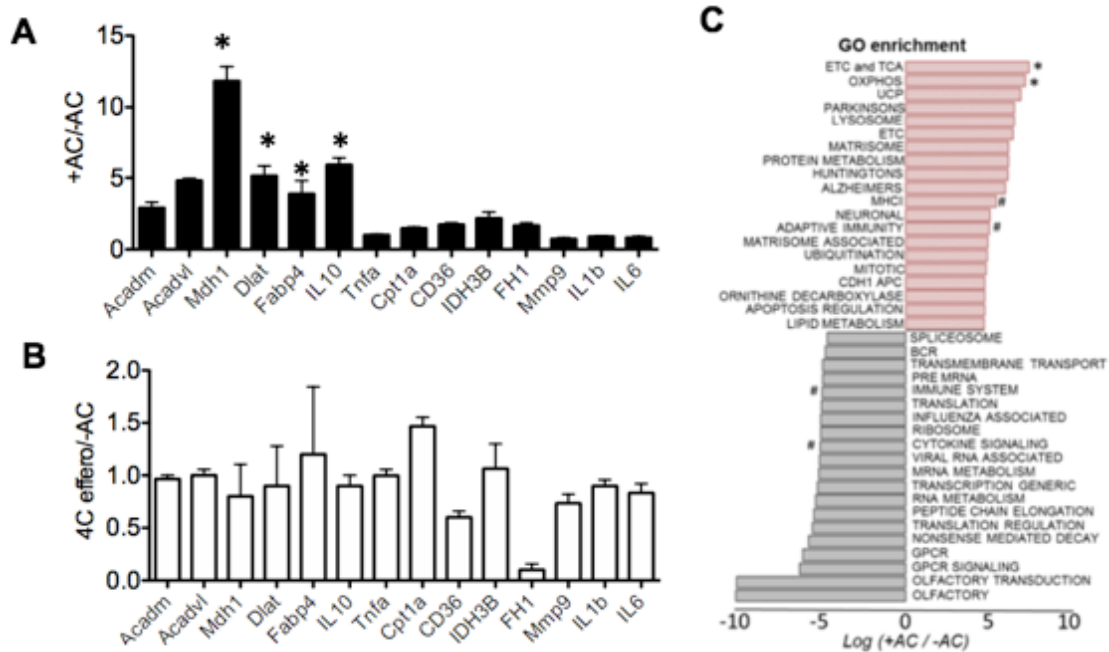


**Figure 2-3-2. The efferocytosis transcriptome and metabolome highlight enhanced fatty acid oxidation. (A)** Metabolite set-enrichment analysis of significantly altered core pathways. **(B)** Selected fatty acid metabolites. **(C)** GO enrichment of selected pathway from RNAseq analysis \* $p < 0.05$

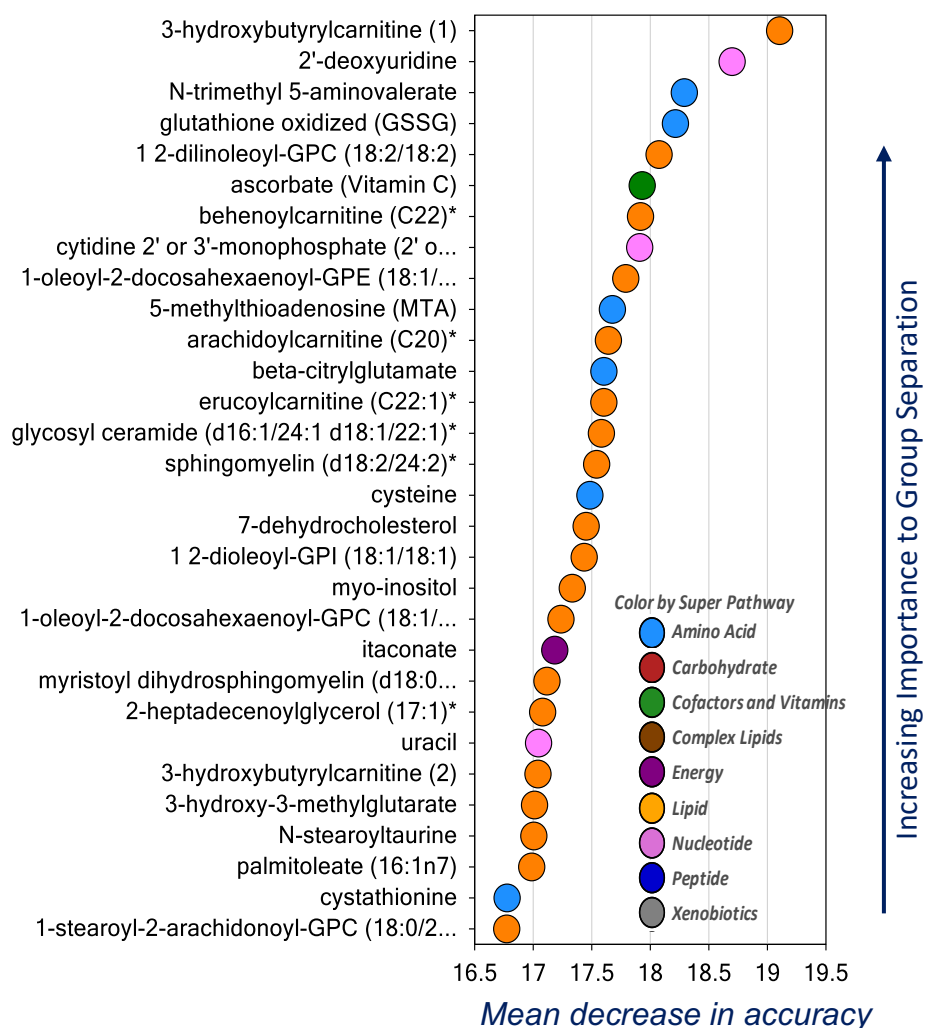


**Figure 2-3-3. Metabolomics of efferocytosis in *Risp-deficient* macrophages.** Biochemical importance plot after non-biased Random Forest Analysis (RFA) for biomarker identification of most significant variables between the following four macrophage groups: (1) *Rispfl/fl* (2) *Rispfl/fl* + AC (3) *Rispfl/fl* + *LysMCre* (4) *Rispfl/fl* + *LysMCre* + AC. Y axis is increasing importance to group separation. Variables with larger mean decrease in accuracy are more important for data classification. Accuracy of prediction determined after identifying the biomarker that changes per specific group. Top hit: 3-hydroxybutyrylcarnitine (ketocarnitine) associated with insulin resistance (PMID 22209095). 2<sup>nd</sup> Top hit: nucleotide (released as find-me signals during efferocytosis); mitochondria regulate nucleotide pools potentially important for DNA/RNA stability.

*Fatty acid oxidation is required for efferocytosis-induced IL-10 generation.* Apoptotic cells contain large amount of fatty acids<sup>128</sup> and we have shown that apoptotic cell stimulation induced fatty acid oxidation in macrophages. We next ask whether IL10 production after efferocytosis is dependent on fatty acid content of engulfed apoptotic cells. We cultivated jurkat cells in media with different fatty acid concentration overnight. Apoptosis was induced as described previously. Apoptotic cells were then co-cultivated with macrophages. We found that apoptotic cells with higher fatty acid content induced more IL10 in macrophages (**Fig 2-4-1A**). To test if fatty acid oxidation is required for anti-inflammatory reprogram of macrophages, we inhibited FAO with etomoxir (ETO), an inhibitor of Cpt1, a key FAO enzyme. We found that ETO reduce OCR in macrophages after efferocytosis (**Fig 2-4-1B,C**). Moreover, ETO inhibited efferocytosis dependent IL10 production without affecting TGF $\beta$  production (**Fig 2-4-1D**). To confirm that off-target effects of ETO did not contribute to this process, we genetically silenced either Cpt1a or Cpt2a expression in macrophages. We found that genetically targeting Cpt1a and Cpt2a also inhibited IL10 production after efferocytosis (**Fig 2-4-1E**). Separately, previous reports elegantly described IL4-induced macrophage polarization that required glucose utilization<sup>110</sup>. Efferocytosis was also distinctly characterized by the inability of glycolysis inhibitors to blunt IL10 production (**Fig 2-4-2A-C**).

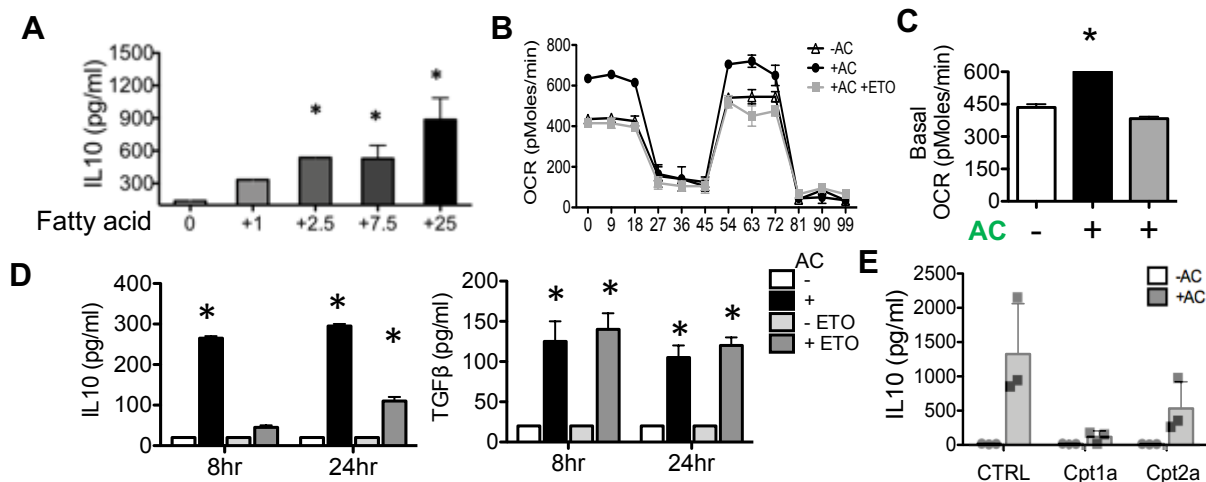


**Figure 2-4-1. Efferocytic IL10 requires fatty acid oxidation/FAO and depends on FA contents from ACs.** (A) IL10 production after treated with ACs cultured in media with different fatty acid content as indicated (ug/L fatty acid per liter of media). (B) seahorse analysis of OCR in ETO treated macrophages. (C) Quantification of basal OCR during efferocytosis with vs without ETO. (D) IL10 and TGFβ production in AC treated macrophages +/- ETO. (E) IL10 production in AC treated cpt1 and cpt2 -/- macrophages.

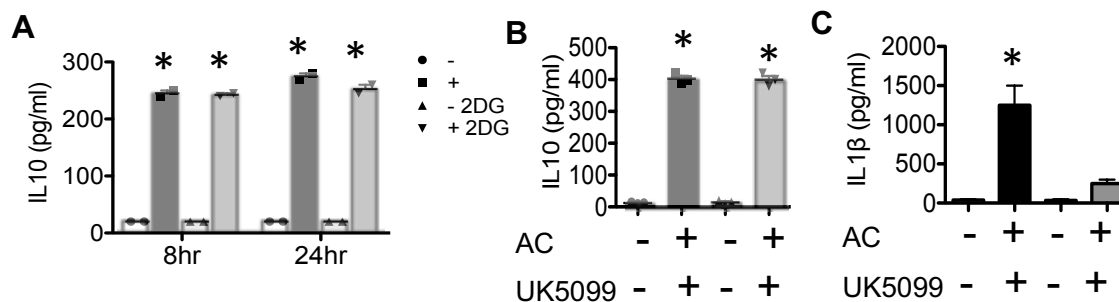


**Figure 2-4-2. Efferocytic IL10 is independent of glycolysis.** (A) IL10 production in AC treated macrophages +/- 2-deoxyglucose/2DG. (B) IL10 production in AC treated macrophages +/- glucose-inhibitor UK5099 and IL1β production in LPS treated macrophages +/- UK5099. (C) IL1β production in AC treated macrophages +/- glucose-inhibitor UK5099 and IL1β production in LPS treated macrophages +/- UK5099. \* p<0.05 versus control.

*Electron transport chain is required for fatty acid induced IL-10 generation during efferocytosis.*

Elevations in oxygen consumption were consistent with heightened mitochondrial electron transport and mitochondrial oxidative phosphorylation. It's been shown that ETC is required for mitochondrial fatty acid oxidation<sup>129,130</sup>. We documented evidence for spatial localization of mitochondria, proximal to phagocytic cups (**Fig 2-5-1**). Electron transport is catalyzed in part by Rieske iron-sulfur protein, or RISP<sup>131</sup>. RISP has been newly implicated in activities beyond electron transport<sup>92</sup>, however such a noncanonical role in macrophages is unclear and of unique significance to inflammation. To test the hypothesis that electron transport contributes to efferocytic anti-inflammatory polarization, we crossed *Rispfl/fl* mice<sup>132</sup> with a macrophage recombinase, *LysMCre*. *Rispfl/fl LysMCre* mice developed and matured to both normal body size and dietary intake and did not present with any significant sign of immuno-compromise. In primary macrophages, immunoblots confirmed reduction of RISP protein (**Fig. 2-5-2A**). RISP is encoded by nuclear gene *ubiquinol-cytochrome c reductase/Uqcrcfs1*, and the failure of RISP to be imported into the mitochondrial inner membrane did not overtly compromise macrophage mitochondrial morphology (**Fig. 2-5-2B**). *Risp-deficient* macrophages also exhibited reduced oxygen consumption at baseline and a compensatory increase in glycolysis as indicated by moderately elevated extracellular acidification (**Fig. 2-5-2C**). Importantly *Risp-deficient* macrophages were proficient at phagocytosis (**Fig. 2-5-2D**). To test if *Risp* was required for anti-inflammatory efferocytic polarization, we measured IL10 production. Supernatants from *Risp-deficient* macrophages exhibited clear reductions in IL10 that were specific to efferocytosis (**Fig. 2-5-3A**). This was not a generalized defect as mutant macrophages were competent at producing pro-inflammatory cytokine TNF $\alpha$  in response to LPS. To address potential off-target

effects during cellular differentiation in germline *Rispfl/fl LysMCre* mice, we reproduced our findings after RNA silencing in mature macrophages (**Fig. 2-5-3B**). We next targeted signaling that was downstream of apoptotic cell binding and added Antimycin A after apoptotic cell engulfment, which inhibits complex III activity<sup>133</sup>. **Fig. 2-5-3C** depicts that Antimycin A also led to IL10 suppression (**Fig. 2-5-3C**). We independently corroborated these findings with a structurally dissimilar complex III inhibitor, myxothiazol (**Fig. 2-5-3D**)<sup>134</sup>. Although ATP in *Risp-deficient* macrophages was acutely reduced during efferocytosis, these levels quickly recovered (**Fig. 2-5-4A, B**). Moreover, efferocytic IL10 was not inhibited by interfering with mitochondrial membrane potential (**Fig. 2-5-4C**). Separately, complex III and RISP are significant sources of mitochondrial reactive oxygen species (mROS)<sup>135</sup>. Efferocytic IL10 was also not blocked with inhibitors of mROS, interestingly in contrast to TGF $\beta$  (**Fig. 2-5-4D**).

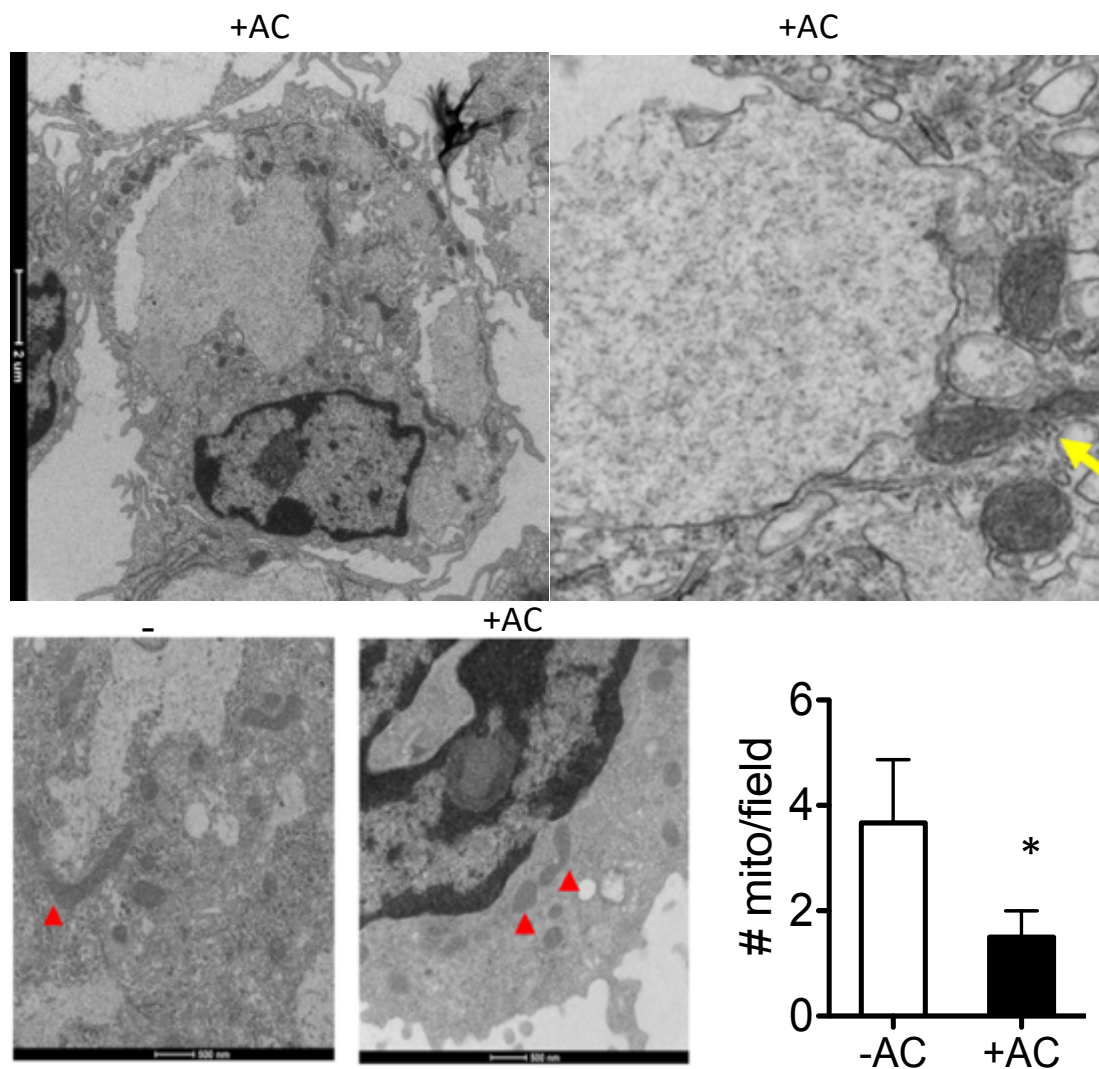


**Fig 2-5-1. Transmission electron micrographs of elicited primary peritoneal macrophages during efferocytosis.** Image depicts macrophage engulfing apoptotic cells. Arrow indicates a focused mitochondrion of the phagocyte. Number of mitochondria per field in macrophages with vs without AC were quantified. \* indicates  $p < 0.05$ .

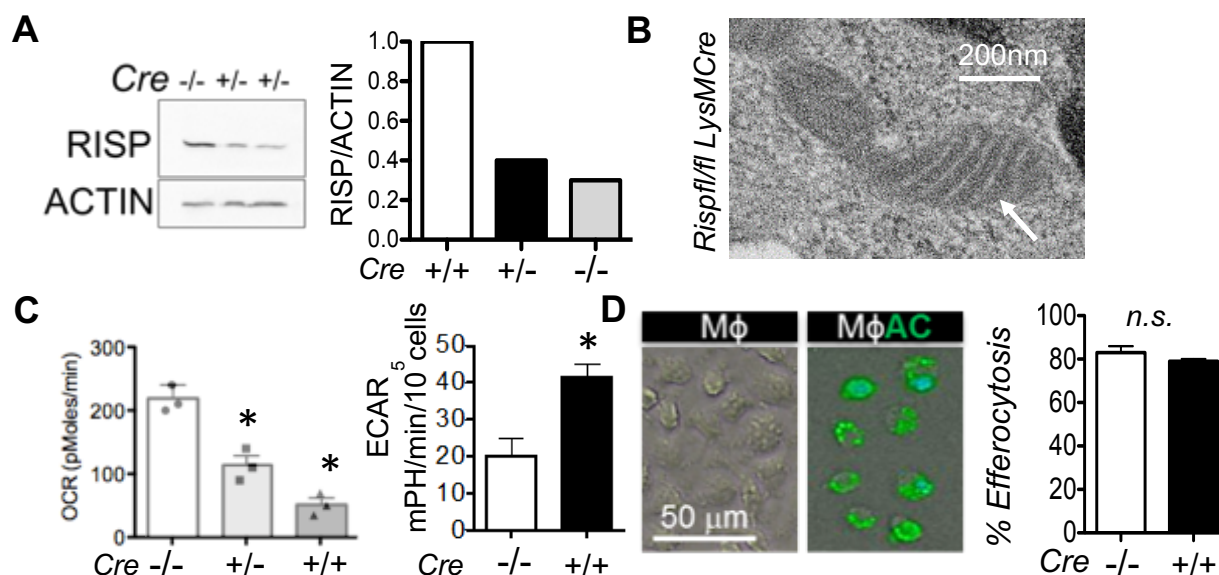


**Fig 2-5-2. Generating electron transport dysfunction macrophage.** Elicited peritoneal macrophages were harvested from *Rispfl/fl* and *Rispfl/fl LysMCre* mice. (A) Macrophage RISP protein was quantified by immunoblot. (B) Transmission electron micrograph of a *Risp*-deficient macrophage. (C) Oxygen consumption rate/OCR and extracellular acidification rate/ECAR profiles of *Risp*-deficient macrophages. (D) Photomicrographs and quantification of efferocytosis. Macrophages remain unlabeled while apoptotic cells (AC) are labelled green. n.s. = not statistically significant.

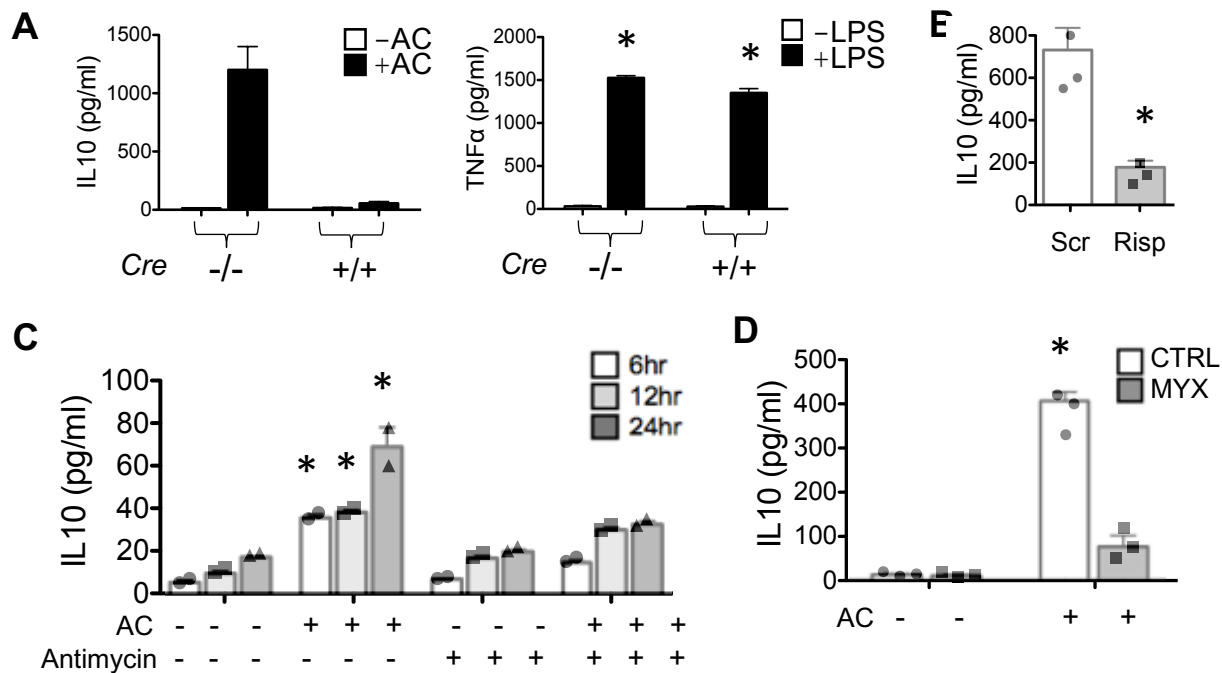


**Fig 2-5-3. Electron transport dysfunction reduces the capacity of efferocytes to produce IL10.** (A) IL10 in cell supernatants 12 hours after efferocytosis. TNFα was measured 6 hours after LPS stimulation. (B) IL10 production was measured in macrophages after *Risp* knockdown with siRNA. (C) Acute inhibitor Antimycin/AntA added at 100nM 1hour post AC feeding. IL10 was measured with ELISA. (D) Myxothiazol inhibitor of electron transfer to RISP was added to efferocytes and IL10 measured by ELISA. \*  $p < 0.05$ .

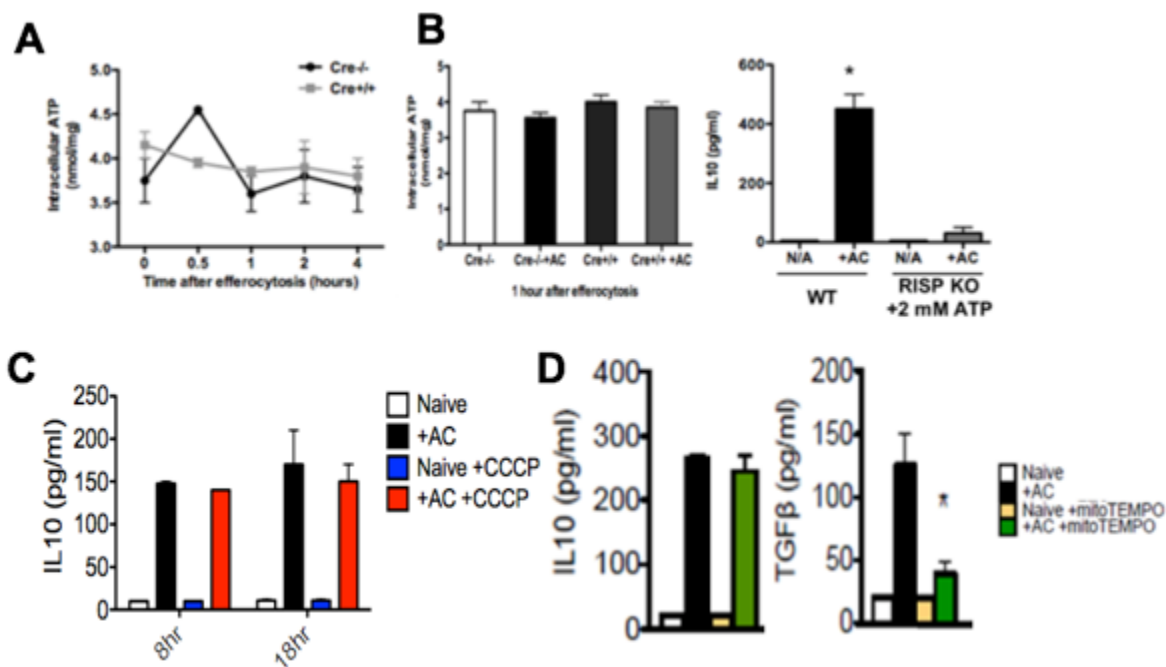


**Fig 2-5-4. ATP kinetics and effects of targeting mitochondrial membrane potential and reactive oxygen species during efferocytosis in Risp-deficient macrophages.** (A) Kinetics of intracellular ATP levels after efferocytosis in *Risp<sup>f1/f1</sup>* macrophages, plus or minus *LysMCre*. (B) Quantification of intracellular ATP in *Risp<sup>f1/f1</sup>* and *Risp<sup>f1/f1</sup> LysMCre* macrophages, plus or minus apoptotic cells (AC) at one-hour post efferocytosis (C) Efferocytosis and IL10 measurement by ELISA +/- carbonyl cyanide *m*-chlorophenyl hydrazine/CCCP to interfere with mitochondrial membrane potential. (D) IL10 and TGFβ was measured by ELISA after treatment of efferocytes with mitochondrial-targeted antioxidant mitoTEMPO/mT. n.s. = not statistically significant. \*  $p < 0.05$ .

*An intact electron transport chain is necessary for increased NAD<sup>+</sup> availability and IL10 production during efferocytosis.* Metabolic rewiring alters the availability of functional metabolites that regulate macrophage function<sup>104</sup>. It has also been shown that both fatty acid oxidation and *Risp* deficiency led to reduced NAD<sup>+</sup>/NADH in cells<sup>92,136,137</sup>. Global analysis of *Risp*-deficiency during efferocytosis revealed reduced nicotinate and nicotinamide metabolism. This included changes in NAD<sup>+</sup> metabolites MNA and adenosine 5'-diphosphoribose (ADP-ribose) (**Fig 2-6-1A**), as well as aspartate, which is dependent on a suitable NAD<sup>+</sup>/NADH ratio within the *Malate-Aspartate Shuttle*. Both global metabolomics and focused pathway analyses corroborated an increased ratio of oxidized coenzyme nicotinamide adenine dinucleotide NAD<sup>+</sup> to NADH in efferocytes, which was further reduced with *Risp*-deficiency (**Fig 2-6-1B**). Thus, aside from its role in metabolic redox reactions, we considered a novel role for NAD<sup>+</sup> during efferocytic anti-inflammatory reprogramming. To test this, we added NAD<sup>+</sup> precursor NMN to *Risp<sup>fl/fl</sup> LysM<sup>Cre</sup>* macrophages during efferocytosis and found that NMN was clearly sufficient to rescue IL10 production (**Fig 2-6-1C**). NAD-dependent IL10 was specific to efferocytosis as NAD<sup>+</sup> supplementation alone, in the absence of apoptotic cell feeding, did not lead to elevated IL10. Elevated NAD<sup>+</sup>/NADH ratios support the activity of sirtuin deacetylases<sup>138</sup>. We found SIRT1 displayed elevated protein levels after efferocytosis (**Fig 2-6-2A**). As predicted from a temporal sequence in which NAD<sup>+</sup> is upstream of SIRT1 protein activity, *Sirt1*-deficient macrophages were refractory to IL10 rescue after supplementation with NAD<sup>+</sup> precursor NMN (**Fig 2-6-2B**). It has been shown that pre-B-cell leukemia transcription factor-1 (Pbx-1) is required for AC-induced IL10 production<sup>139</sup>. We further sought out to test if SIRT1 regulate IL10 production via transcription factor Pbx-1. Chromatin immunoprecipitation (ChIP)-qPCR analysis of Pbx-1 binding was performed in macrophages

treated with scrambled vs sirt1 siRNA. Interestingly, sirt1 deficiency reduced Pbx-1 binding to the apoptotic cell response element on IL10 promoter (**Fig 2-6-2C**). These data support the contention that efferocytic accumulations in NAD<sup>+</sup>, in turn signal through SIRT1/Pbx-1 to induce *IL10* gene expression.

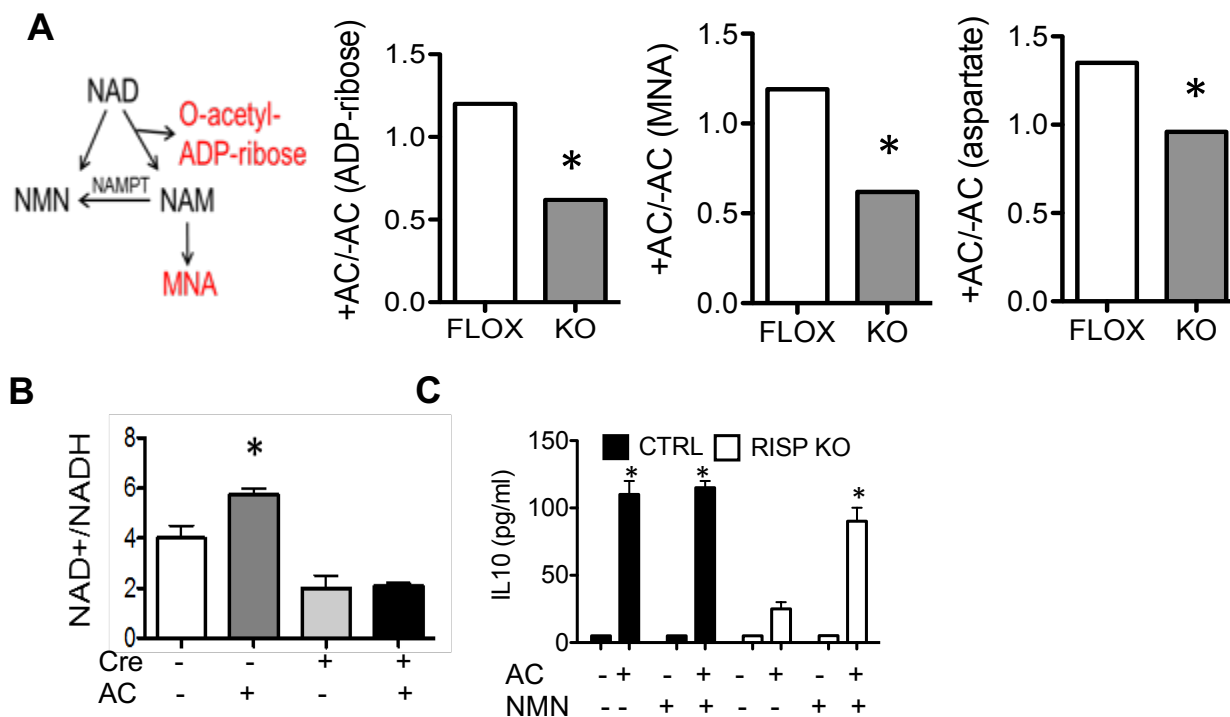


**Fig 2-6-1. NAD<sup>+</sup> is required for efferocytic IL-10 production.** (A) NAD metabolism scheme with a focus on NAD breakdown and buildup of MNA metabolite 1-methylnicotinamide (n-methylnicotinamide). Graphed is the relative levels of indicated metabolites in *Risp-deficient* (KO) versus control (FLOX) efferocytes. (B) *Risp-deficiency* (*LysMCre*) reduces the NAD<sup>+</sup>/NADH ratio in macrophage during efferocytosis of apoptotic cells (ACs). (C) Peritoneal efferocytes were administered NAD<sup>+</sup> precursor NMN and IL10 measured by ELISA.

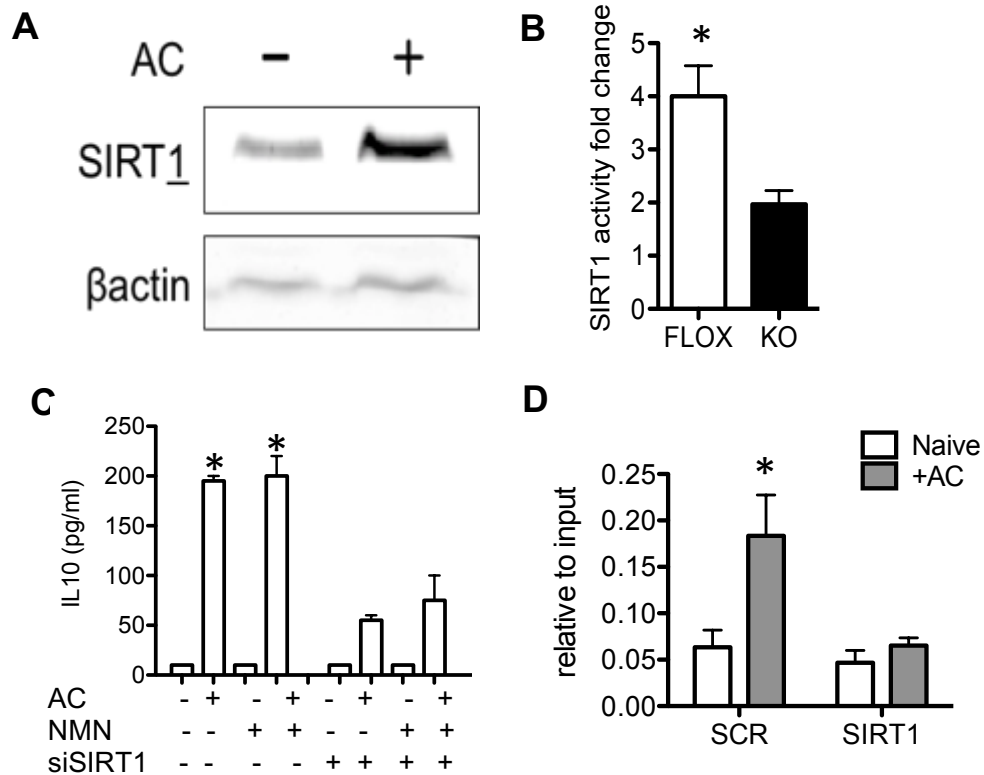


**Fig 2-6-2. Sirt1 is required for efferocytic IL-10 production.** (A) Sirt1 protein level after efferocytosis measured by western blot. (B) sirt1 activity measured in flox vs ko macrophages that are treated with vs without effero. (C) Sirt1 is required for IL10 production after efferocytosis measured in control macrophages vs macrophages treated with sirt1 siRNA. (D) ChIP-qPCR was performed on macrophages treated with scramble vs sirt1 siRNA during efferocytosis. \*  $p < 0.05$  relative to control.

*Macrophage Risp-deficiency impairs IL10-dependent wound healing and inflammation resolution.*

To address the *in vivo* significance of our findings, we examined *Risp*-dependent IL10 in a model of tissue injury requiring efferocytosis<sup>19</sup> and macrophage IL10 polarization<sup>140</sup>, during myocardial infarction/MI. Although MI is ischemic, the repair phase triggers angiogenesis and accumulation of non-hypoxic macrophages that stain low for the hypoxic marker pimonidazole (**Fig 2-7-1A**)<sup>141</sup>. Repair-phase macrophages, isolated directly from the myocardium, were capable of consuming more oxygen relative to other cardiac immune cell monocytes and neutrophils (**Fig 2-7-1B**); this oxygen consumption was lost in cardiac macrophages in the absence of *Risp* (**Fig 2-7-1C**). To isolate myocardial macrophages that were participating in efferocytosis, we induced MI in transgenic mCherry mice that specifically express red cardiomyocytes<sup>142</sup>. Double positive CD64+ (macrophage) mCherry+ efferocytes exhibited heightened *Risp-dependent* expression of genes involved in oxidative phosphorylation (**Fig 2-7-1D**). In macrophage *Risp-deficient* mice, MI also led to acute mortality with more than half of subjects succumbing to death between 4 to 7 days post MI (**Fig 2-7-2A**). Necropsy revealed increased myocardial rupture of the left ventricular free wall and evidence of hemothorax (**Fig 2-7-2B**). Importantly, increases in ventricular rupture were independent of macrophage accumulation, as cardiac flow cytometry revealed similar macrophage levels in the injured myocardium, preceding ventricular rupture (**Fig 2-7-2C**). Within cardiac extracts, IL10 and *TGFβ* mRNA was greatly reduced (**Fig 2-7-2D**). Strikingly, reconstitution of IL10 after MI significantly rescued cardiac rupture to increase organism survival (**Fig 2-7-2E**).

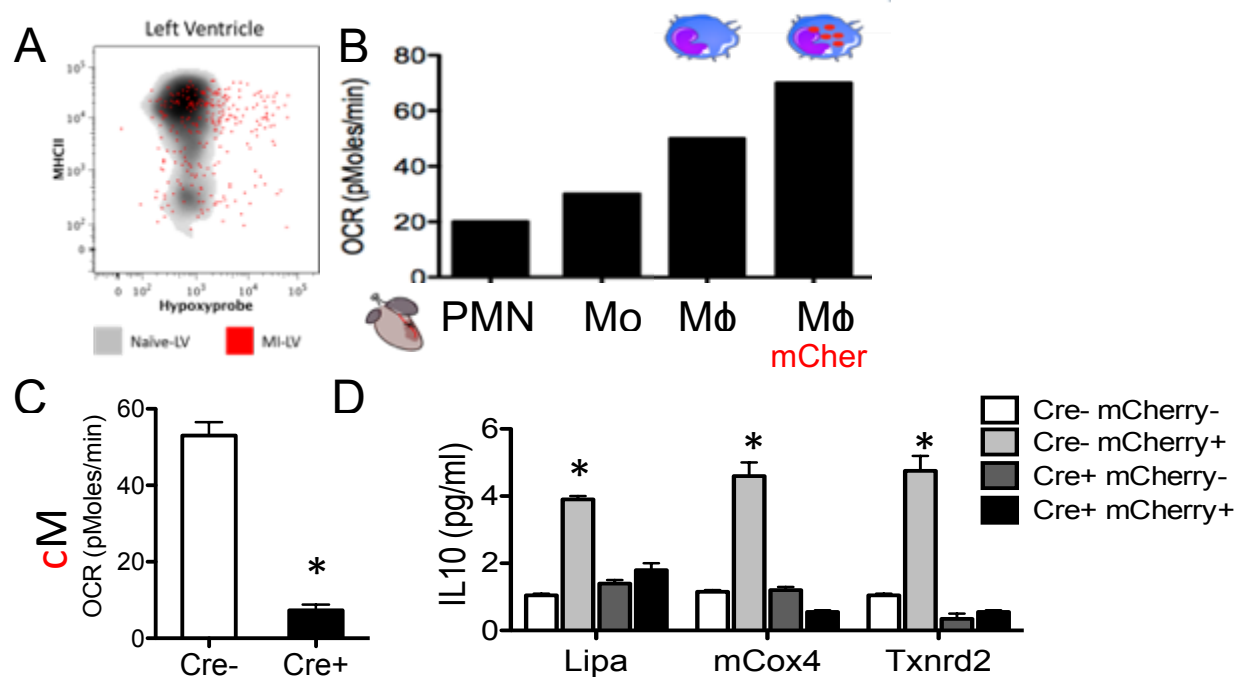


**Fig 2-7-1. . Macrophage mitochondrial dysfunction impairs IL-10-dependent cardiac repair.** *Rispfl/fl* and *Rispfl/fl LysMCre* mice were subjected to experimental myocardial infarction (MI) at the left anterior descending artery, as described in **Materials and Methods**. (A) Cardiac extracts were prepared and flow cytometry employed to isolate left ventricular cardiac macrophages (CD45<sup>+</sup>CD11b<sup>+</sup>F4/80<sup>+</sup>Ly6G<sup>-</sup>CD64) that stained either positive or negative with hypoxia probe pimonidazole. (B) Mice transgenic for cardiac-specific expression of the fluor mCherry, were subjected to MI, and cardiac neutrophils (PMN), monocytes (Mo), macrophages (MF), and macrophages containing mCherry, were interrogated for oxygen consumption rate/OCR. (C) Cardiac macrophages in *Rispfl/fl LysMCre* mice were measured for OCR. (D) Gene expression by qPCR from indicated cell types.

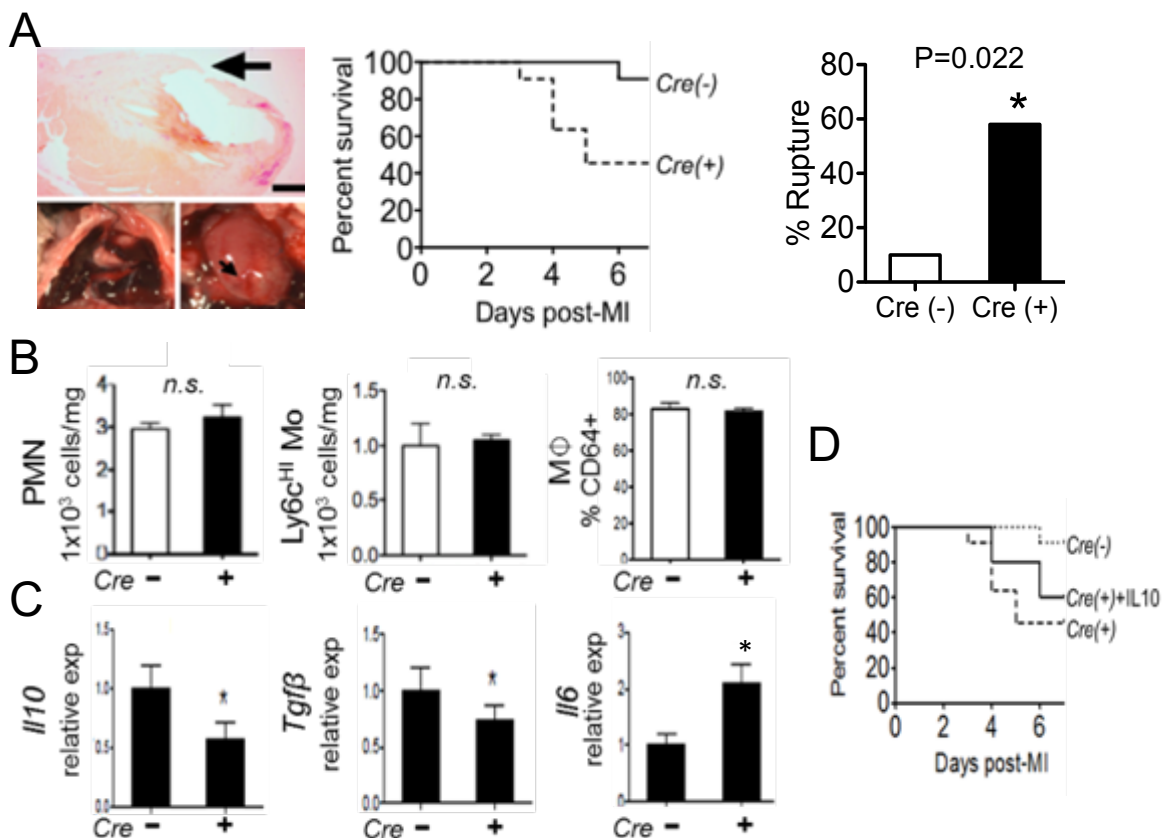


**Fig 2-7-2. . Macrophage mitochondrial dysfunction impairs IL-10-dependent cardiac repair. *Rispfl/fl* and *Rispfl/fl LysMCre* mice were subjected to experimental myocardial infarction (MI) at the left anterior descending artery, as described in Materials and Methods. (A) Kaplan Meier survival plot of indicated mice after MI. (B) Levels of indicated immune cell subsets after MI. (C) Gene expression of indicated inflammatory mediators from cardiac extracts. (D) Survival plots after exogenous IL10 administration.**

## 2.4 Discussion

The clearance of dying cells is a phylogenetically conserved process that has evolved beyond cell engulfment to include the proactive generation of anti-inflammatory cytokines. This integration of immunity with nutrient sensing and nutrient utilization of apoptotic cells makes intuitive sense in the context of efficient energy utilization for increased anabolic demand, and it is perhaps surprising that mitochondrial respiratory connections to the cytokine response of efferocytosis have yet to be clearly documented. This may be in part due to preconceived notions linking metabolism to pure energetic currency. However, these prejudices are waning, as cellular metabolism is now well appreciated to contribute to an array of cell functions beyond biosynthetic demand. Less appreciated are the fundamental mechanisms that explain in what way metabolic intermediates could directly participate in signal transduction that is not linked to cellular bioenergetics. Mitochondria facilitate and dictate varied immunologic functions of innate and adaptive immune cells<sup>143</sup>. Metabolism driven by mitochondrial activity may act as a platform for superoxide-signaling<sup>135</sup> or for the generation of metabolites that control the epigenetic landscape<sup>104</sup>. The unique aspect of apoptotic cell catabolism is the potential of metabolic substrates, derived from the apoptotic cell itself, to directly influence macrophage polarization. It has been shown that upon IL4 stimulation, macrophages use lipids stored in lipid droplet to fuel mitochondrial metabolism<sup>96</sup>. Interestingly, here we showed that apoptotic cells can serve as an extracellular source of fatty acids and anti-inflammatory reprogramming of efferocytes depends on fatty acid content of engulfed apoptotic cells. In this scenario, cellular imbalances of

lipids and proteins during disease could in principle significantly compromise the integrated metabolic response of macrophages to promote tissue repair.

Macrophage receptors have long been simply seen as extracellular stimuli sensors. Upon stimulation, toll like receptors or TAM receptors such MERTK and AXL simply induce signaling pathways that lead to cytokine production<sup>125,144,145</sup>. However, nothing known about capacities of talking to mitochondria thus modulating cellular metabolism. Febbraio group recently reported that TLR4 is not a fatty acid receptor but mediates lipid-induced inflammation by reprogramming macrophage metabolism<sup>146</sup>. Interestingly, here we also showed that MERTK, upon AC stimulation, signal to mitochondria to induce oxygen consumption and fatty acid oxidation. We hypothesize that TAM receptor on macrophages can also as cellular metabolism regulator that primes macrophage to be metabolically ready for immune responses.

During the early stages of inflammation, acute phase monocytes and differentiated macrophages are highly glycolytic, particularly under limiting oxygen tensions. Glycolytic remodeling is both important for inflammatory macrophage polarization, as well as other phases of inflammation<sup>101</sup>. For example, macrophages that are in contact with *Th2*-derived cytokines such as IL4, utilize glucose for alternative macrophage polarization<sup>110</sup>. This is particularly relevant to immunity against allergic and parasitic reactions. In our hands, the generation of anti-inflammatory IL10 was not blocked by inhibitors of glycolysis, although extracellular acidification did trend higher during efferocytosis. One likely explanation is the abundant substrate supply provided by the apoptotic cell, which could preclude any need to mobilize metabolite pools that are pre-stored

in the phagocyte. Interestingly, a recent report has uncovered that recognition of apoptotic cells and IL4 can work together to specifically program macrophages for tissue repair<sup>126</sup>. It will be informative in this aspect to examine the metabolome of macrophages simultaneously exposed to apoptotic cells and IL4. Relative to modest effects on glycolysis, oxygen consumption rate was significantly elevated during apoptotic cell metabolism. This phenotype was interestingly specific to apoptotic cells, as necrotic cells did not trigger macrophages to consume more oxygen. We speculate that damage associated molecular patterns released from necrotic cells, activate toll like receptors to rewire the metabolic bias. Elevated oxygen consumption, in conjunction with requirements for SIRT1, also hint that increased mitochondrial biogenesis could be part of the response.

Changes in macrophage metabolites during efferocytosis were both intuitive and less self-evident. Consistent with increased lipid metabolism, efferocytosis led to accumulations of the monoacylglycerol 1-palmitoleoyl glycerol. Monoacylglycerols may be formed by the action of lipases during the breakdown of triglycerides or diglycerides<sup>147</sup>. Efferocytes also accumulated dephosphocoenzyme A, which is the direct precursor of coenzyme A and notable for its role in the initiation of the citric acid cycle. In line with increased gene expression of TCA enzymes, TCA metabolites pyruvate, citrate, and  $\alpha$  ketoglutarate were reduced after apoptotic cell engulfment. Other metabolite escalations had connotations for inflammation. Efferocytosis induced itaconate, which can inhibit the accumulation of proinflammatory succinate during endotoxin challenge<sup>106</sup>. Levels of succinate trended lower in efferocytes (*Table I*) but were not statistically different. An important note is that efferocytosis may also suppress the macrophage response to

lipopolysaccharide/LPS<sup>46</sup>. It remains to be determined if metabolites generated during efferocytosis in turn contribute to this dampening of LPS-induced macrophage activation. These aforementioned changes clearly represent just a snapshot of the dynamic flux occurring during the metabolism of apoptotic cells. Our global analysis provided and provides a foundation from which to test other specific metabolic pathways, one of which was emphasized as follows. This was the efferocytic induction of nicotinamide adenine dinucleotide (NAD<sup>+</sup>), which was required for generation of the key immune modulator IL10.

In the absence of mitochondrial dysfunction, electron transport recycles mitochondrial NADH to NAD<sup>+</sup>. This occurs alongside a secondary oxidation of cytosolic NADH alongside mitochondrial shuttles that transport reducing agents across mitochondrial membranes<sup>148</sup>. Thus, mitochondrial NAD<sup>+</sup> is coupled to NAD<sup>+</sup>/NADH balance in the cytosol. In macrophages, the synthesis of NAD<sup>+</sup> by nicotinamide phosphoribosyl-transferase (NAMPT) promotes cytoskeletal activation during cellular adhesion<sup>149</sup>. NAD<sup>+</sup> accumulation in efferocytes required *Risp*, and additional reductions in nicotinate and nicotinamide are consistent with efferocytic regulation of the NAD<sup>+</sup> pool. Decreases in NAD<sup>+</sup>/NADH ratio can also lead to increased 2-hydroxyglutarate (2-HG) and this imbalance can impair hematopoietic stem cell differentiation<sup>92</sup>. 2-HG, as well as alpha-ketoglutarate, are further linked to altered epigenetic methylation on key immunoregulatory genes<sup>150</sup>. Though our data did not reveal *Risp-dependent* changes in 2-HG in the setting of efferocytosis, this does not discount the possibility that other mitochondrial-dependent epigenetic alterations may be functioning.

*The mechanism of IL10 induction by NAD<sup>+</sup> is through SIRT1s.* The integration of NAD<sup>+</sup> with sirtuin histone deacetylases <sup>138</sup> supports the concept of gene regulation by metabolic signaling. The seven sirtuin isoforms differ in both subcellular localization and function, and SIRT3, SIRT4, and SIRT5 localize to mitochondria <sup>151</sup>. Our implication of SIRT-1 to efferocytosis is novel. Given that SIRT1 is cytosolic in its localization, this suggests that alterations in the mitochondrial pool of NAD<sup>+</sup>, during efferocytosis, also affect the cytosolic pool. In skeletal cells, SIRT1 controls the transcription of peroxisome proliferator-activated receptor-gamma Co-activator-1 $\alpha$  (PGC-1 $\alpha$ ) <sup>152</sup>, which separately has been linked to IL10 induction <sup>153</sup>. PGC-1 $\alpha$  may also be directly and reversibly acetylated <sup>154</sup> and the early kinetics of efferocytic *IL10* gene expression is consistent with such a post-translational modification. Interestingly, PGC-1 $\beta$  and oxidative metabolism attenuate inflammation by macrophages <sup>155</sup>, however PGC isoforms have overlapping and unique functions. Current studies are underway to identify potential PGC-1 $\alpha$  transcriptional partners that depend on electron transport.

Our findings in heart support the physiologic relevance of our cellular working model (**Fig 2-8**). Within the myocardium, efferocytosis is required to preserve ventricular systolic function after myocardial infarction/MI <sup>19</sup>. Similarly, impairment of macrophage scavenger receptors increases risk of cardiac rupture <sup>156</sup>. Although MI creates an acutely ischemic microenvironment that dampens oxidative respiration, the resolving phase of inflammation accumulates non-hypoxic macrophages, some of which may generate IL10 in the myocardium. *Risp-dependent* reductions in cardiac IL10 were significant given the sufficiency of exogenous IL10 to rescue cardiac rupture. IL10 is a key protective factor in heart <sup>157</sup> and its secretion is necessary for wound closure through

activation of epithelial proliferation<sup>158</sup>. Importantly, exogenous IL10 did not completely protect from cardiac rupture suggesting additional respiratory-dependent pathways. Indeed, *Risp* was required for efferocytic TGF $\beta$ , which contributes to early replacement fibrosis. A caveat to our findings in heart is that *LysMCre* may be expressed in certain non-macrophage cells such as the neutrophil. Neutrophil lipolysis and fatty acid oxidation were recently linked to cellular autophagy, differentiation, and inflammation<sup>159</sup>. In our hands, *LysMCre* deletion of *Risp* did not alter cardiac neutrophil accumulation, nor were autophagy genes significantly altered in macrophages (*data not shown*).

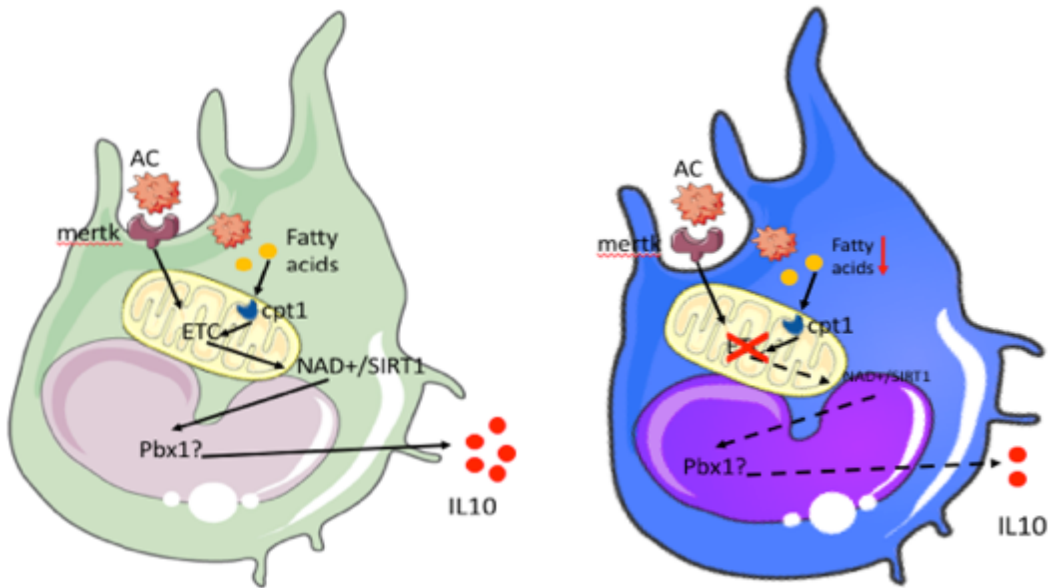


**Fig 2-8 Working model of efferocytic reprogramming through the mitochondrial electron transport chain.** Depicted in schematic is a working model from the experimental data. Shown are macrophages (Mφs), during the process of apoptotic cell (AC) metabolism, and effects on wound healing. Fatty acids from apoptotic cells feed into electron transport I and III complexes as depicted. NAD<sup>+</sup> is nicotinamide adenine dinucleotide. SIRT1 is Sirtuin1. IL10 is interleukin 10. TGFβ is transforming growth factor beta. mROS is mitochondrial reactive oxygen species. See text for details

Additional aspects of our working model warrant future study. For example, potential signaling axes between apoptotic cell receptors and the mitochondria remain to be fully elucidated. In this context, non-metabolite priming of mitochondrial enzymes by receptor-mediated signal transduction could cooperatively amplify the mitochondrial response during efferocytosis. Indeed, cross talk between the apoptotic cell receptor MERTK and mitochondrial regulator mammalian target of rapamycin (mTOR) has been previously reported <sup>160</sup>. In addition, the electron transport chain may function during other core macrophage functions. This includes phagocyte recruitment, phagocyte proliferation and survival, or antigen presentation. Although *Risp*-deficient hearts did not show evidence of reduced macrophage accumulation after cardiac injury, the effects of mitochondrial signaling during tissue repair in other organs remains to be fully explored. In the setting of disease, it will be important to elucidate just how varied metabolite composition contributes to macrophage function and NAD<sup>+</sup> generation, such as during cardiometabolic pathophysiology. For example, atherosclerotic progression is characterized by the turnover and pro-inflammatory phagocytosis of cholesterol-laden foam cells and cholesterol-crystals <sup>161</sup>. Carbon tracing during metabolite flux from apoptotic foam cells to phagocyte has the potential to implicate additional unique immunometabolic cues that may fuel these nonresolving inflammatory disorders. These molecular pathways may also be relevant to pathologies where natural somatic mitochondrial mutations contribute to mitochondrial dysfunction.

### **3 CHAPTER 2- Cardiomyocytes induce macrophage receptor shedding to suppress phagocytosis**

### 3.1 Introduction

Following cardiac stress or myocardial infarction, the innate immune response, comprised of cells including neutrophils and monocytes/macrophages, are mobilized to<sup>4,15</sup> or within<sup>22</sup> the infarcted myocardium to clear necrotic and apoptotic cardiomyocytes (CMs)<sup>57</sup> and promote wound repair<sup>162,163</sup>. Inefficient clearance of dying CMs has been associated with suboptimal tissue remodeling after heart attack<sup>34</sup>.

Phagocytic recognition of dying cells is a multi-step process<sup>58</sup> that requires chemotactic-recruitment<sup>164</sup> of phagocytes, receptor-mediated binding of target-cell to phagocyte at a phagocytic synapse, and internalization and metabolism of dying cells<sup>46,165-167</sup>. Whereas efficient and rapid phagocytosis of apoptotic cells (efferocytosis) activates pro-resolving/anti-inflammatory pathways in the phagocyte<sup>32</sup>, defective or delayed efferocytosis leads to secondary post-apoptotic necrosis and expansion of tissue necrosis<sup>29</sup>. Although the mechanisms of efferocytosis of dying cells in general have been extensively studied, in contrast, the cell biology of CM clearance has escaped detailed examination.

Our recent findings in a mouse model of myocardial infarction are consistent with the concept that phagocytic clearance of dying CMs is a significant causal factor in the mitigation of cardiac necrosis and heart failure<sup>19</sup>. Other studies have examined myocyte phagocytosis in skeletal muscle or in neonates in the context of autoimmunity<sup>168</sup>, however, macrophage-mediated phagocytosis of adult-differentiated-CMs remains uncharacterized. In this context, the following studies were undertaken to model *in vivo* cardiac inflammation and elucidate rate limiting and ultimately therapeutically targetable, molecular steps during the recognition and removal of dying CMs by macrophages.

### 3.2 Material and methods

Chemical reagents were from *Sigma Chemical Co.* (St. Louis, MO) unless stated otherwise. Tissue culture dishes were from *Corning*, and fetal bovine serum (FBS) was from *GIBCO*. *Antibodies*: MERTK polyclonal antibody was from *R&D*. Anti-CD68 for IHC was obtained from *Abcam* (ab125212). Anti-actinin and monoclonal mouse anti-Desmin (clone DE-U-10) from mouse ascities fluid was from *Sigma*(D1033).

Primers for semi-quantitative and real-time PCR in this study

*Mertk*: F (forward oligonucleotide): GTG GCA GTG AAG ACC ATG AAG TTG, R (reverse oligo: GAA CTC CGG GAT AGG GAG TCA T. *Ccl2 (MCP1)*: F: CCT GGA TCG GAA CCA AAT GA, R: ACC TTA GGG CAG ATG CAG TTT TA. *Tnf- $\alpha$* : F: CGG AGT CCG GGC AGG T, R: GCT GGG TAG AGA ATG GAT GAA CA. *Il-6*: F: GAG GAT ACC ACT CCC AAC AGA CC, R: AAG TGC ATC ATC GTT GTT CATAACA, *Il-10*: F: GCC AAG CCT TAT CGG AAA TG, R: GGG AAT TCA AAT GCT CCT TGA T. *Gapdh*: F: GGT GGC AGA GGC CTT TG, R: TGC CCA TTT AGC ATC TCC TT. The *Mertk* primers have previously been described<sup>169,170</sup>.

#### *Animals*

WT and *Mertk*<sup>-/-</sup> littermate controls were used in this study after *Mertk*<sup>+/-</sup> heterozygous mating. Unless otherwise stated, mice were male and 8-12 weeks of age; *Mertk* dependency for cardiomyocyte phagocytosis was also found in female mice. *Mertk* mice were backcrossed 10x to a C57BL/6 background. Mice initially described as *Mertk*<sup>KD</sup> are referred to herein as *Mertk*<sup>-/-</sup>

<sup>171</sup>. B6;D2-Tg(Myh6\*-mCherry)2Mik/J mice were from Jackson. Mice were housed in temperature- and humidity-controlled environments (20 +/- 2°C and 55 +/- 10% relative humidity) and kept on a 12:12 hour day-night cycle with access to standard mouse chow and water *ad libitum*. All studies were approved and reviewed by the Institutional Animal Care and Use Committee (IACUC) at Northwestern University, Chicago, IL.

### *Histology*

Human hearts were obtained from Northwestern University Department of Pathology and Universiteit Antwerpen in Belgium. See **Supplementary Table 1** for patient profiles. **Supplementary Figure 3** describes human analysis and as follows: Analysis of human samples was from patients >50years old. A total of 19 human hearts with evidence of inflammatory necrosis were examined. Within each heart, two regions of interest were measured: One inflammatory necrotic ROI and one remote ROI (Supplemental Figure). For each ROI, a minimum of 100 non-myocyte nuclei were assayed for MERTK expression to ascertain % MERTK positive cells. Under the protocol approved by the institutional review board at Northwestern University, #STU00079445, archived formalin fixed paraffin embedded cardiac autopsy samples were obtained through the Department of Pathology. Murine hearts were infused and fixed with 10% phosphate-buffered formalin at physiological pressures. Hearts were cut transversely, parallel to the atrioventricular groove/coronary sulcus. Fixed hearts were embedded in paraffin at the Northwestern University Mouse Histology and Phenotyping Laboratory (MHPL). Blocks were serially cut 6 µm apart. Alternating sections were stained with hematoxylin and eosin. For frozen sections for immunohistochemistry, samples were rinsed and incubated overnight in 7%

sucrose and frozen in freezing medium and examined at 4 days post MI unless otherwise indicated. Transverse cryosections were cut at a thickness of 10  $\mu\text{m}$  on a Leica cryostat and placed on super frost plus-coated slides.

#### *Laser Capture Microdissection (LCM), RT-QPCR, and qPCR*

RNA from myocardial sections was captured by LCM using a Zeiss P.A.L.M. laser microdissection system as previously described by authors herein<sup>172</sup>. Total RNA was isolated using the RNAqueous-Micro kit from *Ambion* and reverse-transcribed into cDNA using *SuperScript III First-Strand Synthesis Mix (Invitrogen)*. For semi-quantitative and Quantitative RT-PCR: Hearts were snap-frozen for RNA. Total RNA was extracted using the RNeasy kit (*Qiagen*). cDNA was synthesized from 4  $\mu\text{g}$  of total RNA using oligo (dT) and Superscript II (*Invitrogen*). cDNA was subjected to quantitative RT-PCR amplification using a SYBR Green PCR Master Mix (*Applied Biosystems*).

#### *In vivo efferocytosis assays with cardiac mCherry reporter mice*

For *in vivo* assays, myocardial infarction was induced in 8-12 week old mice as previously described and after ligating the left anterior descending artery<sup>19</sup>. Transgenic Myh6-driven mCherry mice were subjected to aforementioned surgery and flow cytometry of myocardial extract was performed 4 days post MI to identify CD64, mCherry double positive cells. Cells were trypsinized to dissociate cell-cell interactions and reveal only internalized mCherry signal.

Ex vivo efferocytosis and co-cultivations of primary adult cardiomyocytes (CMs) and macrophages

Adult mouse CMs and cardiac fibroblasts from 10-week-old mice were isolated using a modified *Langendorff* apparatus as previously described<sup>173</sup>. Briefly, hearts were cannulated via the aorta, perfused and ventricular cells were digested in a spinner flask with Collagenase II for 10 minutes. Heart cells were pre-plated on tissue-culture treated dishes for 1hr and non-adherent cells, i.e., CMs, were used for engulfment assays. Bone marrow cells were cultured in DMEM medium with 10% fetal bovine serum, 1% penicillin-streptomycin and 20% L929 cell-conditioned media for 10 days.  $2.5 \times 10^5$  bone marrow macrophages were stained with Calcein AM or as described in quadruplicate in 24 well plates and overlaid with  $0.5 \times 10^5$  R18-labeled apoptotic or non-apoptotic primary, H9C2, or AC16 CMs. For the induction of apoptosis, CMs were UV-treated for 7mins and cells were incubated at 37°C for 2 h and 4h respectively. After incubation, the phagocytes were co-cultured with the CMs at 37°C for 30 and 60 minutes, and then washed thoroughly with PBS to remove non-engulfed cells. Cells were fixed in 2% PFA and percent phagocytosis was calculated as the number of R18, Calcein AM positive macrophages divided by the total number of Calcein AM positive macrophages.

### *Imaging*

Time lapse video microscopy, confocal microscopy, and electron microscopy. Time lapse and confocal microscopy was performed on a Zeiss microscope. For EM, Epoxy resin was partially corroded by etching the sections for 10 seconds in saturated sodium ethoxide diluted to 50% with absolute ethanol. After rehydration and washing in distilled water, antigen retrieval was

carried out by heating the sections for 10 min to 95°C and then cooling them to 21°C at a rate of 0.04°C/sec in a thermocycler UNO-Thermoblock (Biometra; Göttingen, Germany). After washing in three changes of PBS, nonspecific protein binding was blocked by incubation with 5% albumin in saline for 30 min at room temperature. Incubation with the various primary antibodies was carried out overnight at 4°C. After application of the 10-nm gold-labeled secondary antibody for 60 minutes at room temperature at a concentration of 0.8 µg/ml and subsequent washing in saline, the immunoreaction was stabilized with 2.5% glutaraldehyde in PBS for 10 min<sup>174</sup>. The sections were counterstained with uranyl acetate and lead citrate and examined in an electron microscope (Zeiss EM 10 CR) at an acceleration voltage of 80 kV.

#### *Protein analysis*

Myocardial extracts of ventricular tissue were homogenized in 10 mM HEPES pH 7.4, 320 mM sucrose, 3 mM MgCl<sub>2</sub>, 25 mM Na<sub>2</sub>P<sub>4</sub>O<sub>2</sub>, 1mM DTT, 5mM EGTA, 20mM NaF, and 2mM Na<sub>3</sub>VO<sub>4</sub> with protease inhibitor cocktail. Protein extracts were subjected to SDS-PAGE. Anti-MERTK antibody and anti-cleaved CASPASE-3 antibodies were used for immuno-detection. For detection of soluble-MER: aliquots of cardiac extract were treated with 10 U of protein N-glycosidase F (PNGase F) from New England Biolabs for 1 hour at 37°C.

#### *Statistical Analysis*

Results are presented as means +/- SEM. Differences between multiple groups were compared by analysis of variance (1- or 2-way ANOVA and Bonferroni post-test), and differences between

2 groups were compared by paired or unpaired Student *t* test. A *p* value of < 0.05 was considered to be significant. Stated “n” values are biological replicates.

### 3.3 Results

#### 3.3.1 MERTK<sup>+</sup> mononuclear cells juxtapose damaged cardiomyocytes (CMs) in human myocardium

A previous study from our group<sup>19</sup> tested the causal significance of macrophage-mediated phagocytosis to cardiac repair by experimentally inducing myocardial infarction in the absence of the specific macrophage cell-surface marker (Gautier, Shay et al. 2012) and apoptotic cell receptor MER tyrosine kinase (MERTK)<sup>175</sup>. To test the human significance of our findings, we obtained human hearts post autopsy and compared MERTK expression in mouse hearts versus human. **Figure 3-1** shows the expected accumulation of hematoxylin positive mononuclear (**Fig 3-1A**), CD68 and MERTK immuno-positive cells closely juxtaposed to eosinophilic and Desmin and Actinin positive CMs, and were further elevated (**Fig 3-1B**) in necrotic murine myocardial areas. Similar to mouse, human cardiac autopsy sections (**Fig 3-1C**) revealed increased MERTK immuno-positive mononuclear cells proximal to human CMs (**Fig 3-1D and Fig 3-2**). Although no differences in MERTK expression were found between immune cells of healthy hearts and the remote areas of infarcted hearts, increased MERTK<sup>+</sup> cells were measured in areas of inflammatory/necrotic myocardium (**Fig 3-1E**), consistent with a direct role for MERTK during CM interactions in human heart.

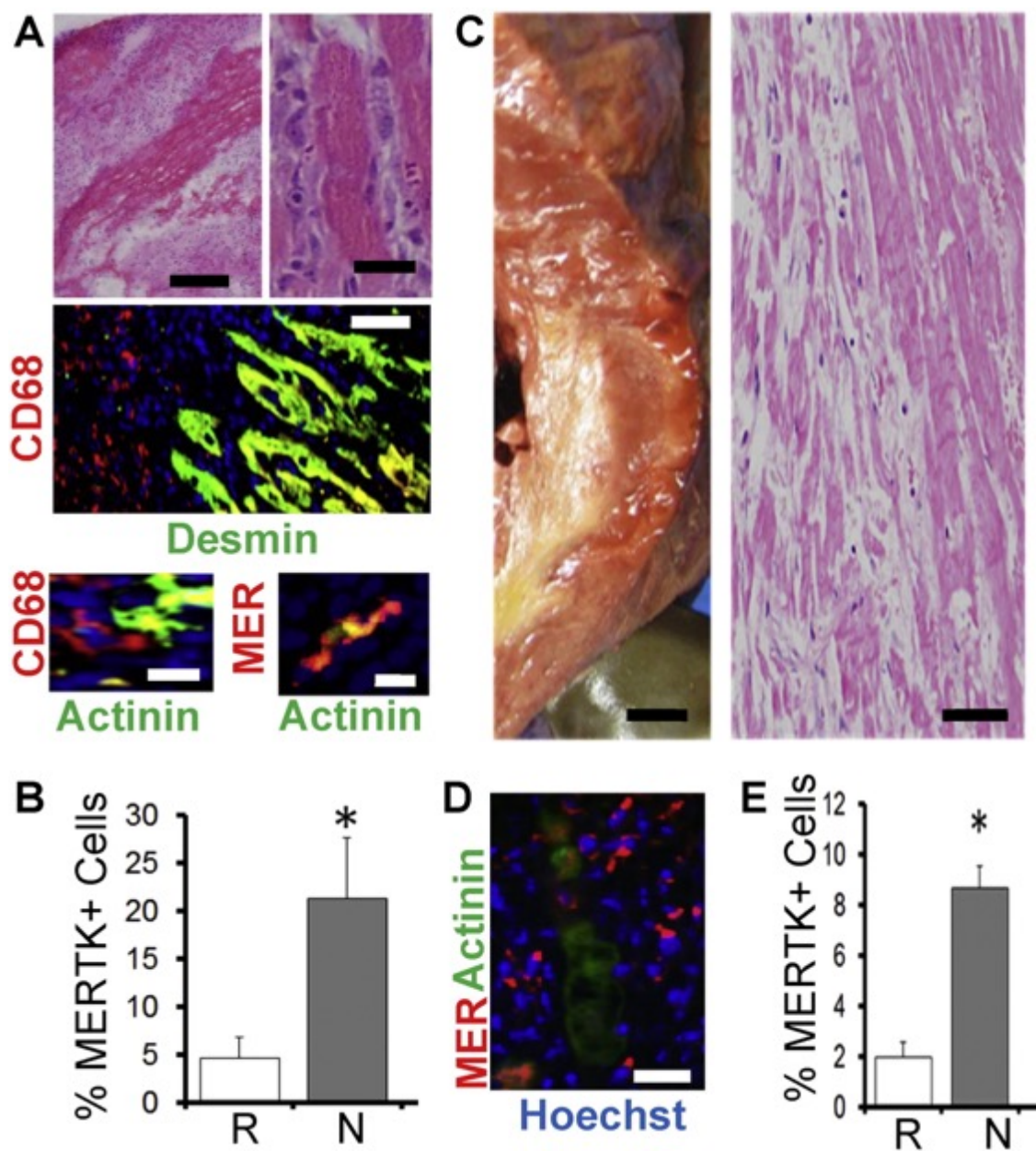


**Fig 3-1 Evidence for MERTK in human myocardium.** A and B is mouse ischemic myocardium and C, D, E is human. **(A)** Hematoxylin and Eosin (H&E) images of mouse myocardium showing hematoxylin+ mono-nuclear cells juxtaposed to hyper-eosinophilic cardiomyocytes. Left scale bar is 500 $\mu$ m and right is 20 $\mu$ m. Below H&E micrographs are Immunohistochemistry (IHC) of mouse heart with indicated markers for macrophages (CD68 and MER-TK) and cardiomyocytes (Desmin & Actinin). CD68 vs Desmin bar = 50 $\mu$ m. Bottom images = 10 $\mu$ m. In **(B)**, results of IHC quantification in Remote (R) vs inflammatory Necrotic (N) myocardial ROIs (regions of interest). **(C, D, E)** Human Myocardium. **(C)** Left is cross-section of myocardium from gross autopsy showing yellow infarct and right is H&E histology of same heart. Left is 0.5cm scale and right is 50 $\mu$ m scale bar. **(D)** IHC (100 $\mu$ m) with indicated markers (Hoechst are nuclei) and **(E)** quantitation of MERTK positive signal in healthy/Remote versus inflammatory/Necrotic myocardial ROIs.

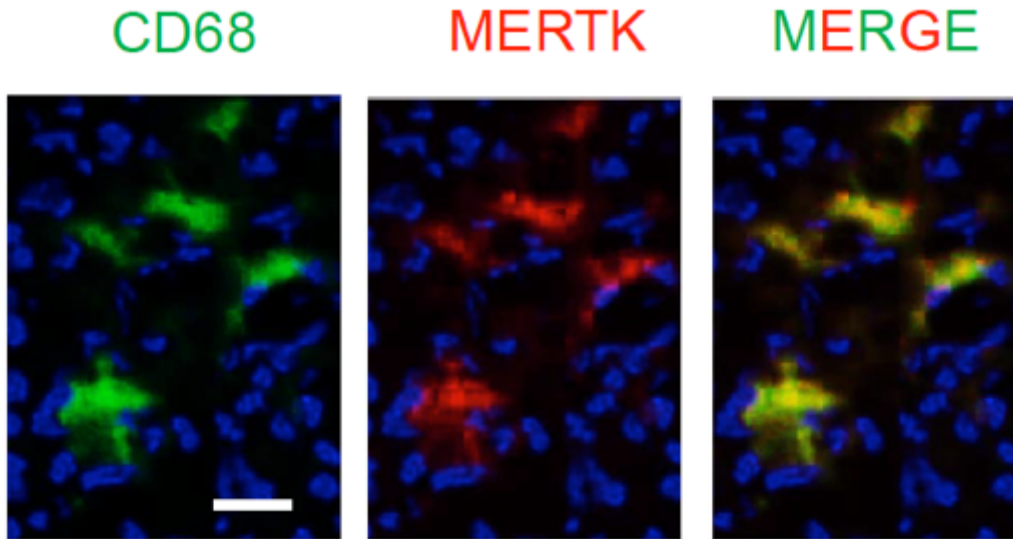


**Fig 3-2 Co-localization of CD68 and MERTK in human myocardium.** Blue is Hoechst for nuclei. Green is CD68. Red is Mertk. Yellow is merge. 67% of CD68+ cells co-stained with Mertk. Scale bar=30um.

### 3.3.2 MERTK localizes to phagocytic cups in ischemic myocardium

To identify MERTK localization in heart at the subcellular level, we imaged ischemic mouse myocardium by transmission electron microscopy (TEM). Cardiac sections were chosen with evidence of inflammatory cell infiltration after TEM-compatible toluidine staining (**Fig 3-3A**). Ultrastructural images readily identified surveying phagocytes with phagocytic vacuoles, electron-dense lysosomes and extended filopodia-like structures surrounding striated myocardial debris. Immunogold TEM (**Fig 3-3B**) revealed MERTK signal (absent in *Mertk*<sup>-/-</sup> hearts) that localized to phagocytic cups and were interacting with target cells that were positive for myocyte markers Desmin and Actinin. Interestingly, *Mertk*<sup>-/-</sup> phagocytes *in situ* seemingly exhibited reduced filopodia-formation (data not shown), similar to that observed in other cell-culture studies where MERTK was inhibited<sup>176</sup>.

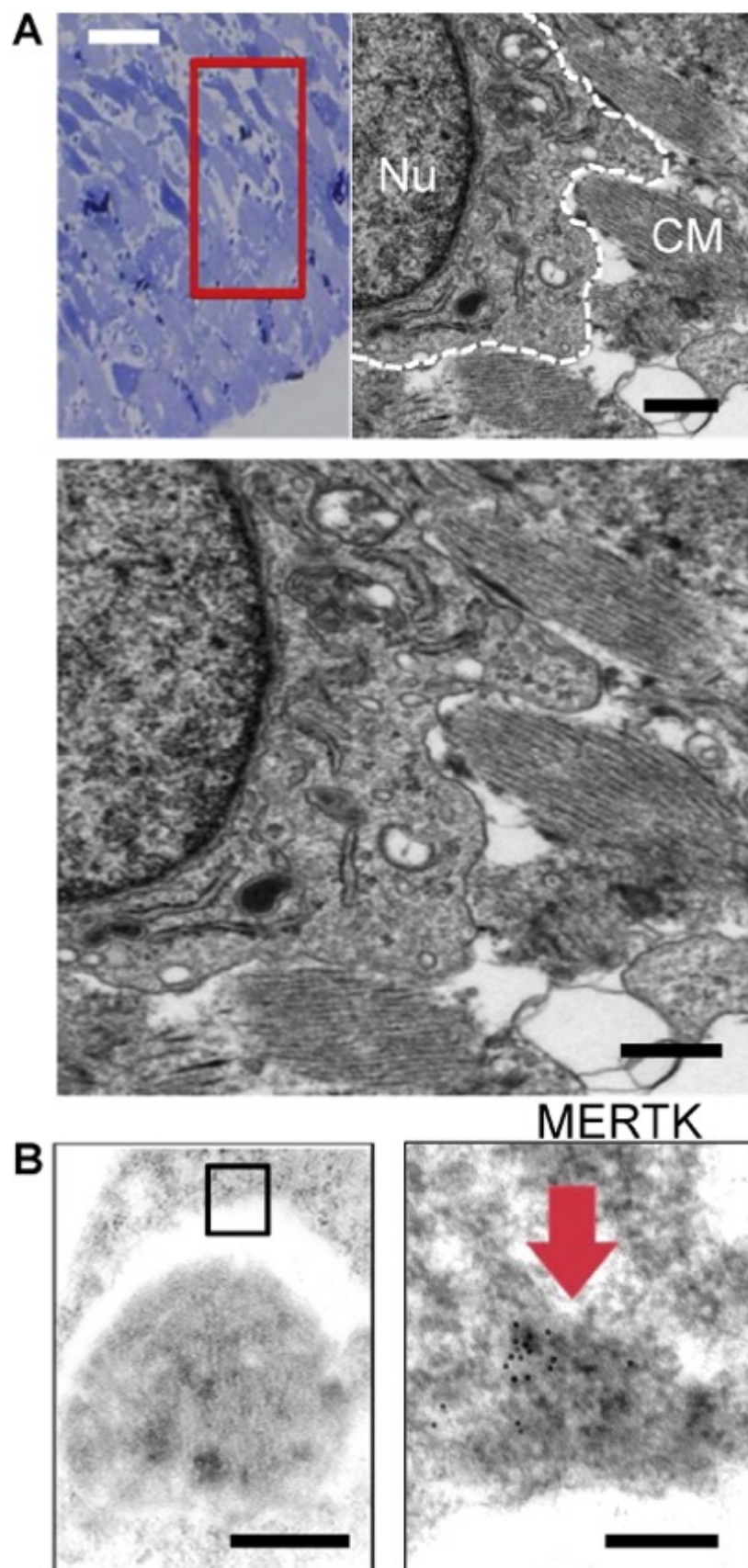


**Fig 3-3. Evidence for MERTK at the phagocytic cup in myocardium.** (A) Toluidine blue staining of cardiac sections after experimental infarction and selection of region of interest with mononuclear infiltration for transmission electron microscopy. TEM image to the right shows putative cardiac macrophage (outlined in white dotted line) and its nucleus (Nu) with extended pseudopods proximal to remnants of striated cardiomyocyte (CM) debris. Image is magnified below. Black bar = 2  $\mu\text{m}$ . (B) Phagocytic pseudopod on top surrounding an apoptotic body that was found to be immunopositive for CM markers Desmin and Actinin. Right: MERTK immunogold staining identified on the phagocytic pseudopod. Black bars = 500 nm to the left and 50 nm to the right.

### 3.3.3 MERTK is required for CM-internalization and digestion in cardiac-derived macrophages

Our past methodologies for quantifying engulfment efficiencies in heart relied on immunohistochemical co-localization of dying CMs with macrophages (**Fig 3-4A**)<sup>19</sup>. Alternative approaches to measure phagocytic activity in heart include optical imaging tomography on injected/ingested probes<sup>177</sup> and flow cytometric co-staining<sup>22</sup>. To definitively test for internalization of CM-derived proteins and any requirement for MERTK, macrophages were isolated by flow cytometry after experimental infarction of mice that were transgenic for cardiomyocyte-specific expression of the mCherry reporter gene. **Figure 3-4B** shows that 4 days after experimental infarction, significant levels of mCherry signal co-localized with CD64+ macrophages. Importantly, direct microscopic imaging of CD64+ sorted cells, revealed mCherry digestion patterns (**Fig 3-4C**) in macrophages that were isolated after light trypsin digestion to dissociate cell-cell binding. Internalization was separately confirmed by confocal microscopy. Importantly, *Mertk* deficiency reduced the extent of CD64+ sorted macrophages containing internalized CM mCherry signal (**Fig 3-4D**).

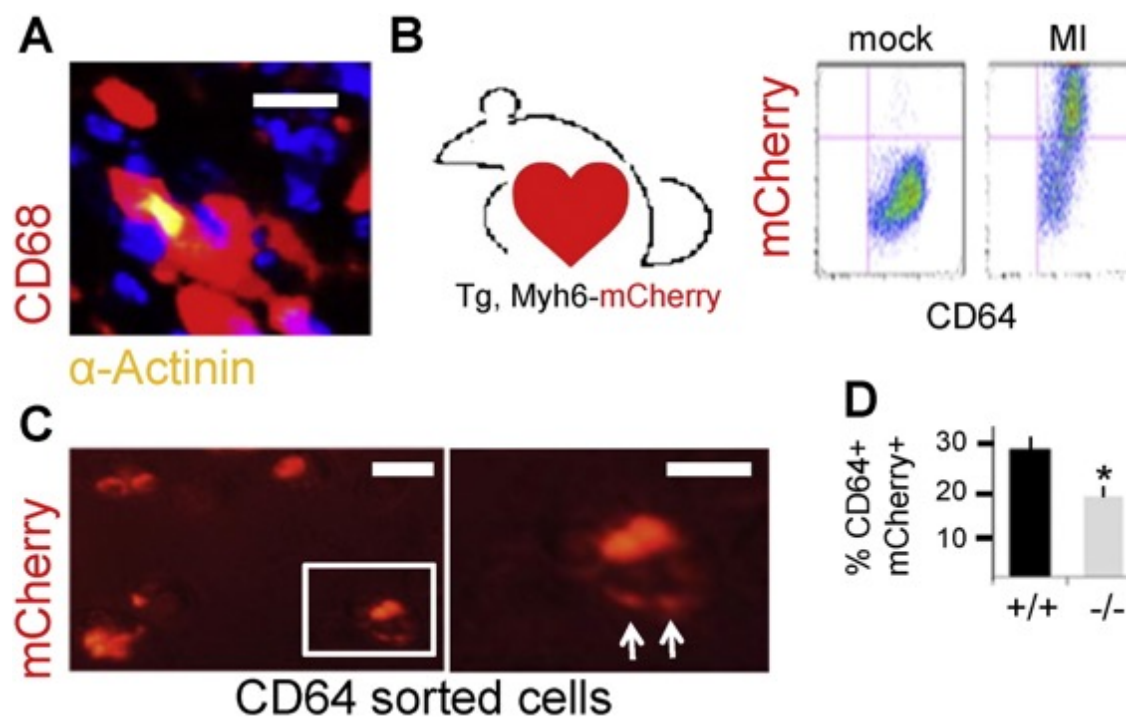


**Fig 3-4. MERTK-dependent internalization of cardiomyocytes by macrophages in myocardium.** (A) Immunohistochemistry shows co-localization of CD68 + macrophages with actinin + cardiomyocytes (yellow). Scale bar = 15  $\mu$ m. (B) Transgenic Myh6-driven mCherry mouse and flow cytograms from myocardial extracts post left anterior descending artery ligation (MI) to induce infarction. MI induces CD64, mCherry double positive cells. (C) CD64 + sorted cells were imaged by fluorescent microscopy for macrophages containing myocardial mCherry signal. Cells were trypsinized to dissociate cell-cell interactions and reveal only internalized mCherry signal. Image to the right is an enlargement of the boxed-in cell, displaying evidence of mCherry digestion (arrows). Scale bar = 15  $\mu$ m. (D) Quantitation of myocardial mCherry internalization in *Mertk*<sup>-/-</sup> mice vs. *Mertk*<sup>+/+</sup> mice after MI.

Having revealed expression of MERTK in human hearts, identified MERTK-signal *in situ* on myocardial phagocytic cups, and validated macrophage internalization and digestion of CMs post infarction, we next co-cultivated primary macrophages with primary adult differentiated CMs *ex vivo* to examine CM phagocytosis in more detail at the cell and molecular level.

### 3.3.4 Co-cultivations reveal cooperative and piece-meal phagocytic processing of dying CMs

Our co-cultivations utilized bone-marrow derived mouse macrophages and primary mouse adult differentiated CMs. Minutes after overlaying macrophages onto dying CMs, brightfield and immuno-epifluorescent microscopy revealed a high ratio of phagocytes engaging and enveloping rod-shaped early-apoptotic CMs (**Fig 3-5A**). The average macrophage: CM ratio was 3.7:1, in contrast to observed ~1:1 ratio between macrophages and cardiac fibroblasts. After staining macrophages with either filamentous actin probe phalloidin or high-affinity aliphatic membrane dye PKH, extensive phagocyte membrane remodeling was observed on macrophages interacting with CMs (**Fig 3-5B**). When CMs were labeled with cytosolic dyes and co-cultured with macrophages for longer durations (>15 minutes), evidence of phagocytic uptake was documented as dye transfer from the CM to macrophage (**Fig 3-5C**). Interestingly, engulfment of CM apoptotic bodies appeared to occur in a piece-meal fashion, consistent with trimming of dying CM apoptotic bodies away from the CM-core. Scanning Electron microscopy showed macrophages seemingly extending pseudopodia along CM surface furrows to promote ingestion. Internalization of CM bodies into macrophages was confirmed by confocal microscopy (**Fig 3-5D**) and consistent with internalization of CM debris, CM bodies co-localized with lysosomal marker lysosomal-associated membrane protein 1 (LAMP1)<sup>178</sup> (**Fig 3-6**). Finally, CM engulfment required

actin polymerization, as engulfment was suppressed after separately treating macrophages with inhibitor of actin polymerization cytochalasin-D (**Fig 3-7**).

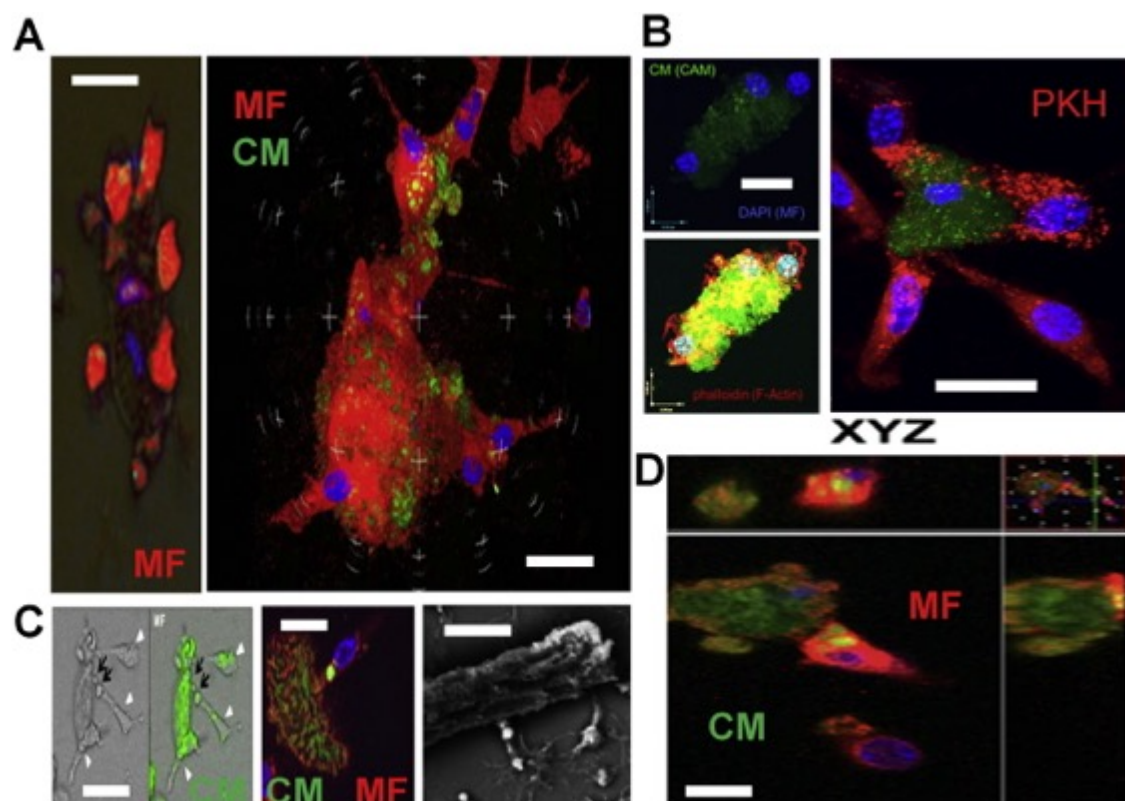


**Fig 3-5 Ex vivo co-cultivations reveal macrophage attraction to dying cardiomyocytes (CMs) and piece-meal phagocytic processing.** (A) Left epi-fluorescent and brightfield merged image displays red pseudo-colored (Calcein-AM/CAM) macrophages (MF) and CM that are solely labeled with DAPI for nuclei. Multiple macrophages engage the singular adult CM. To the right, confocal image shows multiple (nuclei are blue from DAPI) red-immunostained macrophages (F4/80) enveloping a green CM. Scale bars = 30  $\mu\text{m}$ . (B) Evidence of membrane remodeling in MFs upon binding to CMs. Top left shows multiple DAPI-labeled MFs bound to a CAM labeled CM. Below cells are stained for Filamentous Actin (F-actin) dye phalloidin in red. Phalloidin reveals actin polymerization of phagocytes surrounding the CM core. To the right, MFs labeled with membrane dye PKH and CMs are green. MFs directly interacting with CMs show redistribution of PKH dye. Scale bars = 20  $\mu\text{m}$ . (C) Evidence of piece-meal phagocytosis. Left images show green-labeled CMs transferring green dye to attached macrophages (MF, arrowheads). Middle confocal image shows phagocyte appearing to internalize green signal from CM in a phagosome. Right image is scanning electron micrograph of CM and attached MFs appearing to internalize bright/refractile apoptotic bodies. Scale bars = 15  $\mu\text{m}$ . (D) Internalization of green CM apoptotic bodies into green MFs confirmed by confocal microscopy Z sections. Scale bar = 20  $\mu\text{m}$ .

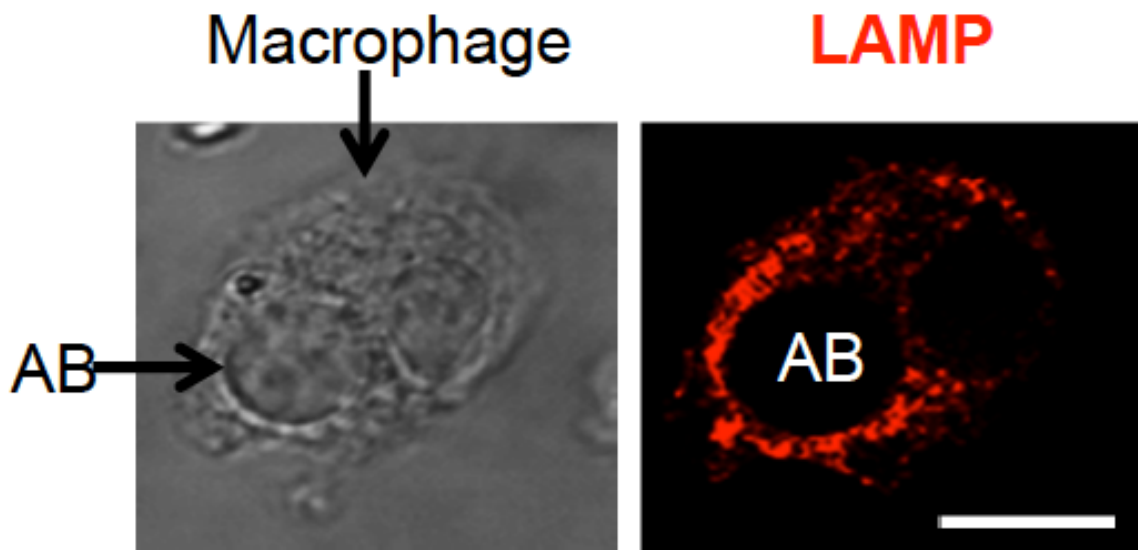


**Fig 3-6 Co-localization of LAMP and cardiomyocyte apoptotic body.** Bright field image of primary macrophage with ingested cardiomyocyte apoptotic body (AB) is shown to the left. To the right is LAMP staining, which surrounds the apoptotic body. Scale bar = 10  $\mu$ m.

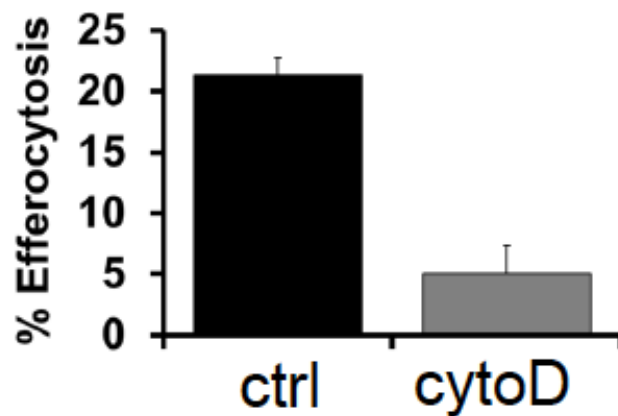


**Fig 3-7 Cardio-myocyte Efferocytosis Requires Actin Polymerization.** Primary murine macrophages were treated with cytochalasin D (cyto D) vs control and cardiomyocyte apoptotic bodies overlaid onto macrophages. Percent efferocytosis was quantified as shown above.

### 3.3.5 CM efferocytosis is inefficient

CM death post MI occurs by both necrosis and apoptosis<sup>57</sup>. CM apoptotic death is found in the zone that borders the infarct area at times that coincide with cardiac MERTK expression<sup>19</sup>. Furthermore, apoptotic bodies by nature of their phosphatidylserine can signal pro-reparative signals in the phagocyte<sup>46</sup>, which likely participate in cardiac wound healing. Therefore, we focused on macrophage engulfment of CM apoptotic bodies. To standardize our initial analyses, we chose to utilize a well-characterized apoptotic inducer, the protein kinase inhibitor staurosporine (STS). We chose a dose of STS that mimicked kinetics of apoptosis similar to that observed during ischemia-induced apoptosis (**Fig 3-8**). As a first approximation of the efficiency of CM efferocytosis, we performed phagocytic assays in comparison to apoptotic cardiac fibroblasts. To achieve this, separate adherent monolayers of CMs and fibroblasts were induced to apoptosis and early non-adherent apoptotic bodies collected, clarified by low speed centrifugation to isolate apoptotic bodies from larger cells, and equivalent numbers of apoptotic bodies overlaid onto phagocytes at a ratio of 5 apoptotic bodies to 1 phagocyte. **Fig 3-9** shows that relative to actin-dependent uptake of cardiac fibroblasts, engulfment of apoptotic bodies from CMs was less efficient (on average 23.7% less than cardiac fibroblasts).

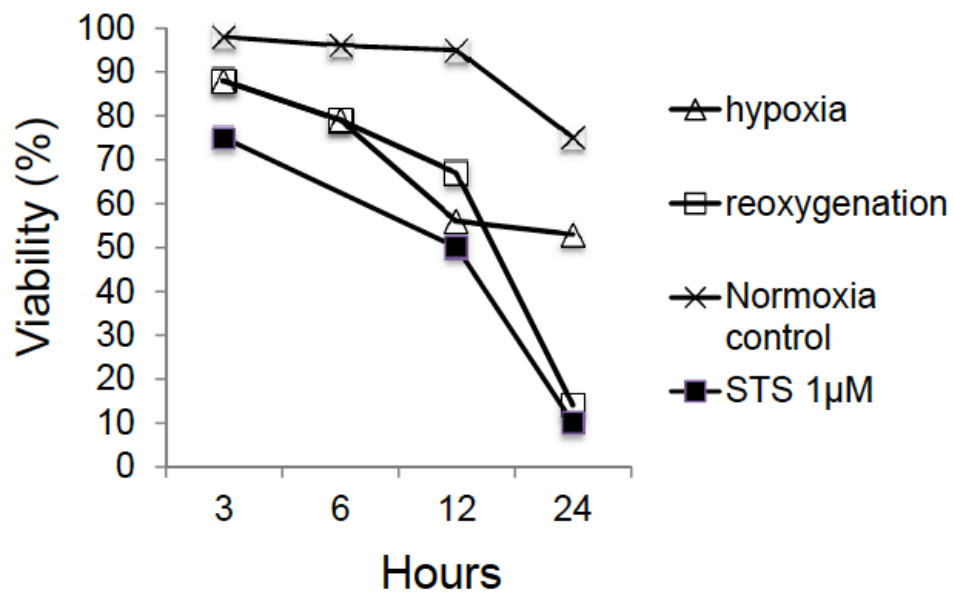


**Fig 3-8** One micromolar protein kinase inhibitor staurosporine (STS) induces cardiomyocyte cell death similar to hypoxia induced cell death. Hypoxia was induced in a Coy Hypoxia Chamber at 1% oxygen. CMs are adult mouse left ventricular myocytes separated from cardiac fibroblasts.

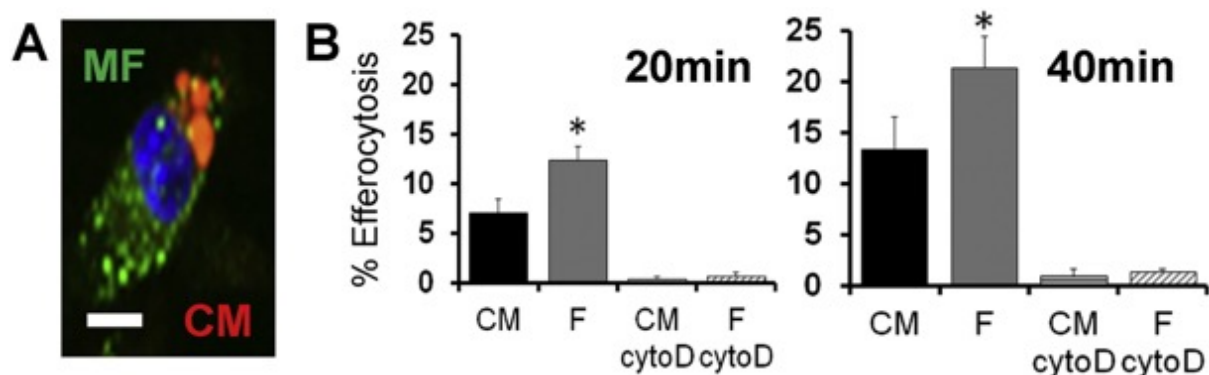


**Fig 3-9 Inefficient phagocytic uptake of CM apoptotic bodies (ABs).** (A) Micrograph of epifluorescent macrophage (green) engulfing red cardiomyocyte (CM) apoptotic bodies. Scale bar = 7  $\mu$ m. (B) Primary resident cardiac fibroblasts (F) and adult ventricular myocytes were adhered onto tissue culture plates and induced to apoptosis (1 h 1  $\mu$ M staurosporine/STS followed by 6 h treatment for CF and 18 h CF to achieve ~ 80% morphological cell death). Non-adherent/floating apoptotic bodies were harvested and separated from larger-CM-core bodies by low-speed centrifugation at 50  $\times$ g to isolate apoptotic bodies from cells and overlaid under saturating conditions onto adherent primary bone-marrow derived macrophages for efferocytosis enumeration. Cytochalasin D (cytoD) was added to macrophages to inhibit actin polymerization and control for engulfment-specificity vs. non-specific binding.

Unlike CM efferocytosis, chemotaxis and binding to CMs was not significantly reduced

We next considered that other stages of CM phagocytosis might also be attenuated relative to cardiac fibroblasts. Phagocytosis during inflammation requires the chemotactic migration of phagocytes to dying cells, followed by intercellular binding to form the phagocytic synapse. To test the ability of macrophages to chemotax to dying CMs, transwell cultures were utilized. **Fig 3-10** shows that relative to apoptotic fibroblasts, macrophages migrated to dying CMs at an efficiency that trended lower, but was not statistically significant. We also measured tethering of CM-apoptotic bodies to macrophages at 4°C and did not find evidence of reduced binding, relative to apoptotic fibroblasts. Rather, macrophage affinities for dying CMs trended higher, versus fibroblasts. Furthermore, corroborative video microscopy (on a Bio-Station Video Microscope station; see **Fig 3-11**) also showed macrophages with CM attachments that were maintained, even after collapse of rod-shaped CMs into large apoptotic bodies. When 4°C cultures were thermo-shifted to 37°C, defects in engulfment were revealed, suggesting that the mechanism of inefficient uptake was at the level of internalization, after chemotaxis and binding.

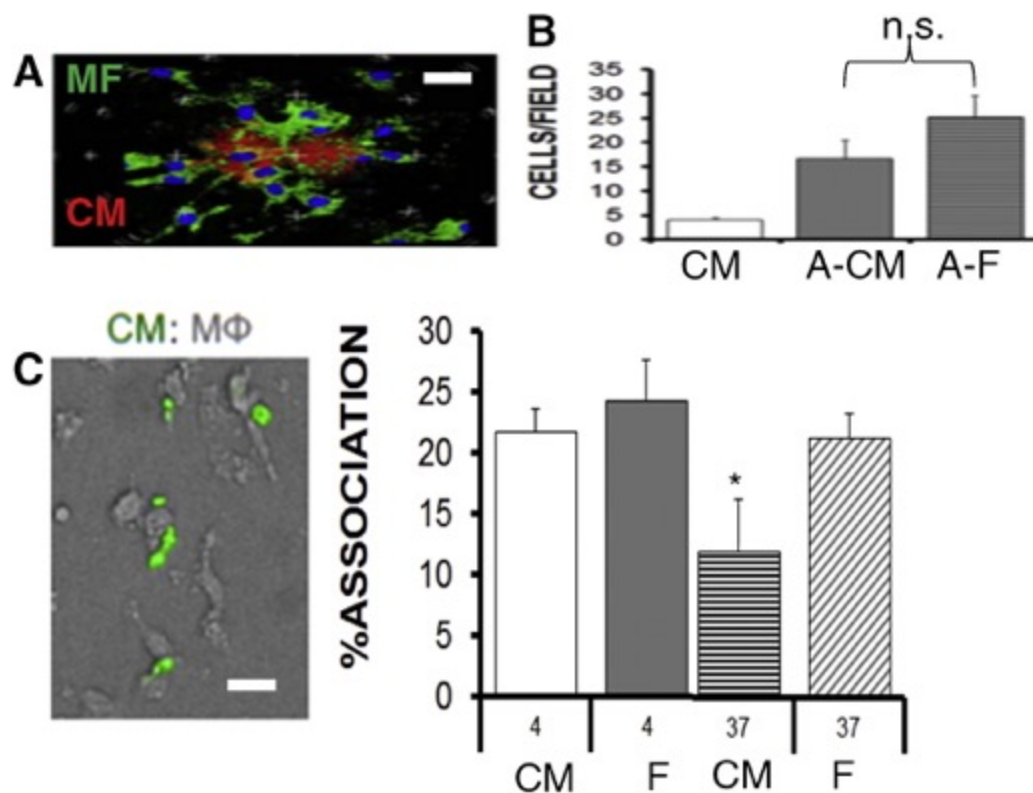


**Fig 3-10 Steps leading (chemotaxis) and preceding (binding) engulfment of cardiomyocytes do not differ significantly relative to cardiac fibroblasts.** (A) Macrophages (green) swarm to apoptotic cardiomyocytes (CM) (red). Scale bar = 20  $\mu$ m. (B) Bar graph displays quantification of macrophage chemotaxis to live CMs vs apoptotic cardiomyocytes (A-CMs) versus apoptotic cardiac fibroblasts (A-F). n.s. = not statistically different. (C) Micrograph shows green CM apoptotic bodies bound to non-labeled macrophages. Binding assay bar graph for affinity of macrophages to dying CMs versus dying cardiac fibroblasts (F) at temperature of 4  $^{\circ}$ C. After thermoshift to 37  $^{\circ}$ C and rinsing away of non-engulfed cells, % association in an indication of engulfment. Scale bar is 15  $\mu$ m.

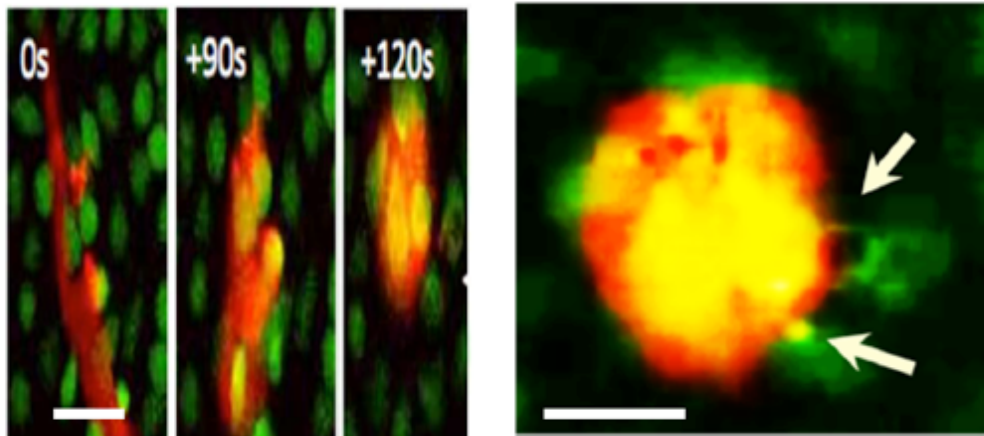


**Fig 3-11** Time lapse images (0seconds, 90 seconds, and 120 seconds) provide evidence that macrophage (green) binding to dying cardiomyocytes (CM; red) is maintained during collapse of CMs from rod-shaped to rounded. Yellow color is merge of Green and Red. Arrows point to phagocytic cups appearing to remove pieces of CM away from the CM core. Scale bars = 50  $\mu$ m.

### 3.3.6 Inefficient efferocytosis is not associated with CM large apoptotic body size

Phagocytic removal of dying CMs is a unique challenge in that myocytes are larger than macrophages. Nevertheless, previous studies have shown that phagocytes can engulf particles as large as themselves<sup>179,180</sup>. Consistently, apoptotic bodies of large and heterogenous size blabbed off the larger cardiomyocyte core after apoptosis induction (**Fig 3-12**). Direct quantitation and flow cytometric analysis indicated that on average, CM apoptotic bodies were larger than apoptotic bodies from cardiac fibroblasts. Microscopic images revealed macrophages interacting with apoptotic bodies of diverse sizes. To determine if large CM apoptotic body size affects efferocytosis efficiency, we normalized size by size exclusion filtration to remove larger apoptotic bodies, and overlaid onto macrophages. As indicated in **Figure 3-12D**, overlay of filtered apoptotic bodies from CMs and cardiac fibroblasts revealed that CMs were still less efficiently engulfed. These data suggested a contributing molecular factor in the reduced phagocytic phenotype.

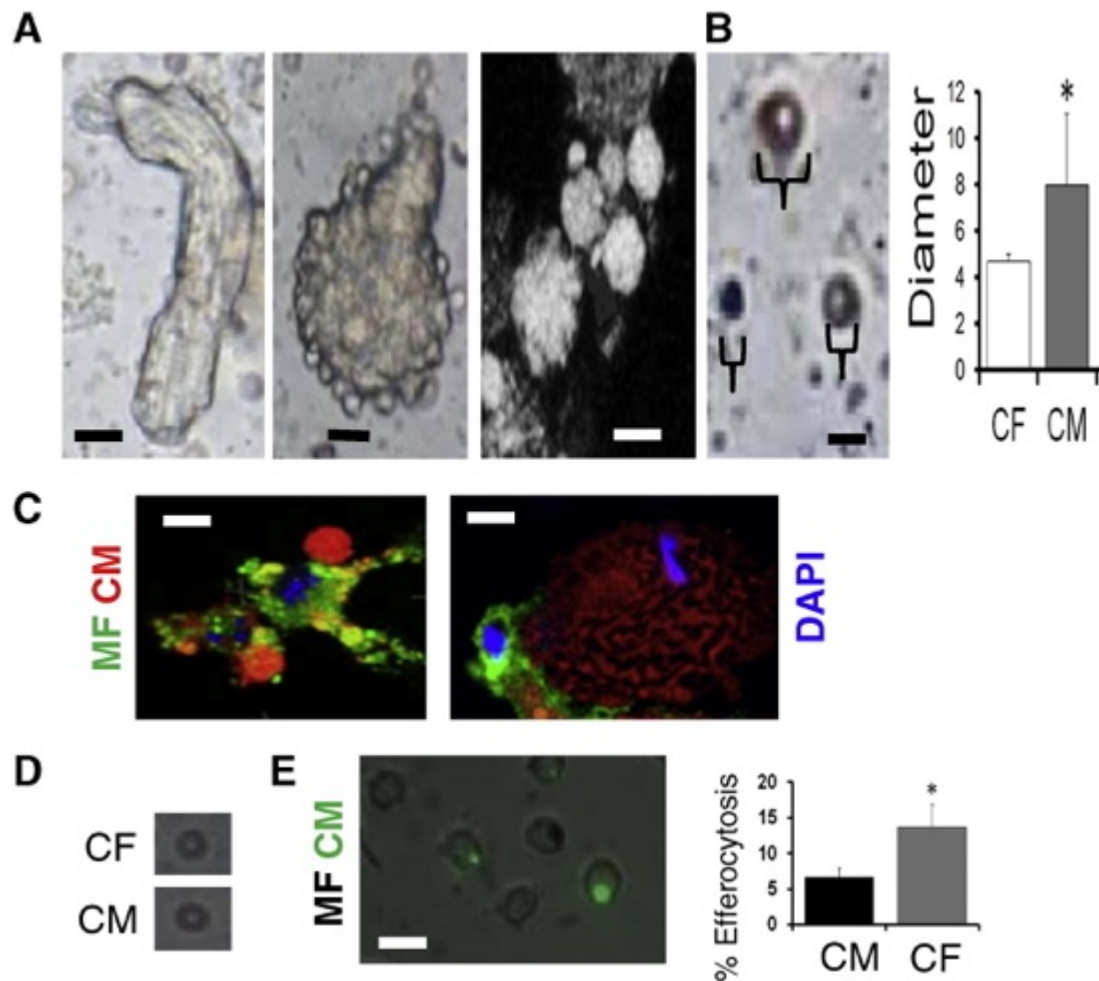


**Fig 3-12 Inefficient cardiomyocyte (CM) efferocytosis is largely independent on the size of CM apoptotic bodies.** (A) Leftmost bright-field image depicts rod-shaped CM in the beginning stages of cell death. To the immediate right is a collapsed rounded CM exhibiting protruding apoptotic body blebs. Next image is confocal microscopy and shows apoptotic bodies of varying sizes forming on a dying CM. Scale bars = 15 µm. (B) Soluble apoptotic bodies (ABs) of various sizes are depicted in photomicrograph. Scale bar = 4 µm. Quantification of CM vs cardiac fibroblast (CF) apoptotic body size. (C) Phagocytes engage CM ABs of various sizes. Scale bar is 10 µm. (D) Average size of largest CM and CF apoptotic bodies after filtration was < 5 µm. (E) Normalized efferocytosis after filtration with size exclusion filter. Scale bar is 10 µm.

### 3.3.7 CMs induce shedding of macrophage apoptotic cell receptor MERTK to reduce efferocytosis efficiency

Multiple mechanisms on the CM or macrophage-side could explain reduced efferocytosis efficiencies. We recently reported evidence of lower molecular weight MER isoforms in extracts of cardiac tissue post ischemia, consistent with shedding of MER ectodomains from cardiac macrophage cell surfaces<sup>19</sup>. Shedding of MER, after its cleavage by proteolysis, can reduce efferocytosis efficiency during inflammation by inhibiting post-binding engulfment signaling<sup>84,85</sup>. Interestingly, our co-cultivation experiments exposed extra-cellular speckles of MER immunostaining, consistent with shedding of MER (**Fig 3-13**). We therefore measured cell surface MERTK levels by flow cytometry, after co-cultivation with CMs, and found significantly reduced MERTK signal. Western blots and ELISA also revealed elevated shed, or soluble-MER in the supernatant of macrophages that were co-cultivated with dying CMs. To test if inefficient CM phagocytosis could be enhanced by blockade of MERTK cleavage, we transfected *Mertk*-deficient HEK cells with wild type *Mertk* cDNA, and compared phagocytic efficiency relative to our previously characterized cleavage resistant (cr) *Mertk*cDNA<sup>85</sup>, in which the protease susceptibility site has been genetically deleted. **Fig. 3-13D** shows that relative to cells transfected with equal masses of WT *Mertk*, cells harboring the crMERTK isoform promoted enhanced CM efferocytosis.

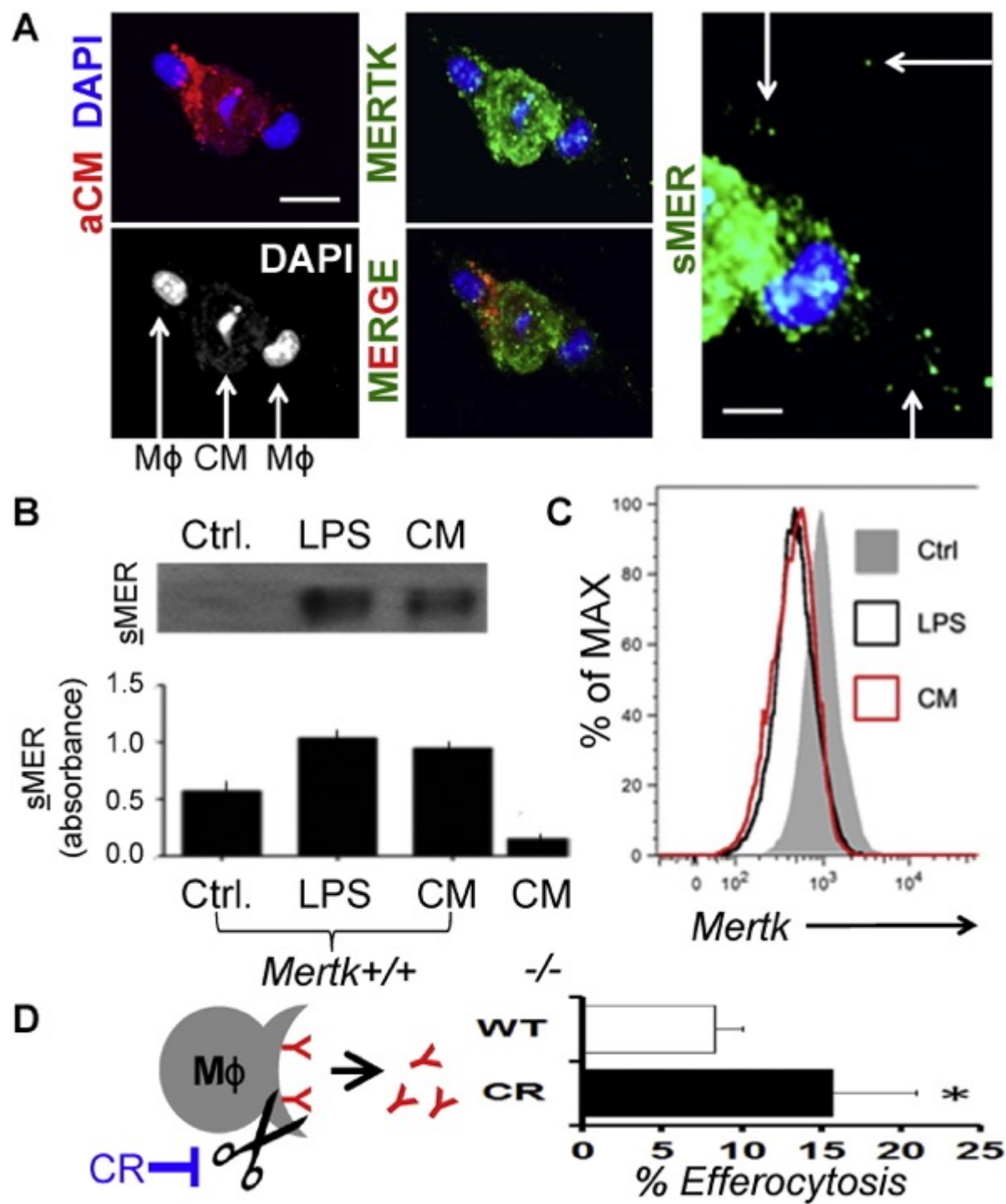


**Fig. 8. Dying cardiomyocytes (CMs) induce MERTK cleavage in macrophages to inhibit efferocytosis.** (A) Confocal images of dying red (PKH) labeled CMs were cocultivated with MERTK-labeled (green) macrophages. DAPI shows macrophage nuclei flanking condensed apoptotic CM nuclei. Scale bar = 20  $\mu$ m. Rightmost panel depicts higher magnification image (white bar = 10  $\mu$ m) of extracellular (arrows) or soluble MER (sMER) signal. (B) Western blots (above) and ELISA (below) for sMER after *Mertk* +/+ or *Mertk* -/- macrophage incubation with positive control lipopolysaccharide (LPS) or CMs. (C) Flow cytometry histograms for cell-surface MERTK after co-cultivation with LPS or CMs (D). Schematic representation of inhibition of sMER cleavage with mutant Cleavage-Resistant (CR) MERTK. Bar graph is enumeration of % CM efferocytosis by HEK293 cells after transfection with equal masses of wild type (WT) vs CR-*Mertk* cDNAs.

### 3.4 Discussion

Herein our study examined *in vivo* validated and rate limiting steps before and during CM engulfment by macrophages. Our focus was on modeling pathways similarly present or required during myocardial wound healing (*Figure 1*)<sup>19</sup>. From these studies, perhaps it is not surprising that macrophage phagocytosis of cardiomyocytes (CMs) was found to be inefficient relative to other parenchymal cell types. For example, the inflammatory response after myocardial infarction (MI) is likely not shaped by selective evolutionary forces, in that the average age of first MI is well after reproductive years. Similarly, and at the cellular level, the long-lived nature and terminally differentiated state of adult CMs limits their phagocytic engagement by phagocyte receptors, in comparison to other cell types with higher turnover kinetics.

Although the predominant form of CM death post MI is necrosis<sup>57</sup>, the significance of apoptotic CMs and their apoptotic bodies are important to examine. For example, apoptotic recognition of non-myocytes is amplified through phosphatidylserine-receptors and other pathways in macrophages, which can transmit intracellular signals to suppress inflammation and promote tissue repair<sup>32</sup>. However, it remains to be conclusively tested as to how recognition of CM apoptotic bodies may regulate macrophage inflammatory signaling. This is an important consideration as potential defects in engulfment, coupled with inefficient activation of pro-resolving immunosuppressive pathways, could cumulatively delay cardiac repair. Given the low regenerative potential of CMs, even slight delays in resolution of cardiac inflammation could promote collateral CM loss and therefore reduce cardiac contractility.

A unique aspect of CMs in the setting of phagocytosis is their larger *size*. Our data indicate minimal changes to efferocytosis efficiency, as a function of CM apoptotic body surface area

(Figure 7). Studies that have examined phagocytic target size and geometry, indicate particle diameter *per se* is not the sole factor in triggering actin-mediated engulfment<sup>181</sup>. Case in point, morphology of the engulfed particle can affect eating efficiency. For example, filamentous bacteria delay timing of phagocytosis through induction of unique phagosome maturation pathways<sup>182</sup>. It will be interesting to determine if larger or stiffer hypertrophic CMs, after pressure overload-associated cardiac syndromes for example, are uniquely engulfed and processed by phagocytes, or alternatively result in unique inflammatory phagocyte polarization<sup>183</sup>. Also important for inflammation resolution is the fate of the large and last CM apoptotic body or “core,” which often represents the final remnant of CM apoptosis<sup>184</sup>.

On the phagocyte side, an important macrophage receptor in cardiac repair is MERTK<sup>19</sup>. During experimental myocardial infarction, evidence suggests that the ectodomain of MERTK is shed from cell surfaces, and our initial analyses indicate this also occurs in humans (data not show). Proteolytic cleavage is known to regulate the activity of many transmembrane anchored proteins. In the case of MERTK, recombinant soluble-MER is modulatory by two accounts: First through suppression of efferocytosis and secondly through affecting thrombus formation *in vivo*<sup>84</sup>. MERTK inactivation by ADAM17-mediated cleavage is predicted to suppress its anti-inflammatory function, thereby permitting the phagocyte to become fully activated<sup>85</sup>. *Ex vivo* enhancement of CM efferocytosis by cleavage-resistant MERTK was significant (Figure 8), however does not rule out other potential contributing mechanisms that affect CM phagocytic efficiency, including on the CM. In addition to identifying potential CM-specific triggers of MERTK cleavage, future studies seeking the physiological relevance of MERTK cleavage post heart attack, will benefit from the identification and blockade of its cleavage site.

*Additional future studies* that model CM clearance pathways should address the role of neutrophils both separately and together with macrophages. This is important in that neutrophils are recruited to the heart prior to monocytes and may contribute to the breakdown of dying muscle cells. Also, cellular cardiac tissue scaffolds<sup>185</sup> may reveal the nature of macrophages with CMs in a more natural three dimensional setting. On the CM side, broader unresolved questions include the identity of CM ligands necessary for interactions with macrophages. On the macrophage, and in the setting of a heterogeneous cardiac macrophage population<sup>22</sup>, distinct phagocyte subsets may promote alternative phagosome maturation pathways and immune responses<sup>186</sup>. In preliminary data, flow cytometry-sorted macrophages from mouse hearts reproduced findings reported herein, however, additional studies should test mechanisms of varying phagocytosis efficiency by these ontogenically unique phagocyte subsets<sup>22</sup>. We anticipate that further studies of macrophage-CM interactions will reveal new strategies to enhance CM clearance efficiency, reduce infarct size, and improve cardiac function.

**4 CHAPTER 3- Acute CD47 blockade during ischemic myocardial reperfusion enhances phagocytosis-associated cardiac repair**

#### 4.1 Introduction

Although clinical management of acute myocardial infarction (AMI) has significantly reduced morbidity and mortality, the consequence of these advances includes an emerging incidence of post-MI heart failure<sup>187</sup>. In turn, new approaches that enhance cardiac wound healing and are complementary to the current standards of care have the potential to improve on left ventricular (LV) systolic function<sup>188</sup>.

A critical determinant of heart failure susceptibility after AMI is infarct size<sup>57</sup>. Infarct size and loss of nonregenerative cardiomyocytes (CMs) by acute necrosis directly correlates with ventricular dysfunction and heart failure<sup>189</sup>. Infarct necrosis can also expand during reperfusion injury or after maladaptive inflammation, leading to accelerated and adverse ventricular remodeling<sup>8,190</sup>. During wound healing, clearance of dying cells must occur efficiently to prevent secondary necrosis and prolonged inflammation. Efficient phagocytic clearance of apoptotic cells by macrophages (Mφs) via *efferocytosis*, actively programs cellular inflammation-resolution and tissue repair signaling pathways<sup>29</sup>. This clearing is particularly important in the heart, where inefficient removal of necrotic CMs may lead to collateral myocyte loss and infarct expansion<sup>162</sup>. In a previous study, we experimentally linked the efficiency of phagocytic clearance to infarct size expansion and discovered that Mφs defective for efferocytosis led to deteriorated cardiac function after MI<sup>19</sup>. These studies begged additional questions, including the natural efficiency of CM clearance by phagocytic cells and whether strategies that target phagocytic enhancement might enhance heart healing. In this study, we focused on CM-intrinsic factors, namely CD47, that regulate phagocytic interactions with Mφs<sup>191</sup>.

Dying cell engulfment requires cell surface presentation of so-called “eat-me” signals, such as phosphatidylserine and calreticulin, which must occur in tandem with downregulation of antiphagocytic “don’t-eat-me” markers, including CD47<sup>191</sup>. Independent of programmed cell death per se, blockade of CD47 and concomitant overexpression of calreticulin can permit phagocyte ingestion of viable cells. In addition to experimental blockade<sup>192</sup>, natural reduced expression of CD47 occurs in vivo, for example, in senescent erythrocytes; this is associated with red blood cell erythrophagocytosis and clearance from the circulation by resident tissue Mφs<sup>193</sup>. A recent study published in the journal *Nature* highlights the potential of CD47 blocking strategies in atherosclerotic cardiovascular disease<sup>194</sup>.

Although CD47 expression has been profiled in neonatal CMs<sup>168</sup>, much less is known about its expression and function in adult CMs. Cd47 deficiency is associated with enhanced cardiac performance after administration of vasoactive agents<sup>195</sup>. In skeletal muscle, CD47 can regulate PGC-1α-dependent mitochondrial biogenesis through recognition of its thrombospondin ligand<sup>196</sup>. CD47 has also been linked to signaling in smooth muscle cells<sup>197</sup>. The significance of CD47 after AMI is unclear.

Our preliminary mechanistic studies suggested elevated CD47 expression in CMs relative to other cardiac cells, leading us to hypothesize that CMs may exhibit natural resistance to phagocytic removal after injury. To test in principle whether acute CD47 blockade during reperfusion of ischemic myocardium enhances cardiac repair, in association with CM phagocytosis, we used an experimental MI model in mice and injected anti-CD47-blocking antibodies during reperfusion. Importantly, CD47 targeting was limited to a single time and dose to focus actions during the height of CM phagocytosis and to avoid targeting alternative postacute CD47 signaling pathways.

## 4.2 Material and methods

### *Human samples*

Human cardiac samples were obtained from the Northwestern University Department of Pathology and the office of the Medical Examiner of Chicago. Under the protocol approved by the institutional review board at Northwestern University (#STU00079445), archived formalin-fixed paraffin-embedded cardiac autopsy samples were obtained and analyzed at Northwestern University Feinberg School of Medicine, as previously described<sup>142</sup>. Specifically, autopsy cases were evaluated by a combination of factors, including serum cardiac enzymes and gross evidence at time of autopsy. Gross evidence consisted of pale or yellow myocardial areas with or without a hyperemic border. Age of infarct ranged from ~6 h to several days. Time from death to autopsy ranged from 18 h to 7 days. Autopsy tissue blocks of myocardium from acutely infarcted areas versus noninfarcted areas and noninfarcted individuals were fixed in 10% formalin and serial 6- $\mu$ m sections were stained with hematoxylin and eosin. In this study, a total of 22 human cardiac autopsy samples were used, 11 from AMI cases and 11 from non-AMI cases.

### *Murine samples*

Murine hearts were infused and fixed with 10% phosphate-buffered formalin at physiological pressures. Hearts were cut transversely, parallel to the atrioventricular groove and coronary sulcus. Fixed hearts were embedded in paraffin at the Northwestern University Mouse Histology and Phenotyping Laboratory. Blocks were serially cut 6  $\mu$ m apart. Alternating sections were stained with hematoxylin and eosin. For frozen sections for immunohistochemistry, samples were rinsed and incubated overnight in 7% sucrose and frozen in freezing medium unless

otherwise indicated. Transverse cryosections were cut at a thickness of 10  $\mu\text{m}$  on a Leica cryostat and placed on super frost plus-coated slides for analysis.

### *Mice*

B6; D2-Tg (Myh6\*-mCherry)2Mik/J mice were from Jackson Laboratory (stock No: 021577, Bar Harbor, Maine). The alphaMHC-mCherry transgene has a modified mouse alpha myosin heavy chain promoter sequence directing cardiac-specific mCherry expression in CMs. Mice were housed in temperature- and humidity-controlled environments and kept on a 12:12-hour day–night cycle with access to standard mouse chow and water ad libitum. All studies were approved and reviewed by the Institutional Animal Care and Use Committee at Northwestern University (Chicago, Illinois). *Cd47*<sup>-/-</sup> mice were obtained from the Jackson Laboratory (stock #003173).

### *Materials and antibodies*

Tissue culture dishes were from Corning (Corning, New York), and fetal bovine serum was from Gibco (Gaithersburg, Maryland). Chemical reagents were from Sigma Chemical Co. (St. Louis, Missouri), unless stated otherwise.

### *Antibodies*

CD47 monoclonal and polyclonal antibodies were as previously described<sup>198</sup>. Anti-CD68 was obtained from Abcam (ab125212, Cambridge, United Kingdom). Monoclonal mouse anti-Desmin (clone DE-U-10) from mouse ascites fluid was from Sigma (D1033). Rat antimouse M $\phi$  antibody

Mac-2 was from Cedarlane (Burlington, Ontario, Canada). Rat antineutrophil antibody was from Serotec (Raleigh, North Carolina).

*Primers for semiquantitative and real-time pcr in this study*

Ccl2: F: CCT GGA TCG GAA CCA AAT GA, R: ACC TTA GGG CAG ATG CAG TTT TA. TNF- $\alpha$ : F: CGG AGT CCG GGC AGG T, R: GCT GGG TAG AGA ATG GAT GAA CA. Il-6: F: GAGGATACCACTCCCAA-CAGACC, R: AAG TGC ATC ATC GTT GTT CAT ACA, Il-10: F: GCC AAG CCT TAT CGG AAA TG, R: GGG AAT TCA AAT GCT CCT TGA T. Gapdh: F: GGT GGC AGA GGC CTT TG, R: TGC CCA TTT AGC ATC TCC TT. hCD47: F: 5'-AGC TCT AAA CAA GTC CAC TGT CCC-3'. hCD47: R: 5'-TCC TGT GTG TGA GAC AGC ATC ACT-3'. Control, hTBP: F 5'-TGA GTT GCT CAT ACC GTG CTG CTA-3', hTBP: R: 5'-CCC TCA AAC CAA CTT GTC AAC AGC-3'.

*Ischemia and reperfusion*

Ischemia and reperfusion injury was performed in male and female B6 mice 8 to 12 weeks of age. Ischemia was produced by occluding the left coronary artery with a 7-0 silk suture on a tapered tube for 45 minutes as we have previously described<sup>199</sup> followed by reopening of the ligature to allow for reperfusion. Mice were anesthetized with tribromoethanol (Avertin) and received buprenorphine (0.1 mg/kg subcutaneously) before surgery and after survival surgery, every 12 h up to 48 h for pain management.

#### Laser capture microdissection

RNA from myocardial sections was captured by LCM using a Zeiss P.A.L.M. laser microdissection system as previously described<sup>172</sup>. Total RNA was isolated using the RNAqueous-Micro kit from Ambion (Waltham, Massachusetts) and reverse-transcribed into cDNA using SuperScript III First-Strand Synthesis Mix (Invitrogen, Carlsbad, California).

#### Semiquantitative and quantitative reverse transcriptase polymerase chain reaction

Hearts were snap-frozen for RNA. Total RNA was extracted using the RNeasy kit (Qiagen, Hilden, Germany). cDNA was synthesized from 4 µg of total RNA using oligo (dT) and Superscript II (Invitrogen). cDNA was subjected to quantitative reverse transcriptase polymerase chain reaction amplification using a SYBR Green PCR Master Mix (Applied Biosystems, Foster City, California).

#### Administration of anti-cd47 via intramyocardial delivery

Five minutes before the ligature was released, 100 µg anti-CD47 (mIAP301) monoclonal antibody was injected at 3 sites into the ischemic myocardium, just distal to the coronary ligation with 30 µl of antibody solution per site. At the end of 45 min of occlusion, the ligature was released, and the heart was reperfused.

#### Adenovirus administration

CM specific-CD47 expression was induced as previously described<sup>200</sup>. Adeno-associated virus1-cTNTp-GFP-2A-mCD47-WPRE and adeno-associated virus1-cTNTp-GFP were from Vector Biolabs

(Malvern, Pennsylvania). We administered  $1 \times 10^{12}$  adeno-associated virus into 6-week-old B6 mice and hearts were harvested for immunohistochemical staining to check for increased protein.

Flow cytometry preparation (cardiac)

Flow cytometric analysis of cells after MI

Mice were anesthetized with isoflurane after MI. Peripheral blood was drawn via retro-orbital bleed with citrate solution (100 mmol/l Na-citrate, 130 mmol/l glucose, pH 6.5), as an anticoagulant. Spleens were removed, triturated in Hank's Balanced Salt Solution (Mediatech, Inc., Manassas, Virginia) at 4°C with the end of a 3-ml syringe and filtered through a nylon mesh. Cell suspension was pelleted and red blood cells were lysed with ACK lysis buffer and resuspended in flow cytometry buffer.

For infarct tissue

Hearts were harvested, perfused with saline to remove peripheral cells, minced with fine scissors, and placed into a cocktail of collagenase and DNase (Sigma-Aldrich, and Worthington Biochemical Corporation, Lakewood, New Jersey) and shaken at 37°C for 1 h. Cells were triturated through nylon mesh or 100 µm strainer and centrifuged at 15 min at 500×g and 4°C. Total cell numbers were determined by Trypan blue staining. The resulting single-cell suspensions were rinsed with Hank's Balanced Salt Solution supplemented with 0.2% (wt/vol) bovine serum albumin and 1% wt/vol fetal calf serum. Flow cytometry was performed as previously described<sup>19</sup> and with indicated antibodies in figure legends.

### Cardiac infarct size measurement

At time of humane killing, mice were anesthetized with a ketamine hydrochloride and xylazine hydrochloride solution C-IIIN from Sigma (K113). The abdominal wall below the ribcage was opened and the diaphragm was cut after lifting the sternum with tweezers. The lower part of ribcage was removed to expose the heart for removal. Fluorescent latex beads were perfused retrograde to determine the area at risk. Subsequently, hearts were sliced into 1-mm transverse cross sections and then incubated with 1% 2,3,5-triphenyl-tetrazolium chloride solution (Sigma T8877) in saline for 15 min at 37°C. Hearts were then placed in 10% formalin. Viable tissue stained red and infarcted tissue white. Heart sections were weighed. Digital photomicrographs were taken and images of infarcts were blinded for analysis. Infarct size was determined as a percentage of the left ventricle. Infarct area and the total area of LV myocardium were traced manually in the digital images. Infarct size, expressed as a percentage of the area at risk, was calculated by dividing the sum of infarct areas from all sections by the sum of LV areas from all sections and multiplying by 100.

### Gadolinium-enhanced magnetic resonance imaging

Digital photomicrographs were taken and images of infarcts were blinded for analysis. Infarct size was determined as a percentage of the left ventricle. Infarct area and the total area of LV myocardium were traced manually in the digital images. Infarct size, expressed as a percentage of area at risk, was calculated by dividing the sum of infarct areas from all sections by the sum of LV areas from all sections and multiplying by 100. Magnetic resonance imaging was performed on a 7-T Clinscan system (Bruker, Ettlingen, Germany) equipped with actively shielded gradients

(BGA12) with a full strength of 440 mT/m and a slew rate of 3,440 mT/m/ms. Images were acquired using a receive only 4-channel phased array radiofrequency coil (using a body coil for radiofrequency transmission) and a magnetic resonance-compatible physiological monitoring and gating system for mice (SA Instruments, Inc., Stony Brook, New York). The magnetic resonance imaging was performed on day 1 after the MI. The magnetic resonance imaging protocol included multislice localizer imaging to select a short axis LV slice. Late gadolinium imaging was performed using a cardiorespiratory gated multislice inversion recovery sequence covering the entire LV from base to apex. Typical imaging parameters included TE/TR, 2.3/4.7 ms; slice thickness, 1 mm; number of slices, 7 to 8; inversion time, 550 ms; number of averages, 2; spatial resolution,  $0.2 \times 0.2 \text{ mm}^2$ ; flip angle, 300; and scan time, 7 minutes. Gadolinium (0.5 mmol/kg body weight) was injected intraperitoneally and late gadolinium enhancement imaging was started 20 minutes after the injection. Image analysis was performed on a workstation using Segment software (Medviso, Lund, Sweden). Using the software, epicardial and endocardial contours were drawn and Otsu thresholding method was used to automatically delineate the infarct zone. Infarct size was calculated as a percentage of the total LV mass.

#### Cardiac efferocytosis assays

Transgenic Myh6-driven mCherry mice underwent the surgery as described and flow cytometry of myocardial extract was performed after the MI to identify phagocyte, mCherry double positive cells, as previously described<sup>142</sup>. Cells were trypsinized to dissociate cell–cell interactions and reveal only internalized mCherry signal. Cardiac phagocytosis was also measured in situ by counting the number of free and ingested apoptotic cells in individual sections. Apoptotic cells

were considered “free” when they were not surrounded by, or in contact with, M $\phi$ s. The analysis was performed in a blinded fashion by 2 independent observers.

### Echocardiography

Two-dimensional transthoracic echocardiography was performed using a 25-MHz probe (Vevo 770, Visualsonics, Toronto, Canada) with mice in a supine position. The mouse chest was treated with a depilatory agent and mice were anesthetized with isoflurane (2% in O<sub>2</sub>) and heart rate was monitored. Left ventricle dimensions were assessed on Visualsonics software in a short axis and long axis views from the mid-left ventricle, just below the papillary muscles. In short axis, 2D (B-mode) images were taken every millimeter starting from apex to base; subsequently, an M-mode was taken 1 mm before, at, and after the papillaries. All measurements were made in 2 to 6 consecutive cardiac cycles and the averaged values used for analysis. The LV end-diastolic and end-systolic dimensions and the thickness of the interventricular septum and posterior wall were made from the M-mode tracings and fractional shortening (ratio between diameter of the LV in diastole or relaxed versus diameter when contracted) was also measured as an indicator of systolic function. Dimensions were measured between the anterior wall and posterior wall. Diastolic measurements were made at the point of minimal cavity dimension, using the leading-edge method of the American Society of Echocardiography.

### Cell types

For isolation of primary M $\phi$ s, when indicated, bone marrow–derived M $\phi$ s were isolated from murine femurs and cultured in L-cell–conditioned medium, containing macrophage colony-

stimulating factor, as described elsewhere<sup>19</sup>. Special care was taken to cultivate Mφs in normoglycemic (5.5 mmol/l glucose) conditions in Dulbecco's modified Eagle's medium culture and to carefully monitor medium pH and lactate accumulation. For peritoneal Mφs, thioglycolate-elicited Mφs were prepared as described previously<sup>201</sup>. The isolation of cardiomyocytes and cardiac fibroblasts from adult hearts was performed as previously described<sup>173</sup>. In brief, 6- to 8-week-old B6 mice were injected intra-peritoneally with 0.5 ml heparin solution before being anesthetized with tribromoethanol. The excised heart was immediately mounted to a modified Langendorff apparatus and perfused with perfusion buffer, digestion buffer, and stopping buffer in sequential order. After enzyme dissociation, CMs were enriched through a gradient of calcium reintroduction buffer, and were plated accordingly for downstream experimentation.

#### In vitro apoptosis

To compare relative efferocytosis efficiency across cell types, a common apoptotic stimulus was selected: staurosporine. CMs, cardiac fibroblasts, and Mφs were incubated with 0.5 μmol/l staurosporine. The morphology of apoptotic blebbing was quantified and confirmed by annexin V staining. Staurosporine was used as a robust means to induce apoptosis across different cell types<sup>202</sup> and also owing to our empirical observations that CMs are relatively resistant to ultraviolet light-induced apoptosis. Fibroblasts, primary Mφs, and CMs were induced to undergo apoptosis with 0.5 μmol/l of staurosporine treatment for 2 h followed by harvest of nonadherent floating cells (approximately 70% of the total cells). Apoptosis was confirmed by microscopic observation of cell size, morphology, and flow cytometric analysis of phosphatidylserine exposure

by binding of annexin V–FITC (catalog no. 556419, 1:50, BD Pharmingen, Franklin Lakes, New Jersey) according to the recommendations of the manufacturer<sup>168</sup>.

#### In vitro efferocytosis assay

Peritoneal Mφs were plated at  $2 \times 10^5$  in 24-well plates 1 day before the experiment. Apoptotic cells were prelabeled with Calcein AM before apoptosis was induced. The Mφ to CM ratio was 1:5. Cells were cocultured for 1 hour before 3 subsequent rinses to remove nonengulfed cells. The phagocytes were then fixed with 4% paraformaldehyde and analyzed by fluorescence microscopy.

#### Statistical analysis

Data are presented as mean  $\pm$  SEM. Data fit a normal distribution. Thus, the Student *t* test was used to determine statistical significance and  $p < 0.05$  were considered significant. SPSS Statistics (SPSS, Inc, Chicago, Illinois) version 17 was used for statistical analyses.

### **4.3 Result**

#### 4.3.1 Evidence for cm-specific cd47 expression in humans and cd47-induction after experimental MI

A previous study characterized CD47 levels from total ventricular biopsy extracts<sup>203</sup>; however, our understanding of CM-specific expression in humans is limited. We, therefore, first used immunohistochemistry of human hearts after autopsy to test for CM-specific CD47. As shown in Figure 4-3A, human (Fig 4-1,2) myocardial CD47 expression was found to colocalize to CMs;

| <b>Cardiac Findings</b> | <b>Infarcted</b> | <b>Non-Infarcted</b> |
|-------------------------|------------------|----------------------|
| Patient #               | 11               | 11                   |
| Male/Female             | 6/5              | 5/6                  |
| Mean Age                | 66               | 62                   |
| <b>RISK FACTORS</b>     |                  |                      |
| Hyperlipidemia          | 8 (73%)          | 1 (36%)              |
| Hypertension            | 7 (63%)          | 5 (45%)              |
| Obesity                 | 5 (45%)          | 5 (45%)              |

**Table 4-1 Autopsy study population.** Table of patient characteristics for human study in fig 4-3

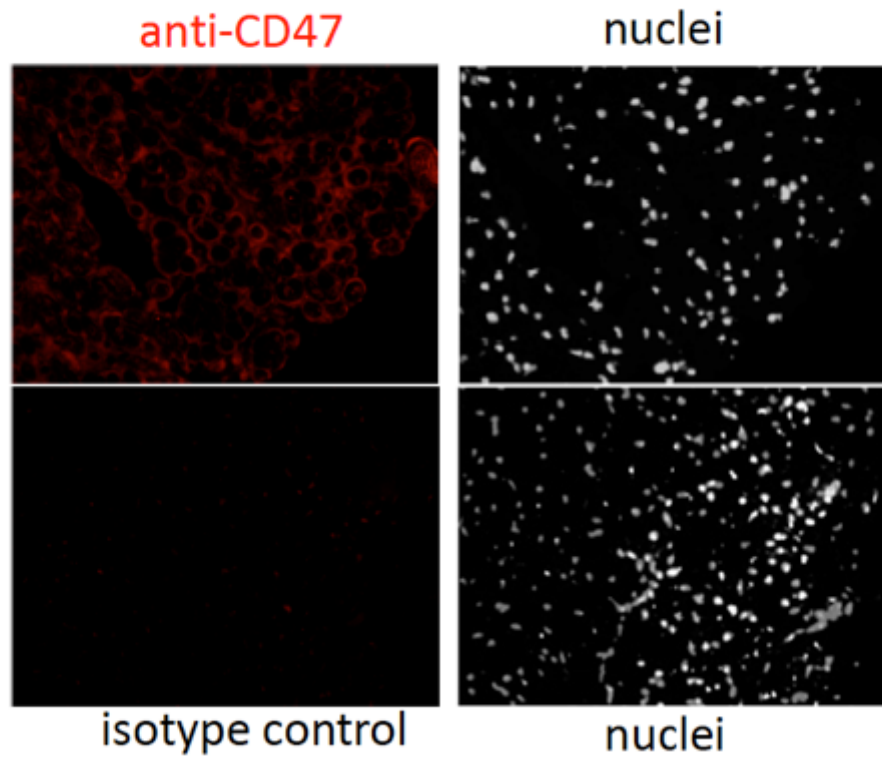


**Fig 4-1 CD47 staining of human cardiac tissue.** Primary Antibody: Rabbit pAB-CD47 (Abcam ab175388) (1:100). Secondary antibody: Alexa Fluor 594 Donkey  $\alpha$ -Rabbit IgG(H+L) (1:100). Nuclei stains are DAPI.

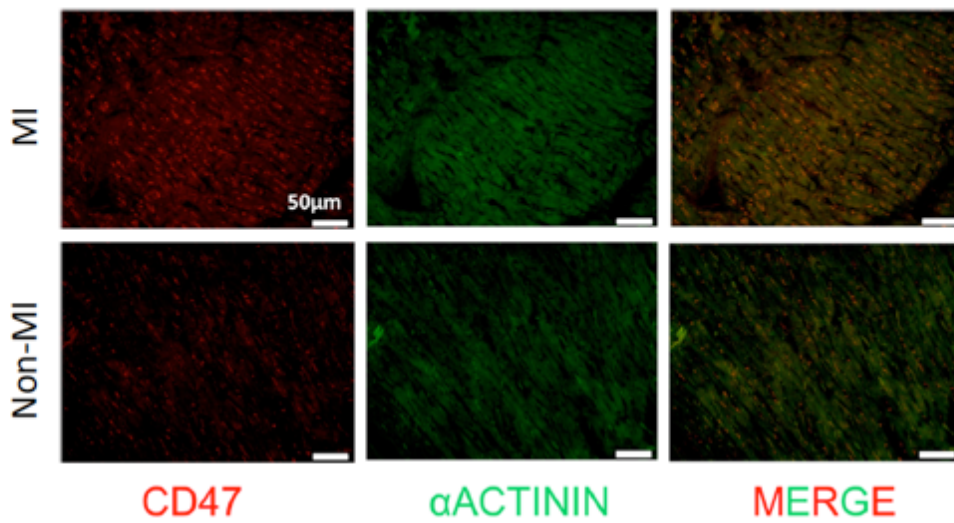


**Fig 4-2 CD47 staining of human myocardial samples.** Autopsy heart immunohistochemistry from myocardial infarction individuals (top panel) versus non-MI (bottom panel) were stained with antibodies against CD47 (red) and cardiomyocyte-marker alpha-actinin (green). To the right is the merge of red and green channels. Scale bar is 50  $\mu$ m.

reduced colocalization was identified on other human cardiac cells, such as endothelial cells (Supplemental Figure 3). In specimens from patients who had succumbed to MI, CD47 staining intensity was interestingly increased (Figure 4-3B). Some of this CD47 colocalized with prophagocytic ligand calreticulin (Supplemental Figure 4), leading us to hypothesize that increased CD47 might interfere with phagocytic efficiency (10). Indeed, increased human CM CD47 levels after acute ischemia is consistent with an impediment to dying myocyte phagocytic clearance and healing. Therefore, we set forth to measure CM CD47 under experimental ischemia and test if CD47 blockade could enhance myocyte phagocytosis and cardiac repair. Similar findings were seen in experimental mouse hearts, where the CD47 signal colocalized with CMs, in contrast with vimentin-positive cardiac fibroblasts (Figures 4-3C,D). To measure CM CD47 levels after MI, experimental mice were subjected to coronary occlusion, as described in the Methods. Interestingly, CD47 levels after MI were significantly increased in the ischemic area at risk versus the remote myocardium (Figure 4-3E). Ex vivo analysis corroborated these findings, revealing significant CD47 protein in isolated adult CMs. Interestingly, CD47 protein was further induced after treatment with stimuli that induced CM death (Supplemental Figure 5). Cell death-induced CD47 was confirmed on the cell surface, and in contrast with primary cardiac fibroblasts.

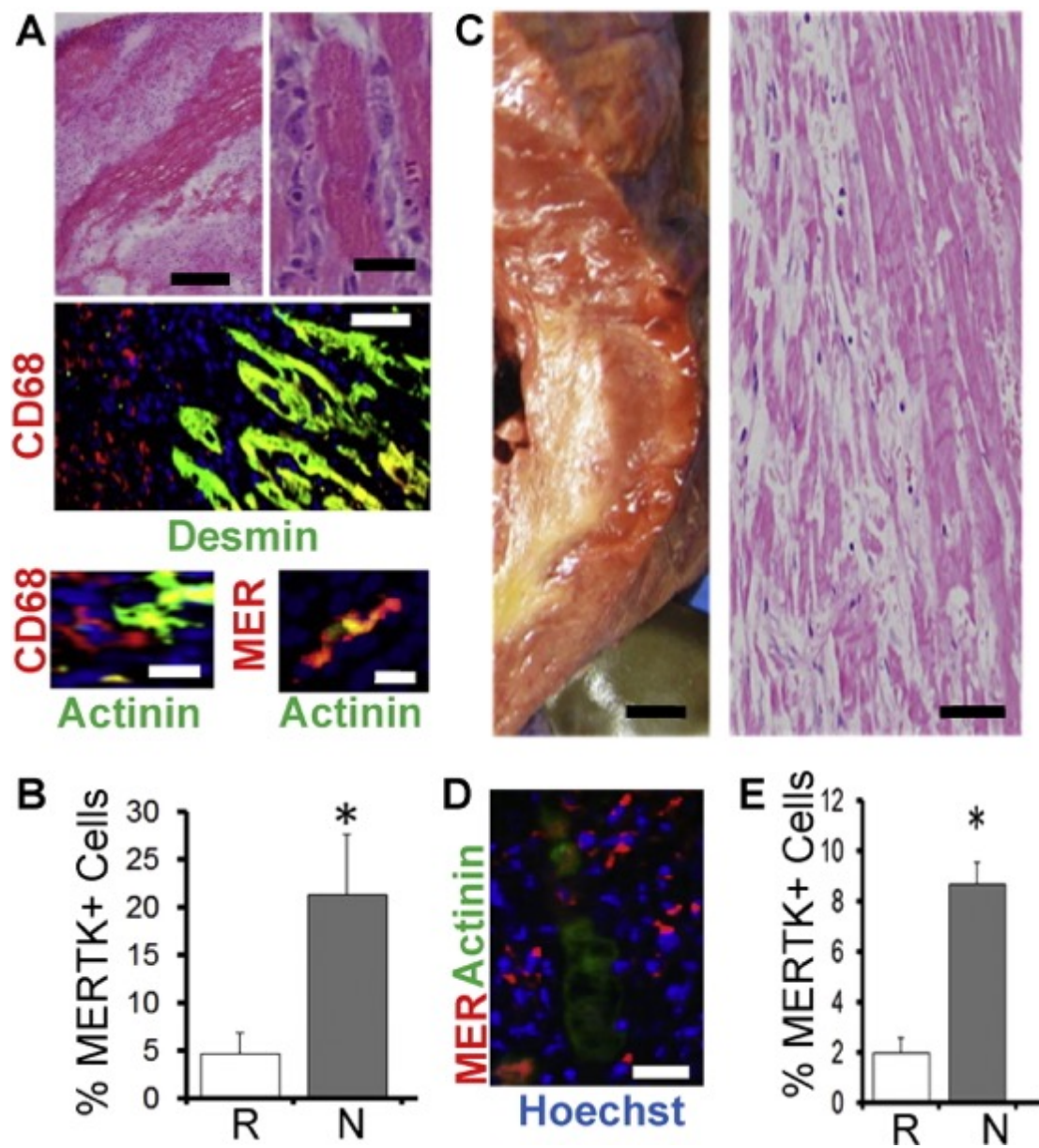


**Fig 4-3. Evidence for MERTK in human myocardium.** A and B is mouse ischemic myocardium and C, D, E is human. (A) Hematoxylin and Eosin (H&E) images of mouse myocardium showing hematoxylin + mono-nuclear cells juxtaposed to hyper-eosinophilic cardiomyocytes. Left scale bar is 500  $\mu\text{m}$  and right is 20  $\mu\text{m}$ . Below H&E micrographs are Immunohistochemistry (IHC) of mouse heart with indicated markers for macrophages (CD68 and MER-TK) and cardiomyocytes (Desmin & Actinin). CD68 vs Desmin bar = 50  $\mu\text{m}$ . Bottom images = 10  $\mu\text{m}$ . In (B), results of IHC quantification in Remote (R) vs inflammatory Necrotic (N) myocardial ROIs (regions of interest). (C, D, E) Human myocardium. (C) Left is cross-section of myocardium from gross autopsy showing yellow infarct and right is H&E histology of same heart. Left is 0.5 cm scale and right is 50  $\mu\text{m}$  scale bar. (D) IHC (100  $\mu\text{m}$ ) with indicated markers (Hoechst are nuclei) and (E) quantitation of MERTK positive signal in healthy/Remote versus inflammatory/Necrotic myocardial ROIs.

#### 4.3.2 Ex vivo uptake of CM apoptotic bodies by mφs is regulated by the CD47–sirpα axis.

We previously reported that phagocytosis is a significant early regulator of cardiac repair after an MI<sup>19</sup>, and furthermore that CMs are engulfed by Mφs at a lower efficiency than other cell types that turnover after an MI<sup>142</sup>. In that the Henson and Weissman groups have shown the potential of blocking CD47 to enhance phagocytosis, we reasoned that increased CD47 might render CMs particularly sensitive to CD47–phagocytic regulation<sup>191,192</sup>. To test the potential of CD47 blockade for rescuing basal CM phagocytosis inefficiency, we added anti-CD47 blocking antibodies to cocultures of primary adult differentiated murine CMs and Mφs. Figure 4-4A shows that CD47 blockade significantly heightened CM efferocytosis, over and above isotype control, and specifically for apoptotic CMs (Figure 4-4B). Efferocytosis enhancements required CD47, because CMs prepared from *Cd47*<sup>-/-</sup> mice were resistant to the effect of anti-CD47 blocking and *Cd47*<sup>-/-</sup> CMs were more susceptible to phagocytic clearance at baseline (Figure 4-4C). These findings predicted similar responses by blocking CD47 ligand, Mφ SIRP-1α. Indeed, anti-SIRP-1α monoclonal antibody, added to Mφs, also increased phagocytosis (Figure 4-4D) of *Cd47*<sup>+/+</sup> CMs. Similar findings were found when inducing iPS-CMs to apoptosis and cocultivating with human Mφs (Fig 4-5).

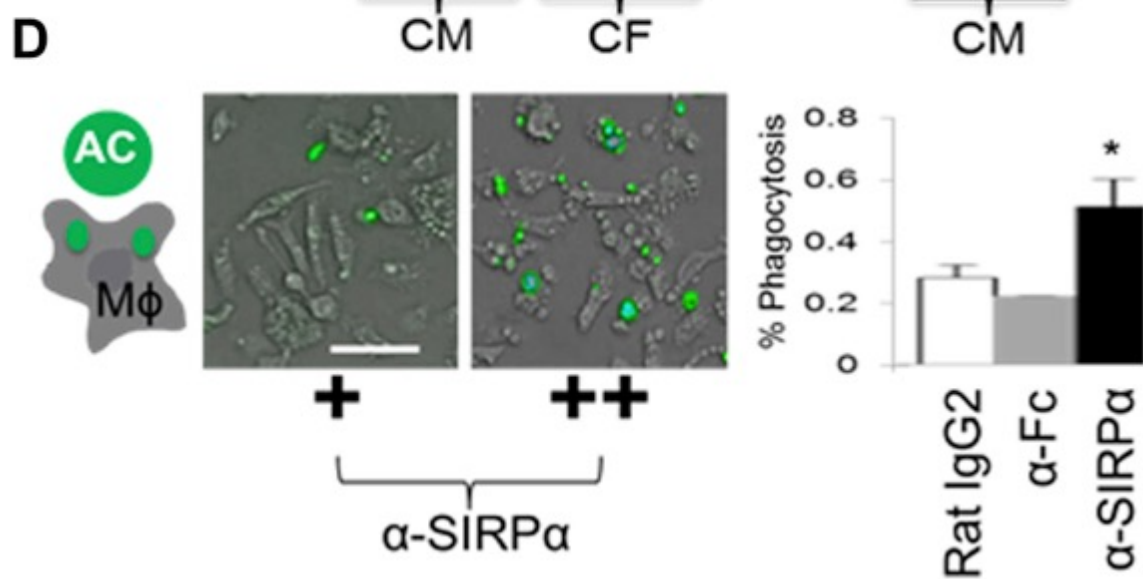
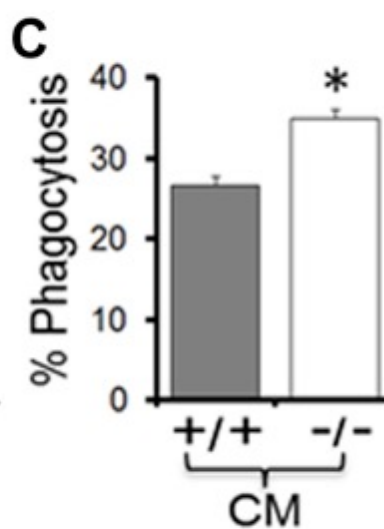
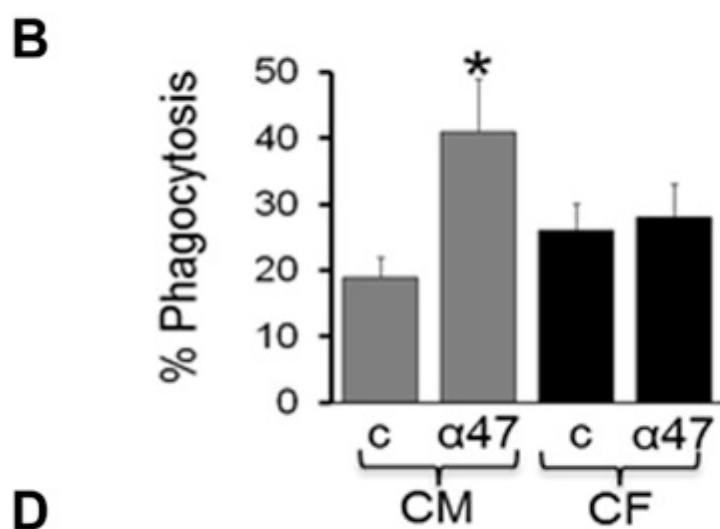
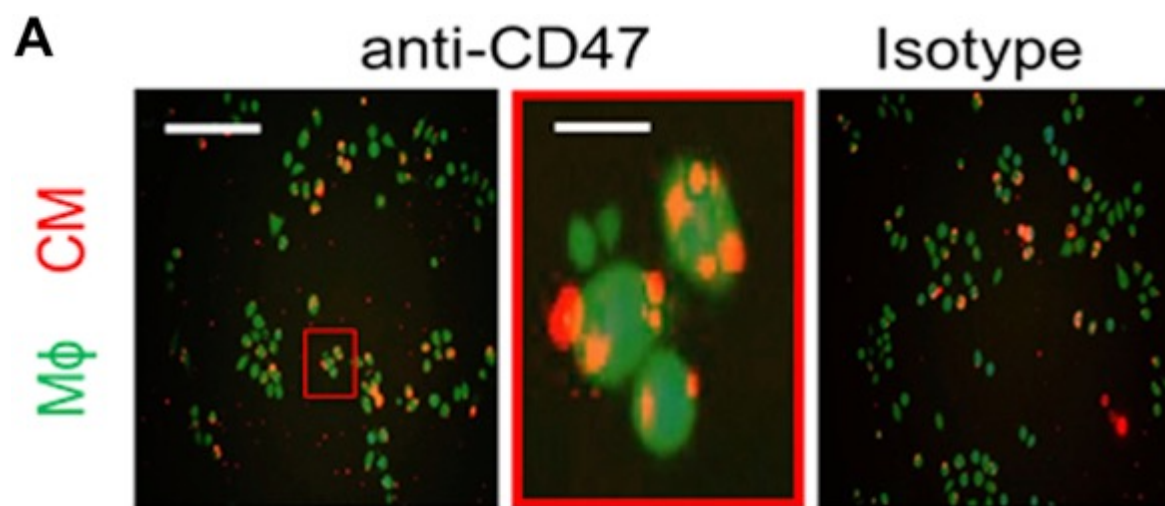


**Figure 4-4. Blockade of the CD47-SIRP-1 $\alpha$  Pathway Specifically Enhances CM Phagocytosis by M $\phi$ s in Culture.** (A) Cocultivations of macrophages (M $\phi$ s) and dying adult mouse ventricular CMs with or without anti-CD47 (a47) versus isotype (C). The CMs were labeled with red R18 dye. The M $\phi$ s were labelled with calcein-AM green. (Left) Scale bar, 300  $\mu$ m. (Right) Scale bar is 20  $\mu$ m. (B) Quantification of percent phagocytosis in CMs versus cardiofibroblasts. Zoom is 600%. \*p = 0.01 relative to CM "c". aCD47, blocking antibody; c, isotype control. (C) Percent phagocytosis of Cd47+/+ versus Cd47-/- CMs by M $\phi$ s. \*p < 0.03. (D) Similar to in (A), except that the antibody treatment is anti-SIRP-1 $\alpha$  versus isotype (Rat IgG2) versus anti-Fc control. Here, CMs were labelled green and M $\phi$ s are not labelled. \*p = 0.04 versus control. Scale bar is 50  $\mu$ m. CF = cardiac fibroblast; other abbreviations as in Figure 4-3.

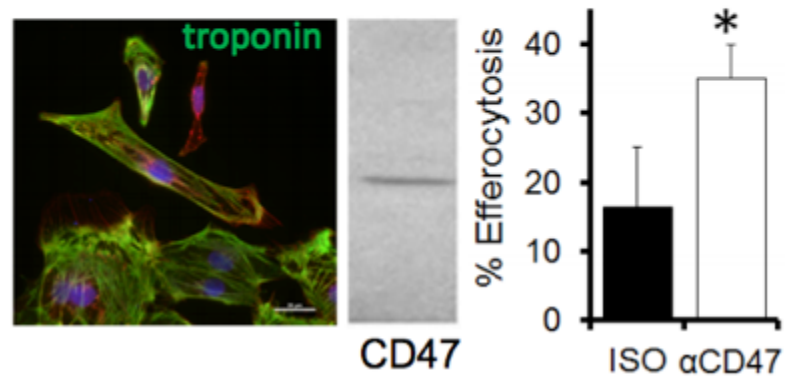


**Fig 4-5 CD47 is expressed in human iPSCMs and its blockade enhances efferocytosis.** Western Blot of CD47 from iPSCMs (micrograph; cardiac troponin TNNT2 is green and ACTN2 actinin is red). iPSCMs were fluorescently labelled and treated with isotype (ISO) control versus antiCD47 and added to human monocyte-derived macrophages to quantify efferocytosis. P = 0.03.

Having tested proof of principle *ex vivo*, we next set out to test physiological relevance. Because of the potential therapeutic implications of our approach, we decided on a reperfusion model of acute murine MI. Also, because of potential nonphagocytic pathways impacted by CD47 signaling, we further decided to limit the blocking of CD47 to acute treatment. Thus, germline deficiency was neither a favorable strategy for our questions nor a viable approach, owing to previously published studies that indicated significant compensatory responses in *Cd47*<sup>-/-</sup> mice<sup>204</sup>.

#### 4.3.3 In vivo testing

Our experimental outline is shown in Fig 4-6. Experimental B6 mice were subjected to ligation of the left anterior descending artery, followed by reperfusion, with or without anti-CD47 treatment. After performing a titration of anti-CD47 concentrations to find the optimal dose for affecting infarct size, we settled on 100 µg. In consideration of potential CD47–thrombospondin interactions, no significant changes in markers of neovascularization were measured (Fig 4-7B). Furthermore, given that global *Cd47*<sup>-/-</sup> knockout mice have been reported to exhibit an increase in arterial diastolic and systolic pressure and that CD47 has also been shown to suppress nitric oxide (NO) signaling in vascular cells after long-term thrombospondin binding<sup>205</sup>, we assessed hemodynamics. However, no differences in systolic blood pressure were found after CD47 blockade (Fig 4-7A).

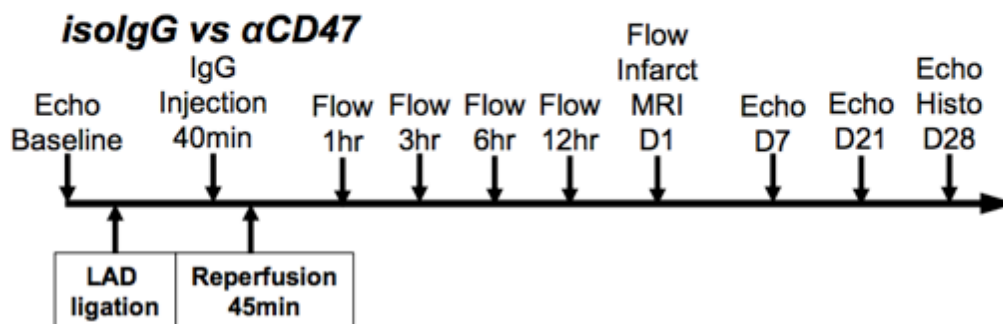


**Fig 4-6 Scheme for in vivo experiments.** Before and after ischemia reperfusion, hearts of control (isIgG injected) vs experimental ( $\alpha$ CD47 igG injected) mice were assessed by Echocardiography, Histology, and MRI for cardiac function and repair, and Flow cytometry for efferocytosis and inflammatory cells.

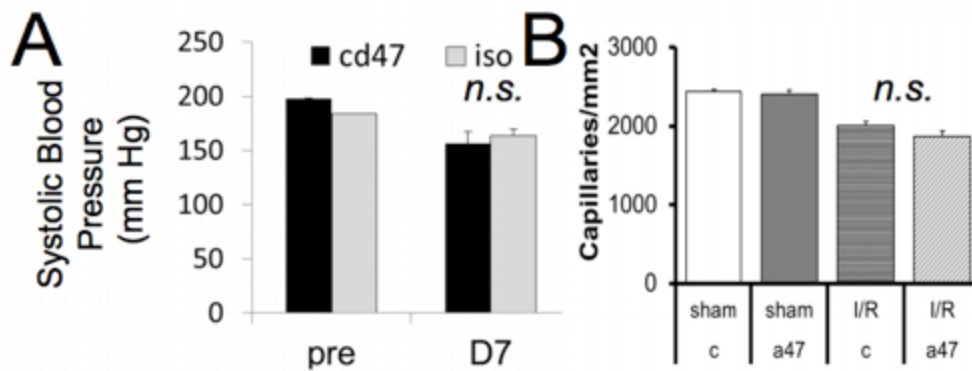


**Fig 4-7 Acute CD47 blockade does not significantly alter systolic blood pressure nor markers of angiogenesis.** (A) Systolic blood pressure was measured on conscious mice using CODA tail-cuff system, pre-surgery and also on day/D7 after ischemia/reperfusion on both CD47 and isotype/IgG injection groups. No significant (n.s.) change was detected between the two groups. (B) Angiogenesis was assessed by lectin antibody staining in the border zone +/- aCD47 treatment, 28 days post I/R.

#### 4.3.4 Acute cd47 blockade during reperfusion after mi enhances myocardial phagocytosis

To specifically measure effects on myocardial phagocytosis, we used mice transgenic for *Mhc6-mCherry*, the fluorescence of which is restricted to CMs<sup>142</sup>. In line with our hypothesis, mice administered anti-CD47 blocking antibody during reperfusion (Fig 4-8A), exhibited an increased profile of myocardial CD11b<sup>+</sup> phagocytes with associated mCherry fluorescence (Fig 4-8B), an indicator of CM phagocytosis. Strikingly, mice administered adeno-associated virus CD47, which increased CD47 levels, exhibited reduced markers of myocardial phagocytosis (Fig 4-8C). Overexpression of CD47 did not affect infarct size, potentially owing to phagocytosis-independent signaling (Fig 4-9). Importantly, anti-CD47 blocking strategies also led to other predicted consequences of enhanced clearance, namely, faster kinetics of cardiac innate immune cell resolution (Fig 4-8D), such as reduced Ly6cHI monocytes and heightened Ly6cLO myeloid cells<sup>15</sup>. Because no differences in neutrophil turnover were found, this suggested specificity for CM uptake. Importantly, administration of antibodies did not affect initial levels or recruitment of blood-borne monocytes (Fig 4-10).

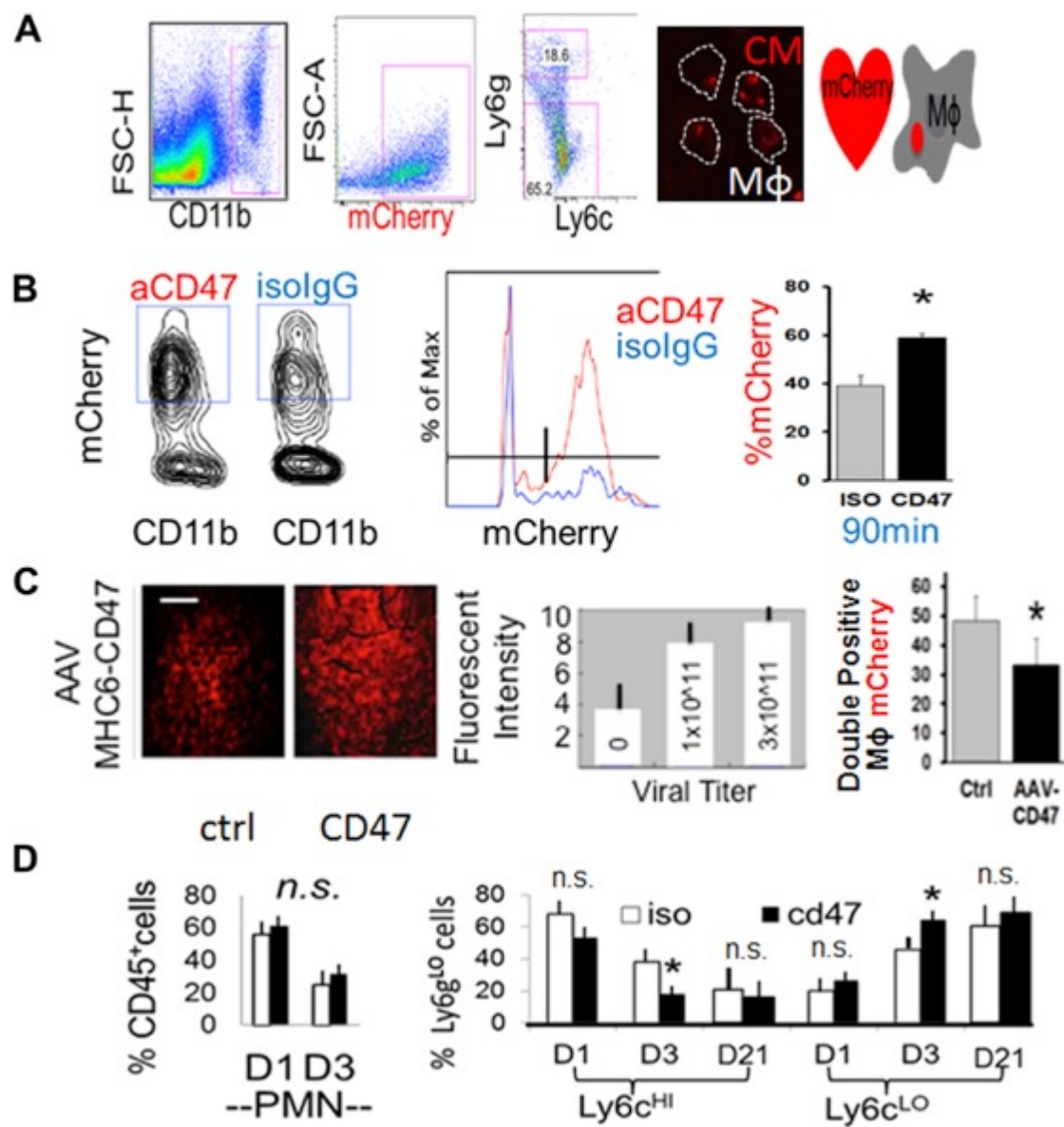


**Figure 4-8. In Vivo CD47 Blockade Versus CD47 Induction Regulates CM Phagocytosis Efficiency and Cardiac Inflammation Resolution.** **(A)** Flow cytometric measure of M $\phi$  engulfment of transgenic mCherry CMs. Gating strategy is shown gating CD11b cells that are mCherry<sup>+</sup> and Ly6g<sup>low</sup> (non-neutrophil phagocytes or M $\phi$ s). Mice were subjected to 45 minutes of ischemia followed by injection of isotype IgG control (ctrl) versus CD47 monoclonal antibodies in phosphate-buffered saline, just before unoccluding the left anterior descending coronary artery. Right image depicts sorted M $\phi$ s with internalized CM mCherry. **(B)** Dot plots, histogram, and bar graph of flow cytometry analysis of CM mCherry-association with myocardial CD11b<sup>+</sup> phagocytes after ischemia and reperfusion of transgenic Myh6-mCherry mice. **(C)** Adeno-associated virus CD47 (myocyte Cre) was injected intravenously before surgery and fluorescent intensity (scale bar, 100  $\mu$ m) is a marker of adeno-associated virus expression and quantified as a function of viral titer. To the right is cardiac phagocytosis enumerated as in **(B and C)**. **(D)** Inflammation resolution kinetics at indicated day **(D)** time points. Flow cytometric analysis of (CD45-hi CD11b-hi Ly6g-lo) Ly6c and CD11c cells in the myocardium. **(Left)** Percentage of CD45-hi CD11b-hi Ly6g-hi neutrophils and polymorphonuclear neutrophils. **(Right)** (CD45-hi CD11b-hi Ly6g-lo) Ly6C-hi monocytes and Ly6c-lo Mo/M $\phi$ s. \*p  $\leq$  0.05 relative to ctrls. ns, not significant. Abbreviations as in Figures 1 and 2.

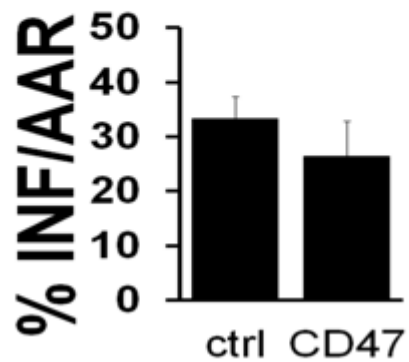


**Fig 4-9. Infarct sizes post ADENO-CD47 treatment vs. control.** Shown are infarcts per area at risk (AAR).

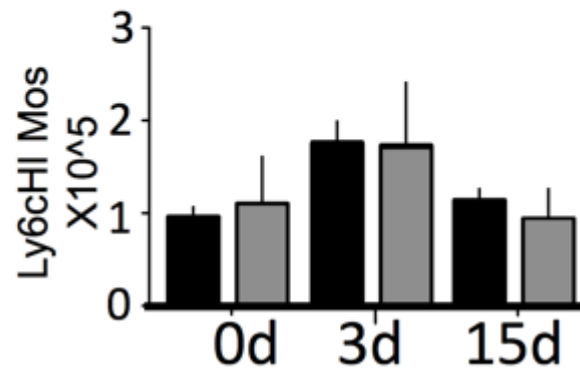


**Fig 4-10. Cellular monocyte inflammation levels in blood post I/R +/- anti-CD47 treatment.** Flow cytometric analyses of myeloid phagocytes at indicated times post I/R from circulating blood.

#### 4.3.5 The effects of acute anti-cd47 on infarct size, systolic function, and cardiac scarring

Impressively, singular administration of anti-CD47 suppressed infarct size and cardiac troponin release (Fig 4-11 A-C). Blockade of CD47 also enhanced systolic cardiac function as indicated by increased LV ejection fraction (Fig 4-12 A-C). Anti-CD47 monoclonal antibody treatment limited ventricular remodeling, because treated mice exhibited reduced scarring, demonstrated by a 2-fold reduction in collagen fraction after Masson's Tri-chrome staining (Fig 4-12D). Taken together, our data suggest a significant potential for incorporating CD47 blocking strategies toward the amelioration of cardiac injury. This approach is unique in its association and targeting of phagocytosis-associated repair.

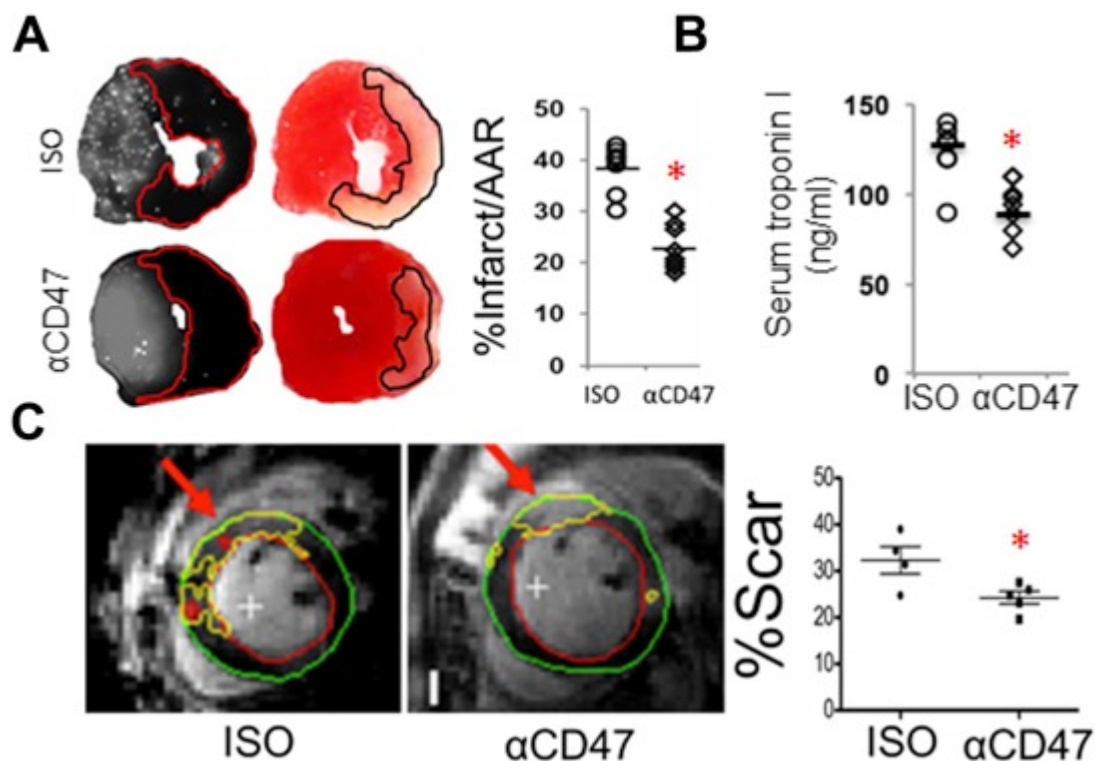


**Fig 4-11. Intramyocardial Injection of Anti-CD47 Reduces Acute Infarct Size.** (A) Fluorescent microspheres were used to measure area at risk (left) at 24 h after reperfusion. Staining with 2,3,5-triphenyl-tetrazolium chloride was performed to measure infarct size (right). Shown here are representative images of myocardial short axis slices and quantification. There were 10 animals in each group ( $p = 0.0001$ ). (B) Serum troponin levels after anti-CD47 treatment at 24 h ( $p = 0.01$ ). (C) CD47 monoclonal antibody injection reduced infarct size as measured by gadolinium enhanced magnetic resonance imaging at 24 h after reperfusion. Example segmentation of the late gadolinium enhancement images. The infarct zones are indicated by the red arrows. The green contours represent the epicardial border, red contours represent the endocardial border, and the yellow contours depict the infarct zones as delineated by automatic thresholding. To the right is quantification of infarct size;  $n = 7$  vs  $7$ .  $p < 0.05$  versus control.

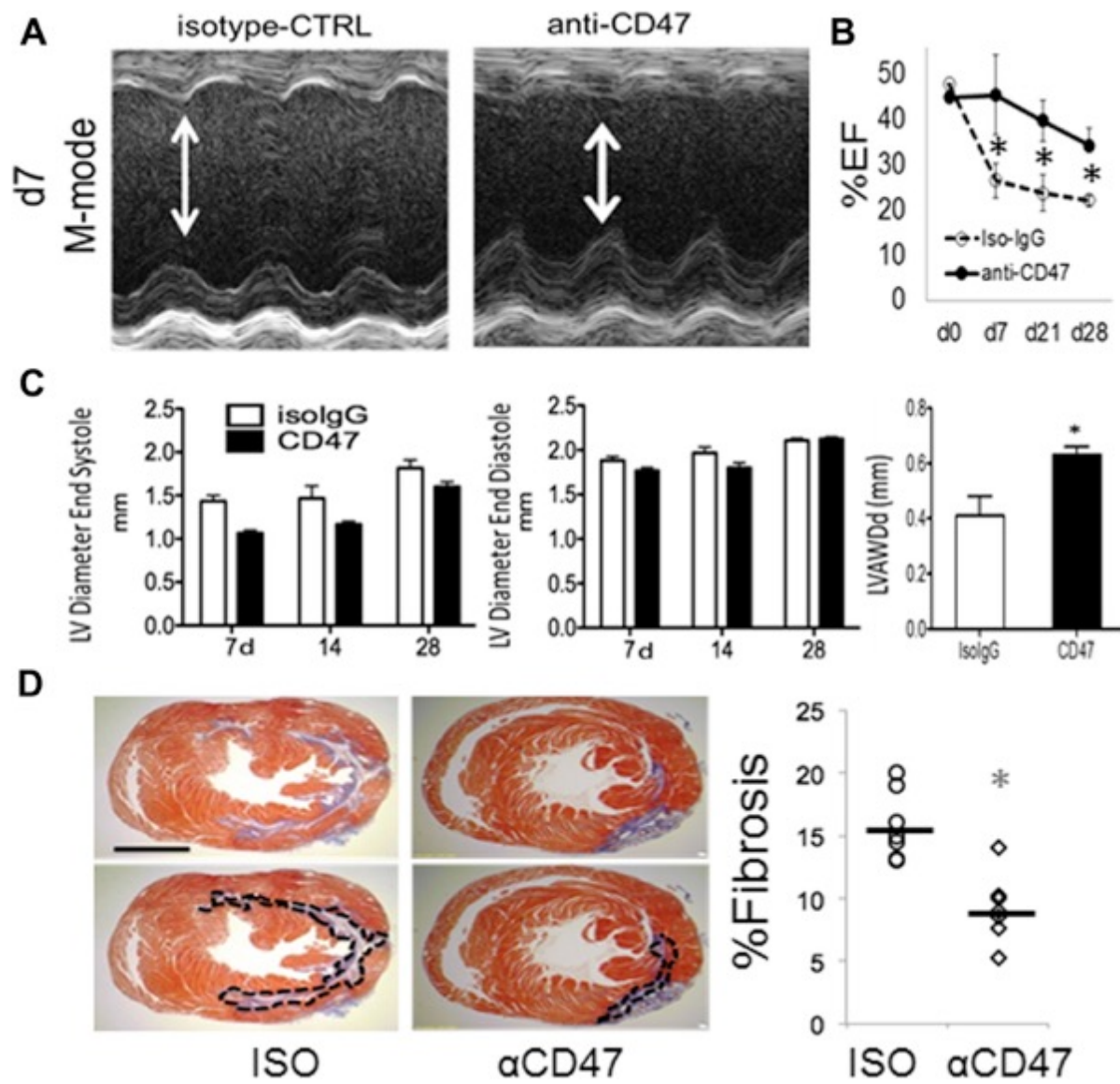


**Fig 4-12. Intramyocardial Injection of Anti-CD47 Improves Systolic Function and Reduces Fibrosis.** (A) Assessment of heart function after ischemia-reperfusion in CD47-antagonized mice at indicated days (d) after I/R. Images are M-mode tracings. Control average heart rate = 474 and anti-CD47 heart rate = 507. (B) Echocardiography analysis of percent ejection fraction. Day 7,  $p = 0.03$ ; day 21,  $p = 0.03$ ; day 28,  $p = 0.03$  (comparisons are between ISO and anti-CD47 at each indicated day). (C) left ventricular systolic and diastolic dimensions. The LV anterior wall diastolic thickness (LVAWDd) (mm) on day 28 from IsoIgG and  $\alpha$ -CD47 antibody-injected mice ( $*p = 0.04$ ). (D) Hearts harvested 21 to 28 days after I/R for staining with Masson's trichrome blue. ISO, isotype control. Scale bar, 1.5 mm.  $*p = 0.04$  relative to control. The number of animals in each group = 10 versus 10.

#### 4.4 Discussion

Although cardiac reperfusion therapies have reduced patient mortality after AMI, improved survival has also led to increases in the frequency of heart failure. A contributing factor to both the benefit and detriment of cardiac repair after ischemia and reperfusion is the innate immune response. Immune cells directly interact with the injured tissue and this includes through binding to the molecular ligand CD47 on parenchymal cells. Herein, we target CD47 with blocking antibodies to enhance phagocytic clearance of dying CMs and in turn, augment cardiac wound healing after MI. Although the gold standard to test molecular requirements is the genetic knockout, *Cd47* germline deficiency tolerizes mice to the CD47–Sirp1 $\alpha$ –phagocytosis pathway, rendering phagocytosis CD47 independent<sup>204</sup>. In this context, CD47-blocking strategies have most notably been pioneered by the Weissman group and to promote tumor cell uptake<sup>192</sup>. During wound healing, CD47 inhibition accelerates wound closure after dermal thermal injury in mice, independent of CD47 ligand thrombospondin-1<sup>206</sup>. Herein, a similar approach is tested in the heart, but with distinct mechanistic and clinical implications. Although multiple cell types turnover after MI<sup>207,208</sup>, distinct myocardial patterns of expression during ischemia and CM-specific mechanisms may render CMs uniquely sensitive to the effects of CD47-blockade. Also, dying cells must both downregulate antiphagocytic signals such as CD47 and concomitantly induce prophagocytic signals. Thus, strategies that target CD47 for phagocytosis should be specific to dying cells, which further require induction of prophagocytic signals.

Previous studies suggest that phagocytosis of adult CMs by M $\phi$ s is naturally inefficient<sup>142</sup>. Indeed, diseases of aging such as MI do not exert evolutionary pressure to optimize CM clearance after

severe MI. During aging, phagocytosis is compromised, including in the heart<sup>34,209</sup>. In the case of CMs, we speculate that low phagocytic efficiency is linked to the low regenerative potential of adult myocytes and could require enhanced mechanisms to prevent phagocytic removal. For example, our data indicate that CD47 surface levels are uniquely heightened after apoptosis and our unpublished experiments suggest novel interactions with membrane scaffolding proteins, which may in turn regulate CD47 cell surface half-life and interactions with other prophagocytic molecules, including calreticulin. In the CM, the function, spatial organization, and interactome of CD47 remains understudied.

Phagocytosis-targeting approaches might be enhanced by the administration of opsonins. For example, natural defects in efferocytosis in cardiovascular disease have been hypothesized to be the result of deficient *Gas6* expression<sup>210</sup>, a critical bridging molecule that facilitates M $\phi$ -mediated engulfment. Similarly, a polymorphism associated with coronary artery disease leads to reduced calreticulin expression on vascular smooth muscle cells and decreased efferocytosis<sup>211</sup>. On the M $\phi$  side, blocking SIRP-1 $\alpha$  may also enhance phagocytic efficiency. This approach is attractive because of the potential to target peripheral blood phagocytes, destined for the heart. Recent advances include the engineering of high-affinity SIRP $\alpha$  variants, which are capable of enhancing CD47 blockade<sup>212</sup>. However, other studies indicate SIRP-1 $\alpha$  is critical to platelet activation<sup>213</sup> and neutrophil and M $\phi$  migration<sup>214</sup>, potentially precluding their efficacy in this regard. Furthermore, cardiac SIRP-1 $\alpha$  protects against myocardial hypertrophy through disruption of TLR4 signaling<sup>215</sup>.

This study has several limitations, including the restricted extent to which murine studies can be extrapolated to humans. Further studies are necessary to test CD47 blockade in large animal

models and examine conservation and reproducibility across species. Also, a closer look at our echocardiography data reveals that the slope of the reduction in the ejection fraction in the anti-CD47 cohort was greater than that in the control group (Fig 4-12). Therefore, additional studies should test the chronic benefit versus the transient nature of this treatment. It is important to consider phagocytosis-independent effects of CD47 blockade. For instance, CD47 targeting during tissue ischemia and reperfusion injury is associated with angiogenesis<sup>216</sup> and efferocytosis in heart can trigger vascular endothelial growth factor A<sup>217</sup>. However, we did not detect significant increases in vascular density. CD47 also has an inhibitory effect on NO signaling. Hypoxia can induce NO synthases and increased NO signaling can improve cell survival under ischemia, in *Cd47*-null mice. In endothelial cells, NO production induces stimulation of vascular smooth muscle cells to promote vascular relaxation; however, induced CD47 ligand thrombospondin-1 inhibits NO production and stimulates production of reactive oxygen species<sup>218</sup>. In our own hands, CD47 blockade does not affect CM viability in vitro. Also, the effects on blood pressure were not found during CD47 blockade (Fig 4-7). Finally, excessive phagocytic uptake has been shown to be detrimental in the central nervous system through phagocytosis-induced cell death<sup>219</sup>. In this context, CD47 may in some instances act as a prophagocytic signal<sup>220</sup>.

An increased understanding of the basic mechanisms of CD47 regulation in CMs holds the potential to uncouple nonphagocytic CD47 signaling to selectively enhance the clearance of dying cells after MI and improve tissue repair. The acute nature of infarct-associated CM death, paired with standards of percutaneous coronary intervention, offer a tractable opportunity for CD47-targeted approaches during clinical reperfusion.

CD47, also known as integrin-associated protein, is known to regulate multiple distinct cellular processes, including the inhibition of phagocytosis of dying cells, or efferocytosis, by immune cell Mφs. Our preclinical studies indicate that CD47-blocking antibodies enhance the phagocytic removal of dying cardiac myocytes, after reperfusion in MI. This intervention also improved the resolution of cardiac inflammation and reduced infarct size.

Further studies are needed to enhance the pharmacological route of administration for anti-CD47 inhibitors and to test the efficacy of humanized anti-CD47 antibodies.

## 5 Concluding Marks

The field of immunometabolism has arisen to merge cellular metabolism with immune function. Much of the initial interest in immunometabolism grew from early links between disease-promoting inflammation and the excess metabolism of obesity<sup>221</sup>. Now, largely absent are preconceived notions that metabolism is solely for the purpose of generating energetic currency. Cellular metabolism is currently well understood to contribute to an array of immune functions beyond biosynthetic demand.

In the case of tissue injury, we found that engulfing apoptotic cells and debris by macrophages are necessary for maintaining tissue homeostasis. Considering apoptotic cells contain large number of intrinsic metabolites, the integration of the inflammatory response with cellular metabolism makes logical sense, where increased anabolic demand requires prioritized and efficient utilization of metabolic substrates. In this context, nutritional status has long been linked to optimal wound healing<sup>222</sup>.

Although metabolism modifying drugs such as metformin and rapamycin have been utilized in clinical fields for inflammatory diseases, one of the challenges is the off-target effects on other cell types and tissues generated by nutrients administration. Thus, future studies require investigation into the fundamental molecular mechanisms to elucidate how metabolic intermediates may directly participate in inflammation and inflammation resolution signal transduction pathways. Approaches targeting macrophage specific downstream molecules such as iNOS, or PKM2 which has been shown to promote angiogenesis at wound site<sup>223</sup>, may yield

less off-target effect. Moreover, future studies looking into metabolites conjugated nanoparticles as delivery vehicles may also contribute to success in therapies.

Because of the complicated integration of numerous metabolic nodes, an informed perspective will benefit from a coupled global network understanding. Integrated top-down transcriptional and metabolic “omics” study revealed that M1 macrophages has a broken TCA cycle at IDH which is required for nitric oxide and IL6 production in M1 macrophages; while in M2 macrophages, intact TCA cycle and glutamine metabolism to UDP-GlcNAc are required for the glycosylation of pathogen recognition receptors<sup>104</sup>. Such network approaches will assist in examination of the heterogeneity of phagocytes in vivo. During wound healing after myocardial infarction, stimuli that activate innate immune cells can be a mixture of tissue debris, hypoxia, cytokines from neighboring cells, and interaction with extracellular matrix. In order to dissect specific metabolic pathways that are activated by environmental stimuli, single cell sequencing of in vivo sorted immune cells coupled with metabolomics analysis is needed to for a more precise prediction of metabolites that are required for alternating immune cell function and understanding of the diversity of the immunometabolic response.

Most conservation of these responses are observed in mouse macrophages. Thus, their applications in human system requires validation. Other than developing integrated network analysis of single cell RNAseq with high resolution metabolomics analysis of human samples, we can take advantage of iPS cells derived from human patients. Induced pluripotent stem cell-derived macrophages (IPSDMs) have been shown to be comparable with human peripheral

blood mononuclear cell-derived macrophages at phenotypic, functional, and transcriptional levels, thus, providing a power tool to study immunometabolism in human systems<sup>224</sup>.

**Reference**

- 1 Lloyd-Jones, D. *et al.* Executive summary: heart disease and stroke statistics--2010 update: a report from the American Heart Association. *Circulation* **121**, 948-954, doi:10.1161/CIRCULATIONAHA.109.192666 (2010).
- 2 Epelman, S., Liu, P. P. & Mann, D. L. Role of innate and adaptive immune mechanisms in cardiac injury and repair. *Nat Rev Immunol* **15**, 117-129, doi:10.1038/nri3800 (2015).
- 3 Tabas, I. Consequences and therapeutic implications of macrophage apoptosis in atherosclerosis: the importance of lesion stage and phagocytic efficiency. *Arterioscler Thromb Vasc Biol* **25**, 2255-2264, doi:10.1161/01.ATV.0000184783.04864.9f (2005).
- 4 Frangogiannis, N. G., Smith, C. W. & Entman, M. L. The inflammatory response in myocardial infarction. *Cardiovasc Res* **53**, 31-47 (2002).
- 5 Swirski, F. K. *et al.* Identification of splenic reservoir monocytes and their deployment to inflammatory sites. *Science* **325**, 612-616, doi:10.1126/science.1175202 (2009).
- 6 Thorp, E. B. Contrasting Inflammation Resolution during Atherosclerosis and Post Myocardial Infarction at the Level of Monocyte/Macrophage Phagocytic Clearance. *Front Immunol* **3**, 39, doi:10.3389/fimmu.2012.00039 (2012).
- 7 Libby, P. Counterregulation rules in atherothrombosis. *J Am Coll Cardiol* **59**, 1438-1440, doi:10.1016/j.jacc.2012.01.023 (2012).
- 8 Panizzi, P. *et al.* Impaired infarct healing in atherosclerotic mice with Ly-6C(hi) monocytosis. *J Am Coll Cardiol* **55**, 1629-1638, doi:10.1016/j.jacc.2009.08.089 (2010).
- 9 Miyamoto, T. *et al.* Bifurcation of osteoclasts and dendritic cells from common progenitors. *Blood* **98**, 2544-2554 (2001).
- 10 Leuschner, F. *et al.* Rapid monocyte kinetics in acute myocardial infarction are sustained by extramedullary monocytopoiesis. *J Exp Med* **209**, 123-137, doi:10.1084/jem.20111009 (2012).
- 11 Shantsila, E. & Lip, G. Y. Monocyte diversity in myocardial infarction. *J Am Coll Cardiol* **54**, 139-142, doi:10.1016/j.jacc.2009.03.047 (2009).
- 12 Shantsila, E. *et al.* Immunophenotypic characterization of human monocyte subsets: possible implications for cardiovascular disease pathophysiology. *J Thromb Haemost* **9**, 1056-1066, doi:10.1111/j.1538-7836.2011.04244.x (2011).
- 13 Nahrendorf, M. & Swirski, F. K. Monocyte and macrophage heterogeneity in the heart. *Circ Res* **112**, 1624-1633, doi:10.1161/CIRCRESAHA.113.300890 (2013).
- 14 Imanishi, T., Tsujioka, H. & Akasaka, T. Endothelial progenitor cell senescence--is there a role for estrogen? *Ther Adv Cardiovasc Dis* **4**, 55-69, doi:10.1177/1753944709353173 (2010).
- 15 Nahrendorf, M. *et al.* The healing myocardium sequentially mobilizes two monocyte subsets with divergent and complementary functions. *J Exp Med* **204**, 3037-3047, doi:10.1084/jem.20070885 (2007).
- 16 Uderhardt, S. *et al.* 12/15-lipoxygenase orchestrates the clearance of apoptotic cells and maintains immunologic tolerance. *Immunity* **36**, 834-846, doi:10.1016/j.immuni.2012.03.010 (2012).

- 17 Auffray, C. *et al.* Monitoring of blood vessels and tissues by a population of monocytes with patrolling behavior. *Science* **317**, 666-670, doi:10.1126/science.1142883 (2007).
- 18 Carlin, L. M. *et al.* Nr4a1-dependent Ly6C(low) monocytes monitor endothelial cells and orchestrate their disposal. *Cell* **153**, 362-375, doi:10.1016/j.cell.2013.03.010 (2013).
- 19 Wan, E. *et al.* Enhanced efferocytosis of apoptotic cardiomyocytes through myeloid-epithelial-reproductive tyrosine kinase links acute inflammation resolution to cardiac repair after infarction. *Circ Res* **113**, 1004-1012, doi:10.1161/CIRCRESAHA.113.301198 (2013).
- 20 Frangogiannis, N. G. *et al.* MCSF expression is induced in healing myocardial infarcts and may regulate monocyte and endothelial cell phenotype. *Am J Physiol Heart Circ Physiol* **285**, H483-492, doi:10.1152/ajpheart.01016.2002 (2003).
- 21 Ben-Mordechai, T. *et al.* Macrophage subpopulations are essential for infarct repair with and without stem cell therapy. *J Am Coll Cardiol* **62**, 1890-1901, doi:10.1016/j.jacc.2013.07.057 (2013).
- 22 Epelman, S. *et al.* Embryonic and adult-derived resident cardiac macrophages are maintained through distinct mechanisms at steady state and during inflammation. *Immunity* **40**, 91-104, doi:10.1016/j.immuni.2013.11.019 (2014).
- 23 Molawi, K. *et al.* Progressive replacement of embryo-derived cardiac macrophages with age. *J Exp Med* **211**, 2151-2158, doi:10.1084/jem.20140639 (2014).
- 24 Mezzaroma, E. *et al.* The inflammasome promotes adverse cardiac remodeling following acute myocardial infarction in the mouse. *Proc Natl Acad Sci U S A* **108**, 19725-19730, doi:10.1073/pnas.1108586108 (2011).
- 25 Bracey, N. A. *et al.* Mitochondrial NLRP3 protein induces reactive oxygen species to promote Smad protein signaling and fibrosis independent from the inflammasome. *J Biol Chem* **289**, 19571-19584, doi:10.1074/jbc.M114.550624 (2014).
- 26 Bracey, N. A. *et al.* The Nlrp3 inflammasome promotes myocardial dysfunction in structural cardiomyopathy through interleukin-1beta. *Exp Physiol* **98**, 462-472, doi:10.1113/expphysiol.2012.068338 (2013).
- 27 Anzai, A. *et al.* Regulatory role of dendritic cells in postinfarction healing and left ventricular remodeling. *Circulation* **125**, 1234-1245, doi:10.1161/CIRCULATIONAHA.111.052126 (2012).
- 28 Zougari, Y. *et al.* B lymphocytes trigger monocyte mobilization and impair heart function after acute myocardial infarction. *Nat Med* **19**, 1273-1280, doi:10.1038/nm.3284 (2013).
- 29 Vandivier, R. W., Henson, P. M. & Douglas, I. S. Burying the dead: the impact of failed apoptotic cell removal (efferocytosis) on chronic inflammatory lung disease. *Chest* **129**, 1673-1682, doi:10.1378/chest.129.6.1673 (2006).
- 30 Chen, W. & Frangogiannis, N. G. The role of inflammatory and fibrogenic pathways in heart failure associated with aging. *Heart Fail Rev* **15**, 415-422, doi:10.1007/s10741-010-9161-y (2010).
- 31 Birge, R. B. & Ucker, D. S. Innate apoptotic immunity: the calming touch of death. *Cell Death Differ* **15**, 1096-1102, doi:10.1038/cdd.2008.58 (2008).

- 32 Serhan, C. N. & Savill, J. Resolution of inflammation: the beginning programs the end. *Nat Immunol* **6**, 1191-1197, doi:10.1038/ni1276 (2005).
- 33 Tabas, I. & Glass, C. K. Anti-inflammatory therapy in chronic disease: challenges and opportunities. *Science* **339**, 166-172, doi:10.1126/science.1230720 (2013).
- 34 Bujak, M. *et al.* Aging-related defects are associated with adverse cardiac remodeling in a mouse model of reperfused myocardial infarction. *J Am Coll Cardiol* **51**, 1384-1392, doi:10.1016/j.jacc.2008.01.011 (2008).
- 35 Frangiannis, N. G. MicroRNAs and endothelial function: many challenges and early hopes for clinical applications. *J Am Coll Cardiol* **63**, 1695-1696, doi:10.1016/j.jacc.2013.10.056 (2014).
- 36 Krishnamurthy, P. *et al.* IL-10 inhibits inflammation and attenuates left ventricular remodeling after myocardial infarction via activation of STAT3 and suppression of HuR. *Circ Res* **104**, e9-18, doi:10.1161/CIRCRESAHA.108.188243 (2009).
- 37 Yang, Z., Zingarelli, B. & Szabo, C. Crucial role of endogenous interleukin-10 production in myocardial ischemia/reperfusion injury. *Circulation* **101**, 1019-1026 (2000).
- 38 Keyes, K. T. *et al.* Resolvin E1 protects the rat heart against reperfusion injury. *Am J Physiol Heart Circ Physiol* **299**, H153-164, doi:10.1152/ajpheart.01057.2009 (2010).
- 39 Schwab, J. M., Chiang, N., Arita, M. & Serhan, C. N. Resolvin E1 and protectin D1 activate inflammation-resolution programmes. *Nature* **447**, 869-874, doi:10.1038/nature05877 (2007).
- 40 Takano, T., Clish, C. B., Gronert, K., Petasis, N. & Serhan, C. N. Neutrophil-mediated changes in vascular permeability are inhibited by topical application of aspirin-triggered 15-epi-lipoxin A4 and novel lipoxin B4 stable analogues. *J Clin Invest* **101**, 819-826, doi:10.1172/JCI1578 (1998).
- 41 Serhan, C. N. *et al.* Design of lipoxin A4 stable analogs that block transmigration and adhesion of human neutrophils. *Biochemistry* **34**, 14609-14615 (1995).
- 42 Stark, M. A. *et al.* Phagocytosis of apoptotic neutrophils regulates granulopoiesis via IL-23 and IL-17. *Immunity* **22**, 285-294, doi:10.1016/j.immuni.2005.01.011 (2005).
- 43 Li, L. *et al.* IL-17 produced by neutrophils regulates IFN-gamma-mediated neutrophil migration in mouse kidney ischemia-reperfusion injury. *J Clin Invest* **120**, 331-342, doi:10.1172/JCI38702 (2010).
- 44 Fadok, V. A., McDonald, P. P., Bratton, D. L. & Henson, P. M. Regulation of macrophage cytokine production by phagocytosis of apoptotic and post-apoptotic cells. *Biochem Soc Trans* **26**, 653-656 (1998).
- 45 Fadok, V. A. & Henson, P. M. Apoptosis: getting rid of the bodies. *Curr Biol* **8**, R693-695 (1998).
- 46 Fadok, V. A. *et al.* Macrophages that have ingested apoptotic cells in vitro inhibit proinflammatory cytokine production through autocrine/paracrine mechanisms involving TGF-beta, PGE2, and PAF. *J Clin Invest* **101**, 890-898, doi:10.1172/jci1112 (1998).
- 47 Bassols, A. & Massague, J. Transforming growth factor beta regulates the expression and structure of extracellular matrix chondroitin/dermatan sulfate proteoglycans. *J Biol Chem* **263**, 3039-3045 (1988).

- 48 Bujak, M. *et al.* Essential role of Smad3 in infarct healing and in the pathogenesis of cardiac remodeling. *Circulation* **116**, 2127-2138, doi:10.1161/CIRCULATIONAHA.107.704197 (2007).
- 49 Bujak, M. & Frangogiannis, N. G. The role of TGF-beta signaling in myocardial infarction and cardiac remodeling. *Cardiovasc Res* **74**, 184-195, doi:10.1016/j.cardiores.2006.10.002 (2007).
- 50 Xiong, M., Elson, G., Legarda, D. & Leibovich, S. J. Production of vascular endothelial growth factor by murine macrophages: regulation by hypoxia, lactate, and the inducible nitric oxide synthase pathway. *Am J Pathol* **153**, 587-598, doi:10.1016/S0002-9440(10)65601-5 (1998).
- 51 Medina, R. J. *et al.* Myeloid angiogenic cells act as alternative M2 macrophages and modulate angiogenesis through interleukin-8. *Mol Med* **17**, 1045-1055, doi:10.2119/molmed.2011.00129 (2011).
- 52 Kawamoto, A. *et al.* Therapeutic potential of ex vivo expanded endothelial progenitor cells for myocardial ischemia. *Circulation* **103**, 634-637 (2001).
- 53 Chambers, S. E., O'Neill, C. L., O'Doherty, T. M., Medina, R. J. & Stitt, A. W. The role of immune-related myeloid cells in angiogenesis. *Immunobiology* **218**, 1370-1375, doi:10.1016/j.imbio.2013.06.010 (2013).
- 54 Marchetti, V. *et al.* Differential macrophage polarization promotes tissue remodeling and repair in a model of ischemic retinopathy. *Sci Rep* **1**, 76, doi:10.1038/srep00076 (2011).
- 55 Takeda, Y. *et al.* Macrophage skewing by Phd2 haploinsufficiency prevents ischaemia by inducing arteriogenesis. *Nature* **479**, 122-126, doi:10.1038/nature10507 (2011).
- 56 Hochreiter-Hufford, A. & Ravichandran, K. S. Clearing the dead: apoptotic cell sensing, recognition, engulfment, and digestion. *Cold Spring Harb Perspect Biol* **5**, a008748, doi:10.1101/cshperspect.a008748 (2013).
- 57 Whelan, R. S., Kaplinskiy, V. & Kitsis, R. N. Cell death in the pathogenesis of heart disease: mechanisms and significance. *Annu Rev Physiol* **72**, 19-44, doi:10.1146/annurev.physiol.010908.163111 (2010).
- 58 Ravichandran, K. S. Beginnings of a good apoptotic meal: the find-me and eat-me signaling pathways. *Immunity* **35**, 445-455, doi:10.1016/j.immuni.2011.09.004 (2011).
- 59 Singer, II *et al.* Sphingosine-1-phosphate agonists increase macrophage homing, lymphocyte contacts, and endothelial junctional complex formation in murine lymph nodes. *J Immunol* **175**, 7151-7161 (2005).
- 60 Lauber, K. *et al.* Apoptotic cells induce migration of phagocytes via caspase-3-mediated release of a lipid attraction signal. *Cell* **113**, 717-730 (2003).
- 61 Peter, C. *et al.* Migration to apoptotic "find-me" signals is mediated via the phagocyte receptor G2A. *J Biol Chem* **283**, 5296-5305, doi:10.1074/jbc.M706586200 (2008).
- 62 Daleau, P. Lysophosphatidylcholine, a metabolite which accumulates early in myocardium during ischemia, reduces gap junctional coupling in cardiac cells. *Journal of molecular and cellular cardiology* **31**, 1391-1401, doi:10.1006/jmcc.1999.0973 (1999).
- 63 Matloubian, M. *et al.* Lymphocyte egress from thymus and peripheral lymphoid organs is dependent on S1P receptor 1. *Nature* **427**, 355-360, doi:10.1038/nature02284 (2004).

- 64 Truman, L. A. *et al.* CX3CL1/fractalkine is released from apoptotic lymphocytes to stimulate macrophage chemotaxis. *Blood* **112**, 5026-5036, doi:10.1182/blood-2008-06-162404 (2008).
- 65 Chekeni, F. B. *et al.* Pannexin 1 channels mediate 'find-me' signal release and membrane permeability during apoptosis. *Nature* **467**, 863-867, doi:10.1038/nature09413 (2010).
- 66 Dolmatova, E. *et al.* Cardiomyocyte ATP release through pannexin 1 aids in early fibroblast activation. *Am J Physiol Heart Circ Physiol* **303**, H1208-1218, doi:10.1152/ajpheart.00251.2012 (2012).
- 67 Ayata, C. K. *et al.* Purinergic P2Y(2) receptors promote neutrophil infiltration and hepatocyte death in mice with acute liver injury. *Gastroenterology* **143**, 1620-1629 e1624, doi:10.1053/j.gastro.2012.08.049 (2012).
- 68 Chen, Y. *et al.* ATP release guides neutrophil chemotaxis via P2Y2 and A3 receptors. *Science* **314**, 1792-1795, doi:10.1126/science.1132559 (2006).
- 69 Elliott, K. J. *et al.* A porphyrin-polyoxometallate bio-inspired mimic for artificial photosynthesis. *Phys Chem Chem Phys* **11**, 8767-8773, doi:10.1039/b905548g (2009).
- 70 Bournazou, I. *et al.* Apoptotic human cells inhibit migration of granulocytes via release of lactoferrin. *J Clin Invest* **119**, 20-32, doi:10.1172/JCI36226 (2009).
- 71 Zakharova, E. E., Korneeva, V. A., Briukhanov, A. L. & Pimenov, N. V. [Psychrophilic sulfate reducing bacterium from aerobic Black Sea waters]. *Mikrobiologiya* **81**, 812-814 (2012).
- 72 Fiane, A. E. *et al.* Mechanism of complement activation and its role in the inflammatory response after thoracoabdominal aortic aneurysm repair. *Circulation* **108**, 849-856, doi:10.1161/01.CIR.0000084550.16565.01 (2003).
- 73 Kempf, T. *et al.* GDF-15 is an inhibitor of leukocyte integrin activation required for survival after myocardial infarction in mice. *Nat Med* **17**, 581-588, doi:10.1038/nm.2354 (2011).
- 74 Singh, M. V. *et al.* MyD88 mediated inflammatory signaling leads to CaMKII oxidation, cardiac hypertrophy and death after myocardial infarction. *Journal of molecular and cellular cardiology* **52**, 1135-1144, doi:10.1016/j.yjmcc.2012.01.021 (2012).
- 75 Nie, H. J., Tian, Y. M., Zhang, D. X. & Wang, H. [Changes of erythrocyte deformability in rats acclimatized to hypoxia and its molemechanism]. *Zhongguo Ying Yong Sheng Li Xue Za Zhi* **27**, 23-28 (2011).
- 76 Arur, S. *et al.* Annexin I is an endogenous ligand that mediates apoptotic cell engulfment. *Dev Cell* **4**, 587-598 (2003).
- 77 Blume, K. E. *et al.* Cleavage of annexin A1 by ADAM10 during secondary necrosis generates a monocytic "find-me" signal. *J Immunol* **188**, 135-145, doi:10.4049/jimmunol.1004073 (2012).
- 78 Ma, Y. J. *et al.* Ficolin-1-PTX3 complex formation promotes clearance of altered self-cells and modulates IL-8 production. *J Immunol* **191**, 1324-1333, doi:10.4049/jimmunol.1300382 (2013).
- 79 Tsai, R. K. & Discher, D. E. Inhibition of "self" engulfment through deactivation of myosin-II at the phagocytic synapse between human cells. *J Cell Biol* **180**, 989-1003, doi:10.1083/jcb.200708043 (2008).

- 80 Izmirly, P. M. *et al.* Maternal and fetal factors associated with mortality and morbidity in a multi-racial/ethnic registry of anti-SSA/Ro-associated cardiac neonatal lupus. *Circulation* **124**, 1927-1935, doi:10.1161/CIRCULATIONAHA.111.033894 (2011).
- 81 Swinnen, M. *et al.* Absence of thrombospondin-2 causes age-related dilated cardiomyopathy. *Circulation* **120**, 1585-1597, doi:10.1161/CIRCULATIONAHA.109.863266 (2009).
- 82 Rogers, N. M. *et al.* Activated CD47 regulates multiple vascular and stress responses: implications for acute kidney injury and its management. *Am J Physiol Renal Physiol* **303**, F1117-1125, doi:10.1152/ajprenal.00359.2012 (2012).
- 83 Cheong, H. S. *et al.* MERTK polymorphisms associated with risk of haematological disorders among Korean SLE patients. *Rheumatology (Oxford)* **46**, 209-214, doi:10.1093/rheumatology/kel182 (2007).
- 84 Sather, S. *et al.* A soluble form of the Mer receptor tyrosine kinase inhibits macrophage clearance of apoptotic cells and platelet aggregation. *Blood* **109**, 1026-1033, doi:10.1182/blood-2006-05-021634 (2007).
- 85 Thorp, E. *et al.* Shedding of the Mer tyrosine kinase receptor is mediated by ADAM17 protein through a pathway involving reactive oxygen species, protein kinase Cdelta, and p38 mitogen-activated protein kinase (MAPK). *J Biol Chem* **286**, 33335-33344, doi:10.1074/jbc.M111.263020 (2011).
- 86 Satoh, M. *et al.* Expression of Toll-like receptor 4 is associated with enteroviral replication in human myocarditis. *Clin Sci (Lond)* **104**, 577-584, doi:10.1042/CS20020263 (2003).
- 87 Munoz, X. *et al.* Human vitamin K-dependent GAS6: gene structure, allelic variation, and association with stroke. *Hum Mutat* **23**, 506-512, doi:10.1002/humu.20025 (2004).
- 88 Hammerman, H. *et al.* Indomethacin-induced scar thinning after experimental myocardial infarction. *Circulation* **67**, 1290-1295 (1983).
- 89 Terry, R. L. *et al.* Defective inflammatory monocyte development in IRF8-deficient mice abrogates migration to the West Nile virus-infected brain. *J Innate Immun* **7**, 102-112, doi:10.1159/000365972 (2015).
- 90 Majmudar, M. D. *et al.* Monocyte-directed RNAi targeting CCR2 improves infarct healing in atherosclerosis-prone mice. *Circulation* **127**, 2038-2046, doi:10.1161/CIRCULATIONAHA.112.000116 (2013).
- 91 Harel-Adar, T. *et al.* Modulation of cardiac macrophages by phosphatidylserine-presenting liposomes improves infarct repair. *Proc Natl Acad Sci U S A* **108**, 1827-1832, doi:10.1073/pnas.1015623108 (2011).
- 92 Anso, E. *et al.* The mitochondrial respiratory chain is essential for haematopoietic stem cell function. *Nat Cell Biol* **19**, 614-625, doi:10.1038/ncb3529 (2017).
- 93 Weinberg, F. *et al.* Mitochondrial metabolism and ROS generation are essential for Kras-mediated tumorigenicity. *Proc Natl Acad Sci U S A* **107**, 8788-8793, doi:10.1073/pnas.1003428107 (2010).
- 94 Sena, L. A. *et al.* Mitochondria are required for antigen-specific T cell activation through reactive oxygen species signaling. *Immunity* **38**, 225-236, doi:10.1016/j.immuni.2012.10.020 (2013).

- 95 Garaude, J. *et al.* Mitochondrial respiratory-chain adaptations in macrophages contribute to antibacterial host defense. *Nat Immunol* **17**, 1037-1045, doi:10.1038/ni.3509 (2016).
- 96 Huang, S. C. *et al.* Cell-intrinsic lysosomal lipolysis is essential for alternative activation of macrophages. *Nat Immunol* **15**, 846-855, doi:10.1038/ni.2956 (2014).
- 97 Usui, F. *et al.* Inflammasome activation by mitochondrial oxidative stress in macrophages leads to the development of angiotensin II-induced aortic aneurysm. *Arterioscler Thromb Vasc Biol* **35**, 127-136, doi:10.1161/ATVBAHA.114.303763 (2015).
- 98 Piquereau, J. *et al.* Mitochondrial dynamics in the adult cardiomyocytes: which roles for a highly specialized cell? *Front Physiol* **4**, 102, doi:10.3389/fphys.2013.00102 (2013).
- 99 Zheng, Y., Gardner, S. E. & Clarke, M. C. Cell death, damage-associated molecular patterns, and sterile inflammation in cardiovascular disease. *Arterioscler Thromb Vasc Biol* **31**, 2781-2786, doi:10.1161/ATVBAHA.111.224907 (2011).
- 100 O'Sullivan, D. *et al.* Memory CD8(+) T cells use cell-intrinsic lipolysis to support the metabolic programming necessary for development. *Immunity* **41**, 75-88, doi:10.1016/j.immuni.2014.06.005 (2014).
- 101 Haschemi, A. *et al.* The sedoheptulose kinase CARKL directs macrophage polarization through control of glucose metabolism. *Cell Metab* **15**, 813-826, doi:10.1016/j.cmet.2012.04.023 (2012).
- 102 Tannahill, G. M. *et al.* Succinate is an inflammatory signal that induces IL-1beta through HIF-1alpha. *Nature* **496**, 238-242, doi:10.1038/nature11986 (2013).
- 103 Rodriguez-Prados, J. C. *et al.* Substrate fate in activated macrophages: a comparison between innate, classic, and alternative activation. *J Immunol* **185**, 605-614, doi:10.4049/jimmunol.0901698 (2010).
- 104 Jha, A. K. *et al.* Network integration of parallel metabolic and transcriptional data reveals metabolic modules that regulate macrophage polarization. *Immunity* **42**, 419-430, doi:10.1016/j.immuni.2015.02.005 (2015).
- 105 Chouchani, E. T. *et al.* Ischaemic accumulation of succinate controls reperfusion injury through mitochondrial ROS. *Nature* **515**, 431-435, doi:10.1038/nature13909 (2014).
- 106 Lampropoulou, V. *et al.* Itaconate Links Inhibition of Succinate Dehydrogenase with Macrophage Metabolic Remodeling and Regulation of Inflammation. *Cell Metab* **24**, 158-166, doi:10.1016/j.cmet.2016.06.004 (2016).
- 107 Mills, E. L. *et al.* Succinate Dehydrogenase Supports Metabolic Repurposing of Mitochondria to Drive Inflammatory Macrophages. *Cell* **167**, 457-470 e413, doi:10.1016/j.cell.2016.08.064 (2016).
- 108 Wu, Z. *et al.* Mechanisms controlling mitochondrial biogenesis and respiration through the thermogenic coactivator PGC-1. *Cell* **98**, 115-124, doi:10.1016/S0092-8674(00)80611-X (1999).
- 109 Nomura, M. *et al.* Fatty acid oxidation in macrophage polarization. *Nat Immunol* **17**, 216-217, doi:10.1038/ni.3366 (2016).
- 110 Huang, S. C. *et al.* Metabolic Reprogramming Mediated by the mTORC2-IRF4 Signaling Axis Is Essential for Macrophage Alternative Activation. *Immunity* **45**, 817-830, doi:10.1016/j.immuni.2016.09.016 (2016).

- 111 Ip, W. K. E., Hoshi, N., Shouval, D. S., Snapper, S. & Medzhitov, R. Anti-inflammatory effect of IL-10 mediated by metabolic reprogramming of macrophages. *Science* **356**, 513-519, doi:10.1126/science.aal3535 (2017).
- 112 Quirino, I. E. *et al.* Arginine Supplementation Induces Arginase Activity and Inhibits TNF-alpha Synthesis in Mice Spleen Macrophages After Intestinal Obstruction. *JPEN J Parenter Enteral Nutr* **40**, 417-422, doi:10.1177/0148607114546374 (2016).
- 113 Gundra, U. M. *et al.* Vitamin A mediates conversion of monocyte-derived macrophages into tissue-resident macrophages during alternative activation. *Nat Immunol* **18**, 642-653, doi:10.1038/ni.3734 (2017).
- 114 Biswas, S. K. & Mantovani, A. Orchestration of metabolism by macrophages. *Cell Metab* **15**, 432-437, doi:10.1016/j.cmet.2011.11.013 (2012).
- 115 Park, D. *et al.* Continued clearance of apoptotic cells critically depends on the phagocyte Ucp2 protein. *Nature* **477**, 220-224, doi:10.1038/nature10340 (2011).
- 116 Poon, I. K., Lucas, C. D., Rossi, A. G. & Ravichandran, K. S. Apoptotic cell clearance: basic biology and therapeutic potential. *Nat Rev Immunol* **14**, 166-180, doi:10.1038/nri3607 (2014).
- 117 N, A. G. *et al.* Apoptotic cells promote their own clearance and immune tolerance through activation of the nuclear receptor LXR. *Immunity* **31**, 245-258, doi:10.1016/j.immuni.2009.06.018 (2009).
- 118 Palsson-McDermott, E. M. *et al.* Pyruvate kinase M2 regulates Hif-1alpha activity and IL-1beta induction and is a critical determinant of the warburg effect in LPS-activated macrophages. *Cell Metab* **21**, 65-80, doi:10.1016/j.cmet.2014.12.005 (2015).
- 119 Oren, R., Farnham, A. E., Saito, K., Milofsky, E. & Karnovsky, M. L. Metabolic patterns in three types of phagocytizing cells. *J Cell Biol* **17**, 487-501 (1963).
- 120 Wang, Y. *et al.* Mitochondrial Fission Promotes the Continued Clearance of Apoptotic Cells by Macrophages. *Cell*, doi:10.1016/j.cell.2017.08.041 (2017).
- 121 Clausen, B. E., Burkhardt, C., Reith, W., Renkawitz, R. & Forster, I. Conditional gene targeting in macrophages and granulocytes using LysMcre mice. *Transgenic research* **8**, 265-277 (1999).
- 122 Xiao, Y. Q. *et al.* Transcriptional and translational regulation of TGF-beta production in response to apoptotic cells. *J Immunol* **181**, 3575-3585 (2008).
- 123 Turner, J. E. *et al.* IL-9-mediated survival of type 2 innate lymphoid cells promotes damage control in helminth-induced lung inflammation. *J Exp Med* **210**, 2951-2965, doi:10.1084/jem.20130071 (2013).
- 124 Jose, P. J. *et al.* Eotaxin: a potent eosinophil chemoattractant cytokine detected in a guinea pig model of allergic airways inflammation. *J Exp Med* **179**, 881-887 (1994).
- 125 Zagorska, A., Traves, P. G., Lew, E. D., Dransfield, I. & Lemke, G. Diversification of TAM receptor tyrosine kinase function. *Nat Immunol* **15**, 920-928, doi:10.1038/ni.2986 (2014).
- 126 Bosurgi, L. *et al.* Macrophage function in tissue repair and remodeling requires IL-4 or IL-13 with apoptotic cells. *Science* **356**, 1072-1076, doi:10.1126/science.aai8132 (2017).

- 127 Lunetta, K. L., Hayward, L. B., Segal, J. & Van Eerdewegh, P. Screening large-scale association study data: exploiting interactions using random forests. *BMC genetics* **5**, 32, doi:10.1186/1471-2156-5-32 (2004).
- 128 Cui, D. *et al.* Pivotal advance: macrophages become resistant to cholesterol-induced death after phagocytosis of apoptotic cells. *J Leukoc Biol* **82**, 1040-1050, doi:10.1189/jlb.0307192 (2007).
- 129 Wang, Y., Mohsen, A. W., Mihalik, S. J., Goetzman, E. S. & Vockley, J. Evidence for physical association of mitochondrial fatty acid oxidation and oxidative phosphorylation complexes. *J Biol Chem* **285**, 29834-29841, doi:10.1074/jbc.M110.139493 (2010).
- 130 Schonfeld, P., Wieckowski, M. R., Lebedzinska, M. & Wojtczak, L. Mitochondrial fatty acid oxidation and oxidative stress: lack of reverse electron transfer-associated production of reactive oxygen species. *Biochim Biophys Acta* **1797**, 929-938, doi:10.1016/j.bbabi.2010.01.010 (2010).
- 131 Hartl, F. U., Schmidt, B., Wachter, E., Weiss, H. & Neupert, W. Transport into mitochondria and intramitochondrial sorting of the Fe/S protein of ubiquinol-cytochrome c reductase. *Cell* **47**, 939-951 (1986).
- 132 Waypa, G. B. *et al.* Superoxide generated at mitochondrial complex III triggers acute responses to hypoxia in the pulmonary circulation. *Am J Respir Crit Care Med* **187**, 424-432, doi:10.1164/rccm.201207-1294OC (2013).
- 133 Rich, P. R. Electron transfer through the isolated mitochondrial cytochrome b-c1 complex. *Biochim Biophys Acta* **722**, 271-280 (1983).
- 134 Ikeda, M. *et al.* STUDIES ON THE BIOSYNTHESIS OF NICOTINAMIDE ADENINE DINUCLEOTIDE. II. A ROLE OF PICOLINIC CARBOXYLASE IN THE BIOSYNTHESIS OF NICOTINAMIDE ADENINE DINUCLEOTIDE FROM TRYPTOPHAN IN MAMMALS. *J Biol Chem* **240**, 1395-1401 (1965).
- 135 Chandel, N. S. *et al.* Reactive oxygen species generated at mitochondrial complex III stabilize hypoxia-inducible factor-1 $\alpha$  during hypoxia: a mechanism of O<sub>2</sub> sensing. *J Biol Chem* **275**, 25130-25138 (2000).
- 136 Akie, T. E., Liu, L., Nam, M., Lei, S. & Cooper, M. P. OXPHOS-Mediated Induction of NAD<sup>+</sup> Promotes Complete Oxidation of Fatty Acids and Interdicts Non-Alcoholic Fatty Liver Disease. *PLoS One* **10**, e0125617, doi:10.1371/journal.pone.0125617 (2015).
- 137 Kimura, R. E. & Warshaw, J. B. Control of fatty acid oxidation by intramitochondrial [NADH]/[NAD<sup>+</sup>] in developing rat small intestine. *Pediatr Res* **23**, 262-265, doi:10.1203/00006450-198803000-00006 (1988).
- 138 Tanner, K. G., Landry, J., Sternglanz, R. & Denu, J. M. Silent information regulator 2 family of NAD<sup>-</sup> dependent histone/protein deacetylases generates a unique product, 1-O-acetyl-ADP-ribose. *Proc Natl Acad Sci U S A* **97**, 14178-14182, doi:10.1073/pnas.250422697 (2000).
- 139 Chung, E. Y. *et al.* Interleukin-10 expression in macrophages during phagocytosis of apoptotic cells is mediated by homeodomain proteins Pbx1 and Prep-1. *Immunity* **27**, 952-964, doi:10.1016/j.immuni.2007.11.014 (2007).
- 140 Shiraishi, M. *et al.* Alternatively activated macrophages determine repair of the infarcted adult murine heart. *J Clin Invest* **126**, 2151-2166, doi:10.1172/jci85782 (2016).

- 141 Varia, M. A. *et al.* Pimonidazole: a novel hypoxia marker for complementary study of tumor hypoxia and cell proliferation in cervical carcinoma. *Gynecol Oncol* **71**, 270-277 (1998).
- 142 Zhang, S. *et al.* Cardiomyocytes induce macrophage receptor shedding to suppress phagocytosis. *Journal of molecular and cellular cardiology* **87**, 171-179, doi:10.1016/j.yjmcc.2015.08.009 (2015).
- 143 Buck, M. D., Sowell, R. T., Kaech, S. M. & Pearce, E. L. Metabolic Instruction of Immunity. *Cell* **169**, 570-586, doi:10.1016/j.cell.2017.04.004 (2017).
- 144 Fourgeaud, L. *et al.* TAM receptors regulate multiple features of microglial physiology. *Nature* **532**, 240-244, doi:10.1038/nature17630 (2016).
- 145 Lemke, G. Biology of the TAM receptors. *Cold Spring Harb Perspect Biol* **5**, a009076, doi:10.1101/cshperspect.a009076 (2013).
- 146 Lancaster, G. I. *et al.* Evidence that TLR4 Is Not a Receptor for Saturated Fatty Acids but Mediates Lipid-Induced Inflammation by Reprogramming Macrophage Metabolism. *Cell Metab*, doi:10.1016/j.cmet.2018.03.014 (2018).
- 147 Chandak, P. G. *et al.* Efficient phagocytosis requires triacylglycerol hydrolysis by adipose triglyceride lipase. *J Biol Chem* **285**, 20192-20201, doi:10.1074/jbc.M110.107854 (2010).
- 148 Titov, D. V. *et al.* Complementation of mitochondrial electron transport chain by manipulation of the NAD<sup>+</sup>/NADH ratio. *Science* **352**, 231-235, doi:10.1126/science.aad4017 (2016).
- 149 Venter, G. *et al.* NAMPT-mediated salvage synthesis of NAD<sup>+</sup> controls morphofunctional changes of macrophages. *PLoS One* **9**, e97378, doi:10.1371/journal.pone.0097378 (2014).
- 150 Liu, P. S. *et al.* alpha-ketoglutarate orchestrates macrophage activation through metabolic and epigenetic reprogramming. *Nat Immunol* **18**, 985-994, doi:10.1038/ni.3796 (2017).
- 151 Kim, H. S. *et al.* SIRT3 is a mitochondria-localized tumor suppressor required for maintenance of mitochondrial integrity and metabolism during stress. *Cancer cell* **17**, 41-52, doi:10.1016/j.ccr.2009.11.023 (2010).
- 152 Amat, R. *et al.* SIRT1 controls the transcription of the peroxisome proliferator-activated receptor-gamma Co-activator-1alpha (PGC-1alpha) gene in skeletal muscle through the PGC-1alpha autoregulatory loop and interaction with MyoD. *J Biol Chem* **284**, 21872-21880, doi:10.1074/jbc.M109.022749 (2009).
- 153 Morari, J. *et al.* The role of proliferator-activated receptor gamma coactivator-1alpha in the fatty-acid-dependent transcriptional control of interleukin-10 in hepatic cells of rodents. *Metabolism* **59**, 215-223, doi:10.1016/j.metabol.2009.07.020 (2010).
- 154 Coste, A. *et al.* The genetic ablation of SRC-3 protects against obesity and improves insulin sensitivity by reducing the acetylation of PGC-1{alpha}. *Proc Natl Acad Sci U S A* **105**, 17187-17192, doi:10.1073/pnas.0808207105 (2008).
- 155 Vats, D. *et al.* Oxidative metabolism and PGC-1beta attenuate macrophage-mediated inflammation. *Cell Metab* **4**, 13-24, doi:10.1016/j.cmet.2006.05.011 (2006).
- 156 Dehn, S. & Thorp, E. B. Myeloid receptor CD36 is required for early phagocytosis of myocardial infarcts and induction of Nr4a1-dependent mechanisms of cardiac repair.

- FASEB journal : official publication of the Federation of American Societies for Experimental Biology*, doi:10.1096/fj.201700450R (2017).
- 157 Krishnamurthy, P. *et al.* IL-10 inhibits inflammation and attenuates left ventricular remodeling after myocardial infarction via activation of STAT3 and suppression of HuR. *Circulation research* **104**, 18 (2009).
- 158 Quiros, M. *et al.* Macrophage-derived IL-10 mediates mucosal repair by epithelial WISP-1 signaling. *J Clin Invest* **127**, 3510-3520, doi:10.1172/jci90229 (2017).
- 159 Riffelmacher, T. *et al.* Autophagy-Dependent Generation of Free Fatty Acids Is Critical for Normal Neutrophil Differentiation. *Immunity* **47**, 466-480 e465, doi:10.1016/j.immuni.2017.08.005 (2017).
- 160 Linger, R. M. *et al.* Mer receptor tyrosine kinase is a novel therapeutic target in pediatric B-cell acute lymphoblastic leukemia. *Blood* **114**, 2678-2687, doi:10.1182/blood-2009-03-209247 (2009).
- 161 Hansson, G. K., Libby, P. & Tabas, I. Inflammation and plaque vulnerability. *J Intern Med* **278**, 483-493, doi:10.1111/joim.12406 (2015).
- 162 Lambert, J. M., Lopez, E. F. & Lindsey, M. L. Macrophage roles following myocardial infarction. *Int J Cardiol* **130**, 147-158, doi:10.1016/j.ijcard.2008.04.059 (2008).
- 163 Zhang, S. *et al.* Phagocyte-myocyte interactions and consequences during hypoxic wound healing. *Cell Immunol* **291**, 65-73, doi:10.1016/j.cellimm.2014.04.006 (2014).
- 164 Elliott, M. R. *et al.* Nucleotides released by apoptotic cells act as a find-me signal to promote phagocytic clearance. *Nature* **461**, 282-286, doi:10.1038/nature08296 (2009).
- 165 Elliott, M. R. & Ravichandran, K. S. Clearance of apoptotic cells: implications in health and disease. *J Cell Biol* **189**, 1059-1070, doi:10.1083/jcb.201004096 (2010).
- 166 Fadok, V. A., Bratton, D. L., Frasch, S. C., Warner, M. L. & Henson, P. M. The role of phosphatidylserine in recognition of apoptotic cells by phagocytes. *Cell Death Differ* **5**, 551-562, doi:10.1038/sj.cdd.4400404 (1998).
- 167 Henson, P. M., Bratton, D. L. & Fadok, V. A. The phosphatidylserine receptor: a crucial molecular switch? *Nat Rev Mol Cell Biol* **2**, 627-633, doi:10.1038/35085094 (2001).
- 168 Briassouli, P., Komissarova, E. V., Clancy, R. M. & Buyon, J. P. Role of the urokinase plasminogen activator receptor in mediating impaired efferocytosis of anti-SSA/Ro-bound apoptotic cardiocytes: Implications in the pathogenesis of congenital heart block. *Circ Res* **107**, 374-387, doi:10.1161/CIRCRESAHA.109.213629 (2010).
- 169 Camenisch, T. D., Koller, B. H., Earp, H. S. & Matsushima, G. K. A novel receptor tyrosine kinase, Mer, inhibits TNF-alpha production and lipopolysaccharide-induced endotoxic shock. *J Immunol* **162**, 3498-3503 (1999).
- 170 Thorp, E., Cui, D., Schrijvers, D. M., Kuriakose, G. & Tabas, I. MERTK receptor mutation reduces efferocytosis efficiency and promotes apoptotic cell accumulation and plaque necrosis in atherosclerotic lesions of apoE<sup>-/-</sup> mice. *Arterioscler Thromb Vasc Biol* **28**, 1421-1428, doi:10.1161/ATVBAHA.108.167197 (2008).
- 171 Scott, R. S. *et al.* Phagocytosis and clearance of apoptotic cells is mediated by MER. *Nature* **411**, 207-211, doi:10.1038/35075603 (2001).

- 172 Thorp, E. B. Methods and models for monitoring UPR-associated macrophage death during advanced atherosclerosis. *Methods Enzymol* **489**, 277-296, doi:10.1016/B978-0-12-385116-1.00016-9 (2011).
- 173 O'Connell, T. D., Rodrigo, M. C. & Simpson, P. C. Isolation and culture of adult mouse cardiac myocytes. *Methods Mol Biol* **357**, 271-296, doi:10.1385/1-59745-214-9:271 (2007).
- 174 Merighi, A., Cruz, F. & Coimbra, A. Immunocytochemical staining of neuropeptides in terminal arborization of primary afferent fibers anterogradely labeled and identified at light and electron microscopic levels. *J Neurosci Methods* **42**, 105-113 (1992).
- 175 Gautier, E. L. *et al.* Gene-expression profiles and transcriptional regulatory pathways that underlie the identity and diversity of mouse tissue macrophages. *Nat Immunol* **13**, 1118-1128, doi:10.1038/ni.2419 (2012).
- 176 Tang, Y. *et al.* MERTK deficiency affects macrophage directional migration via disruption of cytoskeletal organization. *PLoS One* **10**, e0117787, doi:10.1371/journal.pone.0117787 (2015).
- 177 Swirski, F. K. & Nahrendorf, M. Imaging macrophage development and fate in atherosclerosis and myocardial infarction. *Immunol Cell Biol* **91**, 297-303, doi:10.1038/icb.2012.72 (2013).
- 178 Jehle, A. W. *et al.* ATP-binding cassette transporter A7 enhances phagocytosis of apoptotic cells and associated ERK signaling in macrophages. *J Cell Biol* **174**, 547-556, doi:10.1083/jcb.200601030 (2006).
- 179 Cannon, G. J. & Swanson, J. A. The macrophage capacity for phagocytosis. *J Cell Sci* **101 (Pt 4)**, 907-913 (1992).
- 180 Aderem, A. How to eat something bigger than your head. *Cell* **110**, 5-8 (2002).
- 181 Champion, J. A. & Mitragotri, S. Role of target geometry in phagocytosis. *Proc Natl Acad Sci U S A* **103**, 4930-4934, doi:10.1073/pnas.0600997103 (2006).
- 182 Tollis, S., Dart, A. E., Tzircotis, G. & Endres, R. G. The zipper mechanism in phagocytosis: energetic requirements and variability in phagocytic cup shape. *BMC Syst Biol* **4**, 149, doi:10.1186/1752-0509-4-149 (2010).
- 183 Canton, J., Khezri, R., Glogauer, M. & Grinstein, S. Contrasting phagosomal pH regulation and maturation in human M1 and M2 macrophages. *Mol Biol Cell* **25**, 3330-3341, doi:10.1091/mbc.E14-05-0967 (2014).
- 184 Maruyama, R. *et al.* Dynamic process of apoptosis in adult rat cardiomyocytes analyzed using 48-hour videomicroscopy and electron microscopy: beating and rate are associated with the apoptotic process. *Am J Pathol* **159**, 683-691, doi:10.1016/S0002-9440(10)61739-7 (2001).
- 185 Freytes, D. O., Santambrogio, L. & Vunjak-Novakovic, G. Optimizing dynamic interactions between a cardiac patch and inflammatory host cells. *Cells Tissues Organs* **195**, 171-182, doi:10.1159/000331392 (2012).
- 186 Underhill, D. M. & Goodridge, H. S. Information processing during phagocytosis. *Nat Rev Immunol* **12**, 492-502, doi:10.1038/nri3244 (2012).

- 187 Velagaleti, R. S. *et al.* Long-term trends in the incidence of heart failure after myocardial infarction. *Circulation* **118**, 2057-2062, doi:10.1161/CIRCULATIONAHA.108.784215 (2008).
- 188 Jhund, P. S. & McMurray, J. J. Heart failure after acute myocardial infarction: a lost battle in the war on heart failure? *Circulation* **118**, 2019-2021, doi:10.1161/CIRCULATIONAHA.108.813493 (2008).
- 189 Cesselli, D. *et al.* Oxidative stress-mediated cardiac cell death is a major determinant of ventricular dysfunction and failure in dog dilated cardiomyopathy. *Circ Res* **89**, 279-286 (2001).
- 190 Frangiannis, N. G. The immune system and the remodeling infarcted heart: cell biological insights and therapeutic opportunities. *J Cardiovasc Pharmacol* **63**, 185-195, doi:10.1097/FJC.0000000000000003 (2014).
- 191 Gardai, S. J. *et al.* Cell-surface calreticulin initiates clearance of viable or apoptotic cells through trans-activation of LRP on the phagocyte. *Cell* **123**, 321-334, doi:10.1016/j.cell.2005.08.032 (2005).
- 192 Jaiswal, S. *et al.* CD47 is upregulated on circulating hematopoietic stem cells and leukemia cells to avoid phagocytosis. *Cell* **138**, 271-285, doi:10.1016/j.cell.2009.05.046 (2009).
- 193 Khandelwal, S., van Rooijen, N. & Saxena, R. K. Reduced expression of CD47 during murine red blood cell (RBC) senescence and its role in RBC clearance from the circulation. *Transfusion* **47**, 1725-1732, doi:10.1111/j.1537-2995.2007.01348.x (2007).
- 194 Kojima, Y. *et al.* CD47-blocking antibodies restore phagocytosis and prevent atherosclerosis. *Nature* **536**, 86-90, doi:10.1038/nature18935 (2016).
- 195 Isenberg, J. S. *et al.* Thrombospondin-1 and CD47 regulate blood pressure and cardiac responses to vasoactive stress. *Matrix Biol* **28**, 110-119, doi:10.1016/j.matbio.2009.01.002 (2009).
- 196 Frazier, E. P. *et al.* Age-dependent regulation of skeletal muscle mitochondria by the thrombospondin-1 receptor CD47. *Matrix Biol* **30**, 154-161, doi:10.1016/j.matbio.2010.12.004 (2011).
- 197 Wang, X. Q. & Frazier, W. A. The thrombospondin receptor CD47 (IAP) modulates and associates with alpha2 beta1 integrin in vascular smooth muscle cells. *Mol Biol Cell* **9**, 865-874 (1998).
- 198 Lindberg, F. P., Gresham, H. D., Schwarz, E. & Brown, E. J. Molecular cloning of integrin-associated protein: an immunoglobulin family member with multiple membrane-spanning domains implicated in alpha v beta 3-dependent ligand binding. *J Cell Biol* **123**, 485-496 (1993).
- 199 Yeap, X. Y., Dehn, S., Adelman, J., Lipsitz, J. & Thorp, E. B. Quantitation of acute necrosis after experimental myocardial infarction. *Methods Mol Biol* **1004**, 115-133, doi:10.1007/978-1-62703-383-1\_9 (2013).
- 200 Miao, W., Luo, Z., Kitsis, R. N. & Walsh, K. Intracoronary, adenovirus-mediated Akt gene transfer in heart limits infarct size following ischemia-reperfusion injury in vivo. *Journal of molecular and cellular cardiology* **32**, 2397-2402, doi:10.1006/jmcc.2000.1283 (2000).

- 201 Li, S. *et al.* Defective phagocytosis of apoptotic cells by macrophages in atherosclerotic lesions of ob/ob mice and reversal by a fish oil diet. *Circ Res* **105**, 1072-1082, doi:10.1161/CIRCRESAHA.109.199570 (2009).
- 202 Murphy, B. M., O'Neill, A. J., Adrain, C., Watson, R. W. & Martin, S. J. The apoptosome pathway to caspase activation in primary human neutrophils exhibits dramatically reduced requirements for cytochrome C. *J Exp Med* **197**, 625-632 (2003).
- 203 Sharifi-Sanjani, M. *et al.* Cardiac CD47 drives left ventricular heart failure through Ca<sup>2+</sup>-CaMKII-regulated induction of HDAC3. *J Am Heart Assoc* **3**, e000670, doi:10.1161/JAHA.113.000670 (2014).
- 204 Wang, H. *et al.* Lack of CD47 on nonhematopoietic cells induces split macrophage tolerance to CD47null cells. *Proc Natl Acad Sci U S A* **104**, 13744-13749, doi:10.1073/pnas.0702881104 (2007).
- 205 Isenberg, J. S. *et al.* Thrombospondin-1 inhibits endothelial cell responses to nitric oxide in a cGMP-dependent manner. *Proc Natl Acad Sci U S A* **102**, 13141-13146, doi:10.1073/pnas.0502977102 (2005).
- 206 Soto-Pantoja, D. R. *et al.* Thrombospondin-1 and CD47 signaling regulate healing of thermal injury in mice. *Matrix Biol* **37**, 25-34, doi:10.1016/j.matbio.2014.05.003 (2014).
- 207 Narula, J. *et al.* Apoptosis in myocytes in end-stage heart failure. *N Engl J Med* **335**, 1182-1189, doi:10.1056/NEJM199610173351603 (1996).
- 208 Vivar, R. *et al.* TGF-beta1 prevents simulated ischemia/reperfusion-induced cardiac fibroblast apoptosis by activation of both canonical and non-canonical signaling pathways. *Biochim Biophys Acta* **1832**, 754-762, doi:10.1016/j.bbadis.2013.02.004 (2013).
- 209 Arahamian, T., Takemura, Y., Goukassian, D. & Walsh, K. Ageing is associated with diminished apoptotic cell clearance in vivo. *Clin Exp Immunol* **152**, 448-455, doi:10.1111/j.1365-2249.2008.03658.x (2008).
- 210 Hurtado, B. *et al.* Expression of the vitamin K-dependent proteins GAS6 and protein S and the TAM receptor tyrosine kinases in human atherosclerotic carotid plaques. *Thromb Haemost* **105**, 873-882, doi:10.1160/TH10-10-0630 (2011).
- 211 Kojima, Y. *et al.* Cyclin-dependent kinase inhibitor 2B regulates efferocytosis and atherosclerosis. *J Clin Invest* **124**, 1083-1097, doi:10.1172/JCI70391 (2014).
- 212 Weiskopf, K. *et al.* Engineered SIRPalpha variants as immunotherapeutic adjuvants to anticancer antibodies. *Science* **341**, 88-91, doi:10.1126/science.1238856 (2013).
- 213 Chung, J., Gao, A. G. & Frazier, W. A. Thrombospondin acts via integrin-associated protein to activate the platelet integrin alphaIIb beta3. *J Biol Chem* **272**, 14740-14746 (1997).
- 214 Liu, Y. *et al.* Signal regulatory protein (SIRPalpha), a cellular ligand for CD47, regulates neutrophil transmigration. *J Biol Chem* **277**, 10028-10036, doi:10.1074/jbc.M109720200 (2002).
- 215 Jiang, D. S. *et al.* Signal regulatory protein-alpha protects against cardiac hypertrophy via the disruption of toll-like receptor 4 signaling. *Hypertension* **63**, 96-104, doi:10.1161/HYPERTENSIONAHA.113.01506 (2014).
- 216 Isenberg, J. S., Shiva, S. & Gladwin, M. Thrombospondin-1-CD47 blockade and exogenous nitrite enhance ischemic tissue survival, blood flow and angiogenesis via

- coupled NO-cGMP pathway activation. *Nitric Oxide* **21**, 52-62, doi:10.1016/j.niox.2009.05.005 (2009).
- 217 Howangyin, K. Y. *et al.* Myeloid-Epithelial-Reproductive Receptor Tyrosine Kinase and Milk Fat Globule Epidermal Growth Factor 8 Coordinately Improve Remodeling After Myocardial Infarction via Local Delivery of Vascular Endothelial Growth Factor. *Circulation* **133**, 826-839, doi:10.1161/CIRCULATIONAHA.115.020857 (2016).
- 218 Rogers, N. M., Sharifi-Sanjani, M., Csanyi, G., Pagano, P. J. & Isenberg, J. S. Thrombospondin-1 and CD47 regulation of cardiac, pulmonary and vascular responses in health and disease. *Matrix Biol* **37**, 92-101, doi:10.1016/j.matbio.2014.01.002 (2014).
- 219 Emmrich, J. V., Hornik, T. C., Neher, J. J. & Brown, G. C. Rotenone induces neuronal death by microglial phagocytosis of neurons. *FEBS J* **280**, 5030-5038, doi:10.1111/febs.12401 (2013).
- 220 Burger, P., Hilarius-Stokman, P., de Korte, D., van den Berg, T. K. & van Bruggen, R. CD47 functions as a molecular switch for erythrocyte phagocytosis. *Blood* **119**, 5512-5521, doi:10.1182/blood-2011-10-386805 (2012).
- 221 Hotamisligil, G. S. Inflammation and metabolic disorders. *Nature* **444**, 860-867, doi:10.1038/nature05485 (2006).
- 222 Chow, O. & Barbul, A. Immunonutrition: Role in Wound Healing and Tissue Regeneration. *Adv Wound Care (New Rochelle)* **3**, 46-53, doi:10.1089/wound.2012.0415 (2014).
- 223 Zhang, Y., Li, L., Liu, Y. & Liu, Z. R. PKM2 released by neutrophils at wound site facilitates early wound healing by promoting angiogenesis. *Wound Repair Regen* **24**, 328-336, doi:10.1111/wrr.12411 (2016).
- 224 Zhang, H. *et al.* Functional analysis and transcriptomic profiling of iPSC-derived macrophages and their application in modeling Mendelian disease. *Circ Res* **117**, 17-28, doi:10.1161/CIRCRESAHA.117.305860 (2015).